PARTICLE DYNAMICS IN CENTRIFUGAL FORCE FIELDS

A THESIS

Presented to

The Faculty of the Graduate Division

by

John Henry Burson, III

In Partial Fulfillment

of the Requirements for the Degree

Doctor of Philosophy in the School

of Chemical Engineering

Georgia Institute of Technology

December 1964

PARTICLE DYNAMICS IN CENTRIFUGAL

FORCE FIELDS

Approved: _____

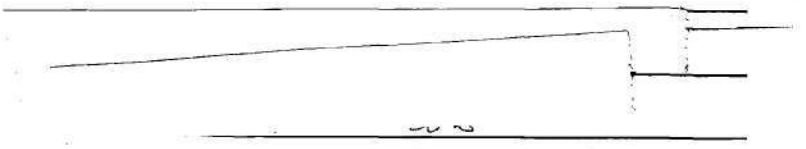

Date approved by Chairman: Dec. 11, 1964

In presenting the dissertation as a partial fulfillment of the requirements for an advanced degree from the Georgia Institute of Technology, I agree that the Library of the Institution shall make it available for inspection and circulation in accordance with its regulations governing materials of this type. I agree that permission to copy from, or to publish from, this dissertation may be granted by the professor under whose direction it was written, or, in his absence, by the Dean of the Graduate Division when such copying or publication is solely for scholarly purposes and does not involve potential financial gain. It is understood that any copying from, or publication of, this dissertation which involves potential financial gain will not be allowed without written permission.

ACKNOWLEDGMENTS

The author wishes to extend his sincere gratitude to the many individuals who have contributed of their time and talents to this study. Particular thanks are expressed to his thesis adviser, Dr. Clyde Orr, Jr., for his encouragement and helpful suggestions throughout the course of this investigation. Thanks are due Dr. Koichi Iinoya, visiting professor from Kyoto University, Kyoto, Japan, who first suggested the subject of this study. Experience and guidelines gained in a previous related study with Dr. Iinoya have been most helpful in the conduct of this research. Valuable assistance was rendered by Drs. C. W. Gorton and W. M. Newton through their comments and suggestions as members of the reading committee, and appreciation is expressed for their conscientious services.

Mr. Edward Y. H. Keng gave much highly useful assistance, and sincere thanks are expressed for his excellent cooperation. Mr. Richard E. Bryan of the Analog Computer Center is also due special thanks for his cooperation and helpful suggestions in programming for the analog computer.

Appreciation is expressed for the support of the Public Health Service and the Engineering Experiment Station of the Georgia Institute of Technology through research grants, employment, and facilities.

For the most valuable assistance of all, the author is greatly indebted to his parents, wife, and children for their continued patience and encouragement throughout the entire program of graduate study.

TABLE OF CONTENTS

LIST OF TABLES

LIST OF FIGURES

LIST OF FIGURES (Continued)

LIST OF FIGURES (Continued)

LIST OF FIGURES (Continued)

LIST OF FIGURES (Continued)

LIST OF FIGURES (Continued)

LIST OF FIGURES (Continued)

Figures Page

NOMENCLATURE

Symbol	Description	Units
A	Constant in slip correction factor	--
A_h	Cross-sectional area of aerosol entry slots	cm^2
a	Size-density parameter, $a=18\mu/\rho\delta^2$	sec^{-1}
B	Constant in slip correction factor	--
C	Particle drag coefficient	--
C'	Constant in slip correction factor	--
D	Inertial parameter in Kriebel's Solution, $D=\rho\Omega\delta^2/18\mu$	--
d	Function of D, $d = \left\{ \left[(1/2)^2 + (2D)^2 \right]^{1/2} + 1/2 \right\}^{1/2}$	--
G	Injection parameter, ratio of initial radial and tangential velocities of a particle	--
g	Function of D, $g= \left\{ \left[(1/2)^2 + (2D)^2 \right]^{1/2} - 1/2 \right\}^{1/2}$	--
j	Function of D, $j=(d^2 + g^2)^{1/2}$	--
F_D	Drag force	dynes
F_L	Lift or Magnus force	dynes
f	Slip correction factor	--
h	Height of classification chamber	cm
k_1	Constant, $k_1 = \mu_\phi / r^{n+1}$	dependent on n
k_2	Constant, $k_2 = Q/2\pi h\, k_1$	dependent on n
M_f	Mass of displaced fluid	gm
M_p	Mass of spherical particle	gm
p	Pressure	$dyne\text{-}cm^{-2}$
Q	Volumetric flow rate	$cm^3\text{-}sec^{-1}$

r	Coordinate direction from axis of rotation	cm
r_o	Initial radial position	cm
Re	Particle Reynolds number, $Re=\delta\bar{V}\rho/\mu$	--
t	Time	sec
u_r	Radial velocity of fluid	$cm\text{-}sec^{-1}$
u_ϕ	Tangential velocity of fluid	$cm\text{-}sec^{-1}$
V_r	Radial velocity of particle	$cm\text{-}sec^{-1}$
V_θ	Tangential velocity of particle	$cm\text{-}sec^{-1}$
$\bar{V}$	Relative velocity of the fluid with respect to the particle $\bar{V}=\left[(u_r-V_r)^2+(u_\phi-V_\phi)^2\right]^{1/2}$	$cm\text{-}sec^{-1}$
x	Dummy variable of integration in drag force term	sec
X,Y	Rectangular coordinates of particle position	cm
$\frac{dr}{dt}$	Radial velocity of particle	$cm\text{-}sec^{-1}$
$\frac{dr_f}{dt}$	Radial velocity of fluid	$cm\text{-}sec^{-1}$
$\frac{d\theta}{dt}$	Angular velocity of particle	sec^{-1}
$\frac{d\phi}{dt}$	Angular velocity of fluid	sec^{-1}
α	Size-density parameter $\alpha=3\rho/4\delta\rho_p$	sec^{-1}
β	Difference in angular displacement of rotor and a fluid contained therein	radians
δ	Particle Diameter	cm
δ	Order of magnitude ($\delta \ll 1$)	--
ϵ	Angular displacement in Kriebel solution	radians
λ	Molecular mean free path	cm
μ	Fluid viscosity	$gm\text{-}cm^{-1}sec^{-1}$

ρ	Fluid density	$gm\text{-}cm^{-3}$
ρ_p	Particle density	$gm\text{-}cm^{-3}$
ψ	Angular displacement of a rotor	radians
ϕ	Angular displacement of a fluid	radians
θ	Angular displacement of a particle	radians
Γ	Angular velocity of a particle about one of its own axes.	sec^{-1}
Ω	Angular velocity of a rotor	sec^{-1}

SUMMARY

The dynamic behavior of small particles when suspended in fluids is an important aspect of many chemical engineering processes. Previous studies in this area have been largely empirical in nature, primarily because of the mathematical complexities normally associated with them. Present-day technology, however, requires a more fundamental knowledge of particle dynamics. Quantitative information is needed for the development of higher efficiency gas cleaners, particle classifiers, and the like. Because response to centrifugal forces is of prime concern in such devices, this research was especially concerned with particle dynamics in strong centrifugal fields.

The specific objectives of this research were to study both theoretically and experimentally the dynamic behavior of particles between one and 50 microns in diameter when suspended in a fluid and undergoing intense vortex motion. A further objective was to develop a centrifugal particle classifier which would efficiently separate particles according to their settling diameters and would also be capable of verifying that the resulting size classifications could be predicted from theoretical considerations.

Fluid velocity components determine to a large extent the trajectories of particles contained therein. Qualitatively correct descriptions of the fluid flow were produced by an approximate analysis for the interaction of radial flow between parallel plates from a source on the axis of rotation and several types of vortex flow. Theoretical predictions of flow patterns

were qualitatively confirmed by flow visualization using tobacco smoke in a classifier rotor illuminated by a high intensity stroboscope.

Equations were developed for the non-steady, two-dimensional motion of particles in viscous fluids. Non-steady drag effects and the slip correction were found to be negligible for the range of particle sizes and fluid densities pertinent to this study. No appreciable lift forces were active due to the absence of strong shear gradients. Simplified forms of the equations were developed for several special cases. Previous best estimates of particle trajectories in centrifugal fields have been restricted to cases in which Stokes law was assumed to represent the particle drag force. The objective of one portion of this research, therefore, was to confirm or reject solutions obtained by previous investigators and, if possible, to extend the results to more general cases.

An analog computer was used to solve the equations of particle motion in their most general form pertinent to the conditions and interest of this study. Solutions were obtained for various particle densities and diameters, initial conditions of motion for the particles, types and strengths of centrifugal fields, and representations of the particle drag force. Theoretical results indicated that particle classification under free vortex conditions in a rotor of the type developed for this study was not feasible and optimum classification should result only under fluid motion conditions described as forced vortex. For good results, the location of each particle must be precisely known as it enters the classification chambers and the initial radial velocity of the particles should be as low as practicable but have the same initial tangential velocity as the fluid. Differences were obtained for particle trajectories when Stokes

law was assumed to represent drag forces and when a more general relation based on the best experimental values for particle drag coefficients was used. Solutions based on Stokes law indicated intersections of particle trajectories with the wall of the classifier rotor at lower angular displacements than did the corresponding solutions based on the more general drag relation. Calculations of particle Reynolds numbers demonstrated that practically every particle exceeded a Reynolds number of unity under typical operating conditions. Since the generally accepted upper limit for the applicability of Stokes law is a particle Reynolds number of one, the results for the more general drag relation should best represent actual particle behavior.

An experimental classifier rotor was developed in which centrifugal fields of known characteristics could be developed and in which the initial conditions of particle motion could be accurately set. Experimental studies were made on the size classification obtained under various operating conditions for dilute aerosols consisting of spherical particles of plastic, glass, aluminum, and zinc having diameters from about one to 50 microns. Excellent results were obtained for each of these materials. Size distributions measured at specified angular locations on the rotor wall demonstrated that the separations were very nearly ideal since essentially mono-disperse sizes were obtained at any one location. Somewhat poorer results were noted at low angular displacements; however, it is believed that this was due primarily to increased radial fluid components and deviations from forced vortex conditions in this small angular sector.

Experimental results were in excellent agreement with analog computer

solutions in which the more general drag relationship was used. Qualitative results with irregular particles showed that separation of these materials according to their effective settling diameters was also possible.

CHAPTER I

INTRODUCTION

Background and Specific Objectives

The dynamic behavior of finely-divided materials in centrifugal force fields is a classical area of chemical and mechanical engineering that has received surprisingly little detailed study. In spite of a scarcity of quantitative information on particle dynamics, many processes involving cyclone separation, spray drying,and centrifugal filtration have been operated quite successfully on the basis of empirical expressions and data correlations. High efficiency gas cleaning devices, particle classifiers and the like, however, demand a more fundamental knowledge of particle behavior.

The overall purpose of this investigation was to study both theoretically and experimentally the dynamic behavior in centrifugal fields of those particles which, when airborne, comprise a "coarse" aerosol. A "coarse" aerosol is here defined as one in which particle diameters are predominantly from about one to 50 microns. Aerosols having particles in this size range, and especially narrowly sized fractions of them, are of particular interest in air pollution research and toxicity response testing because their physiological effects are generally much more significant than those obtained using bulk samples of these same materials. In addition to the obvious value of narrowly sized particle fractions for the calibration of size measuring devices, there are also

demands for quantities of essentially mono-sized particles in studies on catalytic activity, powder metallurgy and high-energy, slurry-type fuels, to mention only a few. Unfortunately, there has previously been no method capable of collecting and simultaneously classifying with high efficiency significant quantities of particles in this size range on a particle number basis. Thus an important part of this investigation, in addition to the theoretical studies, was the design, construction and evaluation of a medium-capacity centrifugal classifier which would be an efficient collection and classification device and capable also of demonstrating that the resulting size-density classifications could be predicted from theoretical considerations.

Aerosol particles between one and 50 microns diameter are generally free of many of the complicating properties of sub-micron particles such as Brownian motion, unusual surface effects, and the slip effect. These advantages are partially offset, however, by the more complicated fluid drag effects for particles much larger than a micron undergoing unsteady motion. The Stokes drag law is generally not valid for the motion of particles in this size range in strong centrifugal fields because of the large particle Reynolds numbers attained. A more general drag force relation in which the drag coefficient is not a simple function of the particle Reynolds number must be employed to describe correctly their dynamic behavior. Particles larger than about 50 microns do not usually form stable aerosols. Also the size classification of these larger particles is readily accomplished by sieving, therefore their classification need not come within the scope of this investigation.

The centrifugation of extremely small particles, i.e., heavy molecules

and atoms, has lately received considerable study because of the potential military and economic ramifications of a cheap and efficient means of separation of isotopes. Classically, centrifugation has been employed as a means of determining molecular weights and the isolation of certain chemical and biological species. Although the same basic principles apply over the entire size spectrum of particle dispersoids, the physical aspects of aerosols as well as the inter-relationships of the laws which govern their behavior change drastically with particle size. This is, perhaps, most vividly revealed in the variations of the drag resistance law with particle size. Particles from atomic dimensions to about one micron are thus excluded from consideration here as are those with greater than 50 microns diameters. This leaves only a narrow portion of the total size spectrum for this study; it encompasses nevertheless, a region of prime concern in current technology.

Previous Related Studies in Fluid Dynamics

The study of particle dynamics in centrifugal fields can logically be divided into several areas, the first of which might be a consideration of the dynamics of various types of vortex motion and the drag forces exerted on submerged bodies. In this area, Stokes[1] was apparently the first investigator, after the formulation of the foundations of mechanics by such notables as Newton, Galileo and Huygens, to obtain meaningful results from purely theoretical considerations of the motion of solid bodies through viscous fluids. His celebrated memoir on pendulums established the force necessary to move a spherical body through a viscous fluid. In the 60 or so years following the formulation of Stokes law, few further

advances were realized in the fundamentals of particle dynamics until 1911 when Lord Rayleigh[2] extended Stokes' solution to the case of accelerating motion of solid bodies in viscous fluids. Subsequent to this, Proudman[3] reported on the motion of solid bodies in a liquid possessing vorticity and Taylor[4][5][6] and Rayleigh[7] extended these results for both viscous and potential flow. Taylor[8] verified many of his theoretical results with a series of ingenious experiments. All of these studies contributed to the overall knowledge of the motion of submerged bodies in rotating fluids; however, they were primarily concerned with specific hydrodynamic problems such as fluid drag rather than with an overall analysis of particle motion.

A large number of other investigations[9][10][11][12][13][14] have reported on many aspects of the fluid dynamics of rotary flow, particularly in connection with the design of turbomachinery and the study of natural vortex motion such as occurs in hurricanes, cyclones and other meteorological phenomena. Indeed, some of the classical exact solutions of the Navier-Stokes equations have been in this realm[15][16]. Although none of these studies was found to be directly applicable to the specific problems of this investigation, valuable guidelines for approaching the problem of the fluid mechanics of rotating fluids were provided by them.

Previous Related Studies of Particle Dynamics

Some of the more important investigations which have been conducted on the rectilinear and curvilinear motion of aerosol particles in various types of force fields are summarized here. In general, they do not utilize equations of particle motion solved analytically except for a few

special cases. Usually, recourse to some method of incremental appoximation provided the method of solution.

Albrecht[17] was one of the first investigators to study the motion of spherical particles as they deviated from the path of flowing fluid when the fluid encountered a cylindrical object in its normal path of flow. These studies were particularly useful in the development of impaction and dust filtration theory. Exact solutions were obtained for a few relatively simple cases in which Stokes law was assumed valid.

Lapple and Shepherd[18] developed equations for calculating the trajectories of particles undergoing accelerated motion in viscous fluids. In several of the cases, curves were prepared by a method of incremental approximation to simplify computations. One of the cases considered was the two-dimensional motion of a particle in a fluid stream undergoing simple rotational motion. No solutions, however, were given for this case except for the greatly simplified situation in which the particle acceleration terms are negligible and the tangential velocities of the fluid and particle are identical.

Narsimhan[19] considered the case of particle motion in a centrifugal field in which tangential forces were negligible and solved the radial component of the equations of particle motion under streamline and eddying conditions. Although Narsimhan noted that a particle in a forced vortex does not attain a constant terminal velocity because the accelerating forces increase as the radius of rotation increases, he nevertheless used what in effect was a constant terminal velocity as a boundary condition. The results were therefore restricted to liquid centrifuges in which tangential forces are usually negligible; they are useful primarily in

calculating optimum feed rates to liquid centrifuges.

Particle motion in a rotating drum aerosol chamber was considered by Calder[20]. Calder's method of vector analysis included the influence of gravity and provided considerable insight into the motion of aerosol particles, particularly for the case of slow rates of rotation and the applicability of Stokes law.

Kriebel[21] studied the motion of particles in a forced vortex of fluid under the assumption of the applicability of Stokes law. This investigation is considered in more detail in the following section on classifier designs.

Bouchillon[22] studied the trajectories of spherical particles in a hydrocyclone. Approximate equations of particle motion in three-dimensional sheared flows were developed and solved by numerical and electrical analog methods. Because of the high shear in a hydrocyclone, lift forces as well as non-steady drag forces were considered for several cases.

Muller and Wessel[23] calculated the trajectories of particles with diameters from 100 to 500 microns in three related types of gravity pneumatic separators. The equations of particle motion were solved for several specific initial conditions with an electrical analog computer.

Some Previous Centrifugal Classifier Designs

Most previous attempts to design centrifugal particle classifiers have been based on the so-called "constant cut-point" theory. Devices of this type include the cyclone and free vortex classifiers. Cyclones are quite useful as gas cleaning devices. Their utility as precision

classifiers is severely limited, however, by the extremely complex turbulent fluid flow generally associated with them. Cyclones are thus excluded from further detailed consideration in this study. The free vortex classifiers were apparently first reported by Wolf and Rumpf[24] in 1941. The principle of operation of this type classifier is to create a free vortex of particle-laden air by introducing an aerosol tangentially with the desired initial angular velocity at the periphery of a centrifugal classifier chamber and have the aerosol flow radially inward to the center of rotation as a spiral vortex. With this arrangement, the centrifugal force acting on a particle is directed radially outward and the fluid drag force radially inward for the ideal case in which no tangential forces are present. Thus for a certain particle diameter and specified flow conditions there will exist a balance of radial forces such that the trajectory of this equilibrium particle will describe a circle in the classification chamber. Particles larger than the equilibrium size will be rejected to the outer wall of the classifying chamber while smaller particles will be collected at or near the center of the chamber. Thus to separate a material into n discrete size fractions, a series of $(n-1)$ runs must be made on the original material and the residue from each of the preceding runs.

Early designs of these free vortex classifiers were generally disappointing, primarily because of poor design features that induced turbulence and secondary flows which re-entrained the separated particles. Later designs[25][26] were based on a more refined mathematical analysis and better mechanical design features which eliminated many of the sources of prior trouble. These later designs have proved to be quite efficient

in separating particles larger than about 10 microns diameter when the separations are considered on a weight basis. If the separations are considered on the numbers of particles present instead of the weights present, then, what was an insignificant contribution by the very small particles becomes a larger contribution on a number per cent basis, and the quality of separation is invariably poorer. Because of the difficulty in generating a laminar free vortex or Archimedian spiral flow pattern in which tangential forces are negligible, it is doubtful if precise classification on a number per cent basis can ever be achieved by centrifugal classifiers of this type.

A recent German classifier described by Wieland[27] combines spiral and axial flow of aerosol along a vertical tube in much the manner of the Sharples super-centrifuge[28]. The former classifier has a compartmented vertical rotor which is supposed to permit separating the feed aerosol into 13 discrete size fractions. No quantitative information has been given on separation efficiencies; however, an examination of published photomicrographs indicates separations of about the same precision as attained in the more-conventional free vortex classifiers.

A somewhat similar device which preceded that of Wieland is the Bahco classifier[29]. This device also operates on the cut-size principle; however, the means of separation is the winnowing of small particles from a radially outward flowing aerosol by a superimposed spiral flow of clean air inward and upward. The smaller particles, i.e., those below the cut-size, are deflected from their radial path and carried out with the air stream while the larger particles are collected on the periphery of the classification chamber. Separation efficiencies

on a number basis are generally low for this device.

A centrifugal classifier for the simultaneous collection and classification of airborne particles according to settling diameters is described by Sawyer and Walton[30]. This device, called the "Conifuge", is based on a conical centrifuge with the internal air flow pattern directed radially outward and downward through the space between two coaxial, conical rotors with parallel surfaces of generation. The aerosol particles are deposited according to their settling diameters on a glass slide positioned on the inner side of the outer rotor. In its present design, this device is capable of collecting and classifying only small quantities of material. Experimental results were reported only for a small range of particle densities. Theoretically calculated and experimentally measured deposition points agreed well for small particles where the mathematical model, which assumed the Stokes drag law, would be expected to be valid. Significant deviations between predicted and experimental results were noted for the larger particle sizes. Because of the method of introducing the aerosol, the incoming particles are distributed over the entire cross-section of the entrance to the separation zone. Consequently, the initial conditions for each particle cannot be accurately specified and the final deposition point does not depend strictly on the undisturbed particle trajectory in the classifying chamber. Although the details of the theoretical analysis were not available, it appears that all particle trajectories were computed for the same initial conditions. Otherwise, precise particle classification is not possible and only accumulative size distributions can be measured.

Goetz et al.[31] have developed a centrifugal particle classifier

that effectively separates and classifies small quantities of particles 0.03 to 3.0 microns in diameter from an aerosol. The device operates by centrifuging a dilute aerosol in a helical rotor designed so that, theoretically, there is no shearing action between the rotor wall and the flowing aerosol and, consequently, no boundary layer present on the rotor wall to prevent the deposition of sub-micron particles. The unit is designed to be self-pumping and is provided with a system of jets and limiting orifices hopefully to assure laminar flow within the helical rotor channels. The device must be calibrated empirically with mono-disperse polystyrene latexes rather than by theoretical considerations, due to the complexity of the rotor geometry and operating conditions.

Kriebel[32] studied the motion of solid particles injected into a cylinder of gas which rotates as a solid body. The equations of motion for small particles with their drag forces governed by Stokes law were solved analytically by use of Laplace transforms for the particular case of solid body rotation of the gas and no radial throughflow of the gas. An air centrifuge was constructed that closely approximated the analytical flow model and experimental data were obtained for glass beads and calcium carbonate powder. Fairly good agreement between theory and experiment was claimed. No size distribution data for various collection points were presented however, so only qualitative estimates could be made of the separations actually achieved. The method of particle feeding consisted of an injection of powder and air into a partially evacuated centrifuge chamber. This feeding method leaves much to be desired when attempting to make analytical studies of particle motion since the initial conditions for the entering particles are difficult, if not impossible,

to determine and because of the secondary flow of air that is invariably associated with the entrance of a high velocity gas jet into a partially evacuated rotor.

CHAPTER II

DEVELOPMENT OF THE EQUATIONS OF MOTION FOR A PARTICLE IN A CENTRIFUGAL FIELD

Background

Derivation of the equations of motion for a particle in a centrifugal field can be accomplished quite simply by the vectorial summation of all forces acting on the particle and the application of Newton's second law of motion. The principal difficulties lie not in the derivation but rather in deciding which of the many forces acting on the particle may be simplified or neglected and still permit meaningful solutions to be obtained. The procedure in this analysis is to discuss in some detail each of the forces and the justifications made in the application or neglect of each. Finally, the equations of particle motion for several cases of interest in this study are developed.

Fluid Flow in Centrifugal Fields

A study of the motion of small particles in centrifugal fields should logically consider first the fundamentals of the fluid mechanics of rotating fluids. Rotating fluids, of course, are but special cases of general fluid motion and as such are described by the same mathematical models used in studying all fluid motions. A meaningful description of the fluid flow within a centrifuge rotor in which a fluid simultaneously moves radially outward from and tangentially about some fixed point on the axis of rotation is of principal concern in the design of a centrifugal

particle classifier. This information is necessary because the fluid velocity components in each of the coordinate directions must be known to solve accurately the differential equations describing trajectories of particles within such a rotor. The actual flow situation within a rotor of this type is a quite complicated function of the rotor speed, the rotor geometry, the volumetric flow rate of the aerosol through the rotor and the efficiency of momentum transfer between the rotor and the confined fluid. Consequently, to avoid insuperable mathematical difficulties, the equations of fluid motion are here considerably simplified to permit the determination of approximate expressions for the fluid velocity components acting in several types of vortex motion. Several simplified cases are considered in the following analysis to show the wide flow variations that exist according to the types of vortex motions considered.

The simplified equations of motion in cylindrical coordinates for the steady, two-dimensional, axisymmetric, incompressible flow of an ideal fluid are:

$$u_r \frac{du_r}{dr} - \frac{u_\phi^2}{r} = - \frac{1}{\rho} \frac{dp}{dr} \tag{1}$$

and

$$\frac{du_\phi}{dr} + \frac{u_\phi}{r} = 0 \tag{2}$$

The continuity equation for these conditions is given by

$$\frac{d}{dr} (ru_r) = 0 \tag{3}$$

Since u_ϕ is a function of r only, equation (2) may be rewritten as

$$\frac{d}{dr}(ru_\phi) = 0 \tag{4}$$

Integration of (2) between limits of r_o and r and u_{ϕ_o} and u_ϕ gives

$$ru_\phi = r_o u_{\phi_o}$$

which is the equation for a free, or potential, vortex. Application of the initial condition that at $r=r_o$ the angular velocity of the fluid must equal the angular velocity of the rotor, Ω, yields for the tangential velocity

$$u_\phi = \frac{r_o^2 \Omega}{r} \tag{5}$$

To satisfy the continuity equation, the product ru_r must be independent of r. This condition is satisfied by the general relationship for radial flow between parallel plates from a source located at the center of rotation, i.e.

$$ru_r = \text{constant} = \frac{Q}{2\pi h} \tag{6}$$

Subsitution of (5) and (6) into equation (1) gives for the radial pressure gradient

$$\frac{1}{r^3}\left[\left(\frac{Q}{2\pi h}\right)^2 + \left(r_o^2\Omega\right)^2\right] = \frac{1}{\rho}\frac{dp}{dr} \tag{7}$$

Integrating equation (7) between the limits of r_o and r and p_o and p gives

$$\frac{\rho}{2}\left[\frac{1}{r_o^2}-\frac{1}{r^2}\right]\left[\left(\frac{Q}{2\pi h}\right)^2+\left(r_o^2\Omega\right)^2\right]=(p-p_o)=\Delta p \tag{8}$$

Approximate expressions for the velocity components for this case therefore are summarized by the following:

$$u_\phi=\frac{r_o^2\Omega}{r} \tag{9}$$

$$u_r=\frac{Q}{2\pi hr} \tag{10}$$

The fluid motion described by equations (9) and (10) has many practical applications as it closely describes the flow within tornados, waterspouts, many types of industrial turbomachinery and in certain regions of cyclone separators. The type of flow characterized by such free vortex motion is typical of conservative fields of force, that is, under those conditions in which no external forces are acting on the fluid and the fluid particles thus tend to conserve angular momentum as their radius of rotation changes. For this situation, the moment of momentum tends to remain constant and the angular velocity of the fluid particles always decreases with increased radius of rotation.

When the motion of rotating fluids is strongly influenced by external forces, such as by the presence of vanes in a rotor or by close spacings between the top and bottom of an enclosed rotor, the vortex motion induced is characterized by a tendency for the fluid elements to attain the angular velocity of the solid wall or vane to which they are closest. These conditions are believed to be most typical of the experimental conditions of

interest in this study. Under these conditions, viscous forces become an important factor in the transfer of torque from the rotor case to the fluid contained therein and the previous analysis for inviscid flow is not applicable.

The approximate Navier-Stokes equations for laminar, steady, two-dimensional, axisymmetric, incompressible flow of a real fluid are given by

$$u_r \frac{du_r}{dr} - \frac{u_\phi^2}{r} = -\frac{1}{\rho}\frac{dp}{dr} + \frac{\mu}{\rho}\left[\frac{d^2u_r}{dr^2} + \frac{1}{r}\frac{du_r}{dr} - \frac{u_r}{r^2}\right] \qquad (11)$$

and

$$u_r \frac{du_\phi}{dr} + \frac{u_r u_\phi}{r} = \frac{\mu}{\rho}\left[\frac{d^2u_\phi}{dr^2} + \frac{1}{r}\frac{du_\phi}{dr} - \frac{u_\phi}{r^2}\right] \qquad (12)$$

and the continuity equation by

$$\frac{du_r}{dr} + \frac{u_r}{r} = 0 \qquad (13)$$

To present a more general analysis for this case, the preceding equations were non-dimensionalized by choosing characteristic values such that the order of magnitude of a dimensionless property formed by dividing the property by a characteristic value was either one or much less than one. The tangential velocity of a fluid entering the rotor of a centrifugal classifier is generally quite high and considerably larger than the radial velocity of the fluid. Thus if the initial tangential velocity of the fluid is chosen as a characteristic velocity, then the

orders of magnitudes of the radial and tangential velocity terms become δ and 1, respectively, where $\delta \ll 1$. A characteristic length term was arbitrarily chosen to be the depth of the classification chamber of the rotor. The resulting reduced variables are summarized by the following:

$$u'_r = \frac{u_r}{u_{\phi_o}} = \delta$$

$$u'_\phi = \frac{u_\phi}{u_{\phi_o}} = 1$$

$$r' = \frac{r}{h} = 1$$

$$\left(\frac{dp}{dr}\right)' = -\frac{1}{\rho}\,\frac{dp}{dr}\,\frac{h}{u_{\phi_o}^2} = 1$$

$$\left(\frac{\mu}{\rho}\right)' = \frac{\mu}{\rho}\,\frac{1}{h\mu_{\phi_o}} = 1$$

Substituting the above quantities with their appropriate orders-of-magnitude into equations (11) and (12) gives the following:

$$\begin{matrix} \delta^2 & 1 & 1 & 1 & \delta & \delta & \delta \end{matrix}$$

$$u'_r \frac{du'_r}{dr'} - \frac{(u'_\phi)^2}{r'} = \left(\frac{dp}{dr}\right)' + \left(\frac{\mu}{\rho}\right)' \left[\frac{d^2u'_r}{dr'^2} + \frac{1}{r'}\frac{du'_r}{dr'} - \frac{u'_r}{r'^2} \right] \qquad (14)$$

$$\begin{matrix} \delta & \delta & 1 & 1 & 1 & 1 \end{matrix}$$

$$u_r \frac{du'_\phi}{dr'} + \frac{u'_r u'_\phi}{r'} = \left(\frac{\mu}{\rho}\right)' \left[\frac{d^2u'_\phi}{dr'^2} + \frac{1}{r'}\frac{du'_\phi}{dr'} - \frac{u'_\phi}{r'^2} \right] \qquad (15)$$

Omitting those terms from (14) and (15) which are negligible then

gives the following equations from which primes have now been dropped for simplicity:

$$\frac{u_\phi^2}{r} = \frac{1}{\rho}\frac{dp}{dr} \tag{16}$$

$$\frac{d^2u_\phi}{dr^2} + \frac{1}{r}\frac{du_\phi}{dr} - \frac{u_\phi}{r^2} = 0 \tag{17}$$

A trial solution for equation (17) is the relation for a forced vortex

$$\frac{d\phi}{dt} = \text{constant; or } u_\phi = r\left(\frac{d\phi}{dt}\right) \tag{18}$$

which, when substituted in equation (17), is found to be a valid solution. The continuity equation is again satisfied by the radial flow equation used previously. Substitution of (18) in equation (16) gives the radial pressure gradient for these conditions, viz.

$$r\left(\frac{d\phi}{dt}\right)^2 = \frac{1}{\rho}\left(\frac{dp}{dr}\right) \tag{19}$$

which, when integrated between r_o and r and p_o and p, gives

$$\frac{\rho}{2}(r^2 - r_o^2)\left(\frac{d\phi}{dt}\right)^2 = (p - p_o) = \Delta p \tag{20}$$

Approximate velocity components for the case of forced vortex motion are thus summarized by

$$u_\phi = r\frac{d\phi}{dt} = r\,(\text{constant}) \tag{21}$$

and

$$u_r = \frac{Q}{2\pi hr} \tag{22}$$

The two examples discussed previously represent the extremes of vorticity. Actual vortices are generally somewhere intermediate in behavior between these two idealizations. If it is now assumed that the *angular velocity of a fluid is a relatively simple function of radius* only, then a generalized expression for the tangential velocity of the fluid may be written as

$$u_\phi = k_1 \, r^{(n+1)} \tag{23}$$

in which k_1 is a constant and the value of n determines the type of vortex. For example if $n=-2$, $u_\phi = k_1/r$; or a free vortex. A value of $n=0$ describes a forced vortex or completely solid body rotation since $u_\phi = k_1 r$, or $d\phi/dt = k_1$. Combination of equations (22) and (23) and elimination of the time dependency gives the following relation which describes the path of fluid elements in a plane perpendicular to the angular velocity vector.

$$\frac{d\phi}{dr} = \frac{r^{(n+1)}}{k_2} \tag{24}$$

where $k_2 = \dfrac{Q}{2\pi h \, k_1}$.

To visualize better the path of the fluid within a rotating enclosure, it is convenient to consider the relative trajectory of the

fluid, i.e., the trajectory of the fluid elements referred to a set of coordinate axes rotating with the speed of the rotor. If the angular velocity of the rotor is constant and equal to Ω, then the relative angular velocity of the fluid is given by

$$\frac{d}{dt}(\psi - \phi) = \Omega - k_1 r^n \tag{25}$$

in which ψ represents the angular displacement of the rotor.

Combining this result with equation (22) gives for the relative trajectory of fluid particles within the rotor

$$\frac{d\beta}{dr} = \frac{2\pi h}{Q}(\Omega r - k_1 r^{n+1}) \tag{26}$$

where β is the difference in angular displacement of the rotor and the fluid within the rotor.

Integrating equation (26) for the relative fluid trajectory between limits of zero to β and r_o to r, gives for $n \neq -2$

$$\beta = \frac{2\pi h}{Q}\left[\frac{\Omega}{2}(r^2 - r_o^2) - \frac{k_1}{n+2}(r^{n+2} - r_o^{n+2})\right] \tag{27}$$

To illustrate the variations in flow patterns for the various types of vortex motion, consider first the case of a forced vortex, i.e., n=0, with the following initial conditions

$$r)_{t=o} = r_o \quad ; \quad \frac{d\phi}{dt})_{t=o} = \Omega$$

Examination of equation (26) then indicates that $d\beta/dr = 0$, or that the relative fluid path may be represented by a straight line along a radius

in a plane perpendicular to the axis of rotation.

For the case of potential flow or a free vortex, n=-2 and equation (26), upon integration again between limits of zero to β and r_o to r, gives

$$\beta = \frac{2\pi h}{Q} \left[\frac{\Omega}{2} (r^2 - r_o^2) - k_1 \ln \left(\frac{r}{r_o}\right) \right] \tag{28}$$

Only slight departures from a forced vortex result in very large angular changes in the flow patterns. Considering the case of n = -0.05, a rather close approximation to the conditions necessary for a forced vortex, equation (27) then becomes

$$\beta = \frac{2\pi h}{Q} \left[\frac{\Omega}{2} (r^2 - r_o^2) - \frac{k_1}{1.95} (r^{1.95} - r_o^{1.95}) \right] \tag{29}$$

Figure 1 illustrates with numerical examples representative of typical experimental conditions the general spiral flow features of the fluid and the wide variations that result for small changes of n . The curves of Figure 1 represent the relative paths of fluid elements emanating from a single point on the axis of rotation.

Drag Force

A general expression for the steady-state force exerted on a submerged sphere by a flowing fluid is given by

$$F_D = \left(\frac{\pi \delta^2}{4}\right) \left(\frac{\rho}{2}\right) C \bar{V}^2 \tag{30}$$

The drag coefficient, C, for spheres in steady motion has been studied extensively and found to be a unique function of the particle Reynolds number. A relation which describes the drag force acting on a spherical

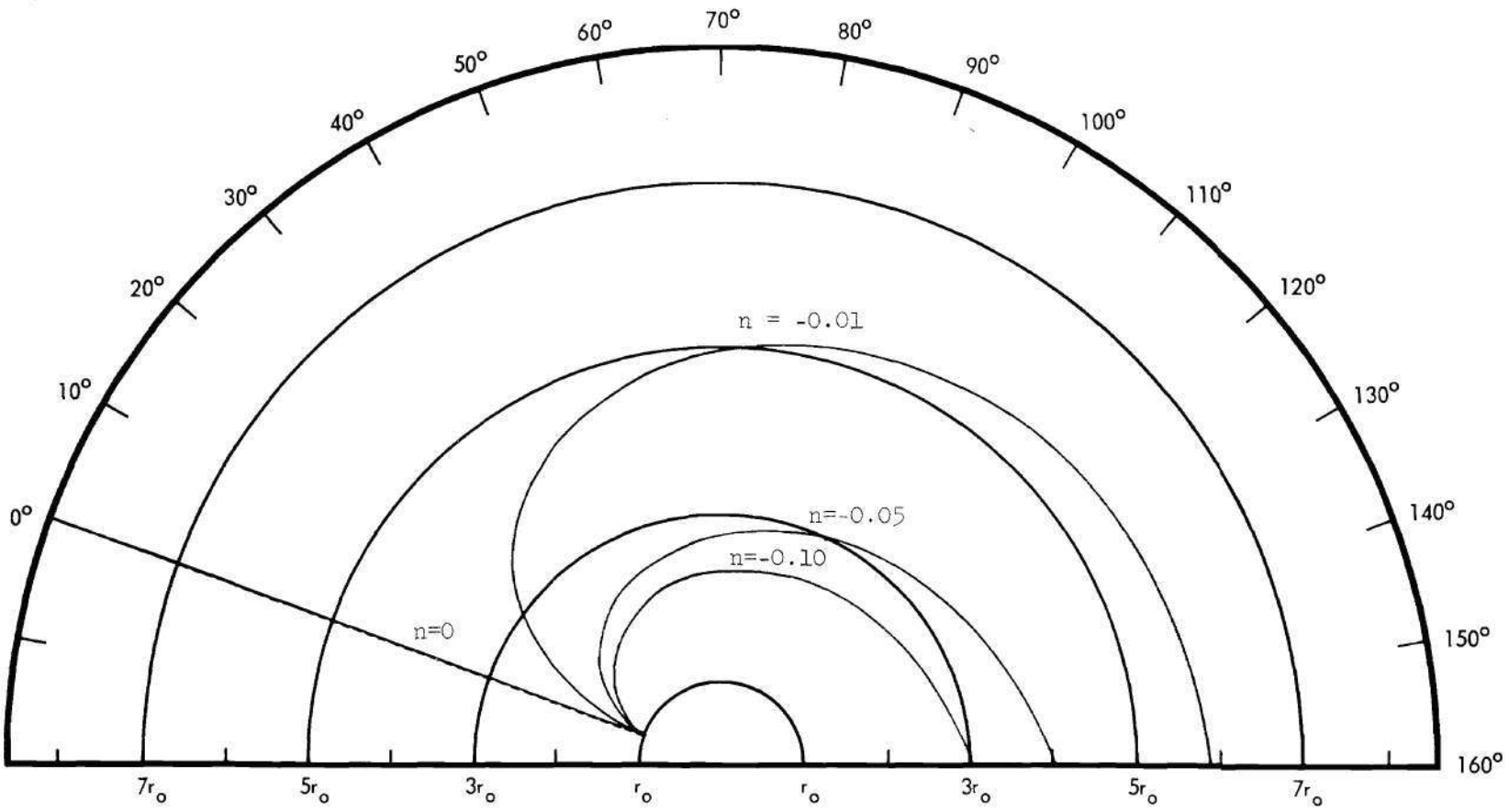

Figure 1. Spiral Flow Streamlines for Several Types of Vortex Flow.

particle at very low relative particle velocity or, more specifically, at particle Reynolds numbers below about 0.1 was first derived by Stokes[1] in 1851 and is now the famous law bearing that name. The familiar expression for Stokes law

$$F_D = 3\pi\mu\delta\bar{V} \tag{31}$$

indicates that the drag force exerted on a spherical particle moving steadily in a static medium is proportional to the first power of the particle diameter and the resultant relative particle velocity.

Many assumptions are implicit in the derivation of Stokes law, and, of course, the result is strictly valid only for those conditions. The more important assumptions include the condition for infinitesimally slow, or "creep" flow; an infinite expanse of a continuous, incompressible fluid medium; a non-deformable, spherical particle; constant velocity with no particle rotation; and no fluid slip at the sphere surface.

The assumption of creep flow omits the inertia terms from the Navier-Stokes equation. Stokes law therefore represents a first approximation to the drag while Oseen's[33], which present a second approximation of the inertia forces, is given by

$$F_D = 3\pi\mu\delta\bar{V}\left[1 + \frac{3}{8}\mathrm{Re}\right] \tag{32}$$

Goldstein[34] carried the approximation a step further; however, the resulting relationship is quite cumbersome and is apparently little better than Oseen's.

In the transition region ($1 < \mathrm{Re} < 500$), the drag coefficient for

spheres can be approximated by

$$C = \frac{18.5}{Re^{0.6}} \tag{33}$$

Above Reynolds numbers of 500, the drag coefficient is essentially constant and has an approximate value of 0.44. This region of constant drag coefficient is termed the Newton's law region. When the Reynolds number increases to about 2×10^5, there is an abrupt decrease in the drag coefficient which is associated with a shift of the boundary layer separation zone from the front of the equator to a region behind the equator of the sphere.

The effects of unsteady motion of a particle with respect to a fluid were also considered by Stokes in the case of a sphere undergoing harmonic motion in an infinite fluid. An expression was obtained for the force on a sphere due to the presence of the surrounding fluid under these particular conditions. This work led to studies by Basset[35] and Boussinesq as reported by Lamb[36] for arbitrary accelerations of a sphere. The latter studies were further extended in a study by Lord Rayleigh[37] of the motions of solid bodies through viscous liquids. According to Rayleigh, the total drag force acting on a sphere in accelerating motion at time t is given by the following expression in which x is a dummy variable of integration:

$$F_D = \frac{\pi\delta^3}{6}\left[\frac{\rho}{2}\frac{d\bar{V}}{dt} + \frac{3\rho C\bar{V}^2}{4\delta} + \frac{9}{\delta}\left(\frac{\mu}{\rho\pi}\right)^{1/2}\int_o^t \frac{d\bar{V}}{dx}\,\frac{dx}{(t-x)^{1/2}}\right] \tag{34}$$

The first and third terms of this relation express a part of the drag

force which results from the expenditure of energy necessary to accelerate the fluid. The first term, which depends on the inertia of the fluid, is the same as would be obtained by a hydrodynamic analysis for inviscid flow. This term leads to an apparent increase in the mass of the particle and is generally referred to as the "added mass" or "virtual mass" term. The integral term has generally been disregarded in pertinent works on particle dynamics with little or no reason offered for its omission. Fuks[38] studied at length the effects of the integral term and concluded, on the basis of an exhaustive mathematical analysis, that this term brings about a small reduction of the particle's acceleration, the effect of which depends primarily on the ratio of the density of a particle and its surrounding medium. The effect of the integral term may become large in liquid media but is generally insignificant in gases, amounting to only about a two per cent correction for a particle with a specific gravity of four in a gaseous medium. Fortunately, this permits the integral term to be omitted from further consideration in this study.

The problem of the influence of wall effects, or the lack of an infinite expanse of fluid medium, has also been studied quite extensively from both a theoretical and an experimental viewpoint. In most instances, no appreciable influences due to wall effects appear until the particle displacement from the walls is of the order of five times the particle diameter. Since the range of particle sizes considered in this study is several orders of magnitude less than the dimensions of and clearances within the rotor, it is believed that wall effects may be justifiably neglected.

The assumption of a continuous fluid medium can be restated by the

condition that the diameter of a particle is very large in comparison to the mean free path of the fluid atoms or molecules. A further correction, however, must be applied to the drag force when the diameter of a particle approaches the mean free path of the fluid because of the slip of the fluid at the sphere surface. Millikan[39], in the celebrated oil drop experiment, first proposed the following equation and Davies[40], from a later analysis of data, provided the best values for the constants A, B, and C'.

$$f = 1 + \frac{2\lambda}{\delta} \left[A + B \exp\left(-C'\delta/2\lambda\right)\right] \qquad (35)$$

The slip factor, f, multiplies the Stokes law velocity to yield the true value. This correction is of only minor importance in gases at ordinary temperatures and pressures until particle diameters are somewhat less than one micron. For particles in liquids, the effect is negligible down to particle diameters of about 0.01 micron. Because this study is primarily concerned with particles larger than one micron diameter in a gas medium, the slip correction is also neglected.

Particle Reynolds numbers between 0.01 and 100 are of greatest interest in this study. Lapple[41] has compiled a plot of experimentally measured drag coefficients for spheres as a function of particle Reynolds number which best represent the available data for the sedimentation of particles through gaseous media. This plot, which is shown in Figure 2 combines the experimental results of at least 17 investigators. The dotted line represents an extrapolation of drag coefficients based on Stokes law to higher particle Reynolds numbers.

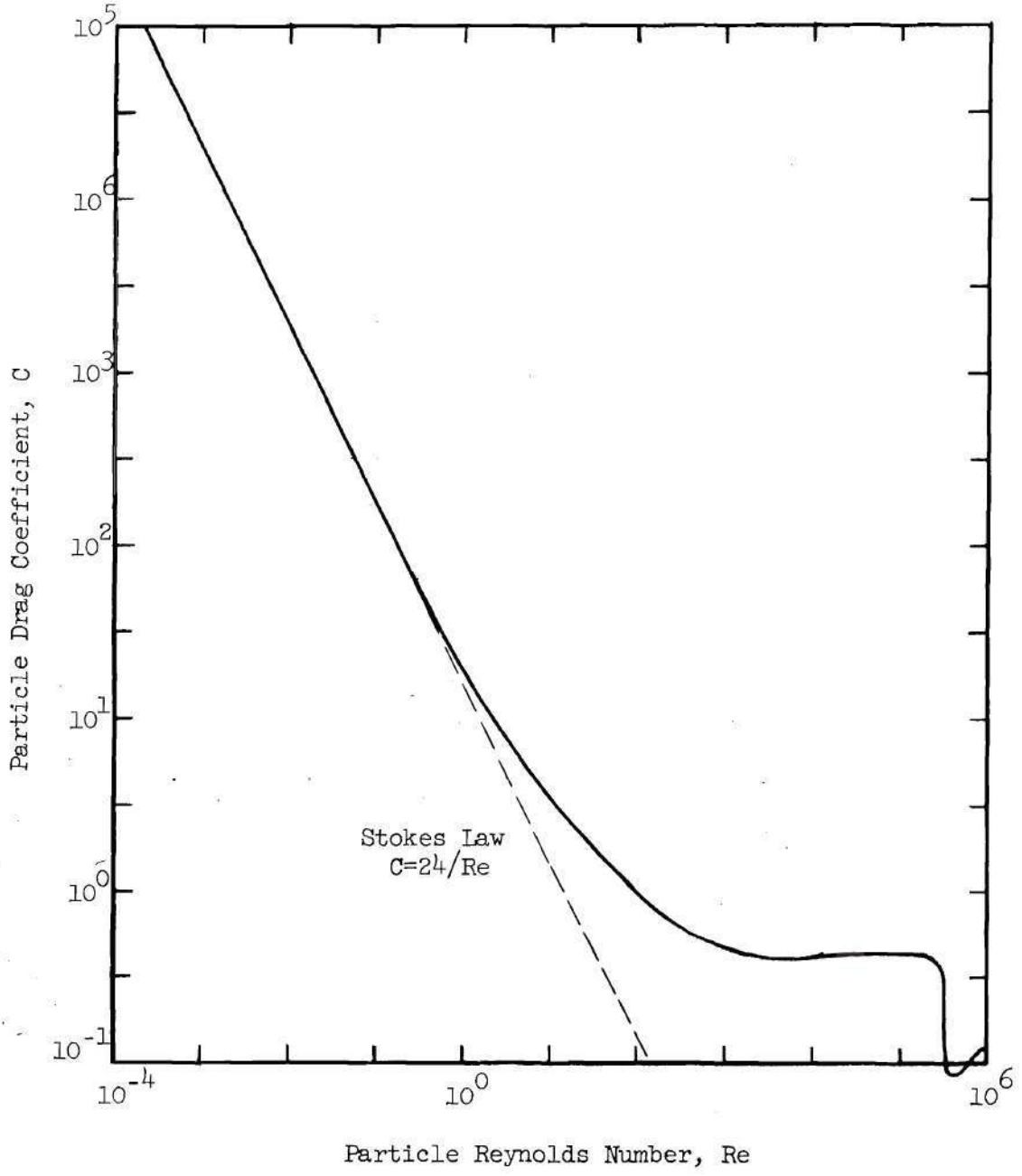

Figure 2. Drag Coefficients for Spheres in Steady Flow

Magnus Force

A particle spinning about one or more of its own axes and simultaneously traveling through a fluid in such a manner that the body axis of rotation is at some angle with the flight path will experience a force in a direction perpendicular to the plane in which the flight path and rotational axis lie. This force, which partially accounts for the slice and hook of a golf ball and the curve of a baseball, is called the Magnus, or lift, force and has been the subject of much investigation to determine its effect on missile flight, the path of spinning artillery shells and as a possible device for producing high lift. Swanson[42] recently published a summary of investigations on this effect and, subsequent to this, Rubinow and Keller[43] derived a theoretical expression for the lift component acting on a spinning sphere moving steadily through an infinite viscous fluid at small Reynolds number. The magnitude of this force is primarily a function of the relative velocity of the sphere with respect to the fluid, and the angular velocity of the sphere as is given by the approximate relation

$$F_L = M_f \left\{ \Gamma \times \overline{V} \left[1 + O(R) \right] \right\} \tag{36}$$

where $O(R)$ is negligible for $R < 1.0$.

Bouchillon[44], in studying particle trajectories in a hydrocyclone, found, by an order of magnitude analysis, that the lift force for highly shearing flows was comparable to the drag force and hence must be included in an analysis of particle trajectories for these conditions.

The fluid flow within a centrifugal classifier of the type used in this study is characterized by a comparatively slow movement of fluid

relative to the rotor surfaces and, consequently, small shear forces. An approximate analysis of the lift forces for typical experimental conditions of this study indicated that the ratio of the drag to the lift force was very large and could be safely neglected. Only for the case of particles larger than about 100 microns diameter in shear flows of such magnitude that particle spins of the order of 1000 radians per second were attained was the lift force comparable to the drag force.

Derivation of Equations and Statement of Assumptions

The equations of particle motion may be developed by vectorial summation of the forces acting on a particle. The net force is then related to the particle motion through Newton's second law.

Since the relative motion of particles with respect to the fluid in a centrifugal field is inherently unsteady, the effects of acceleration on the particle drag forces should be considered for the most general case. The direction of the drag force acting on each particle is assumed to act always in the direction of the relative velocity vector. The magnitude and direction of the drag force components are then obtained by multiplying the total drag force by $(u_r - V_r)/\overline{V}$ and $(u_\phi - V_\phi)/\overline{V}$ for the radial and transverse directions, respectively.

Forces acting radially outward and in a counterclockwise direction are arbitrarily assumed positive when the rotor direction of rotation is counter clockwise. The resulting approximate equations of motion which describe the two-dimensional particle path in a plane normal to the angular velocity vector are given by

$$\frac{dV_r}{dt} = \frac{V_\theta^2}{r} \left[1 - \frac{\rho}{\rho_p} \left(\frac{u_\phi}{V_\theta}\right)^2 \right] + \frac{3 \rho C \bar{V}}{4\delta \rho_p} (u_r - V_r)$$

$$+ \frac{\rho}{2 \rho_p} \frac{d\bar{V}}{dt} \frac{(u_r - V_r)}{\bar{V}} \qquad (37)$$

and

$$\frac{dV_\theta}{dt} = - \frac{V_\theta V_r}{r} \left[1 - \frac{\rho}{\rho_p} \frac{u_\phi u_r}{V_\theta V_r} \right] + \frac{3 \rho C \bar{V}}{4\delta \rho_p} (u_\phi - V_\theta)$$

$$+ \frac{\rho}{2 \rho_p} \frac{d\bar{V}}{dt} \frac{(u_\phi - V_\theta)}{\bar{V}} \qquad (38)$$

The following assumptions are inherent in the preceding equations:

1. The presence of the particles does not alter the velocity field of the fluid.
2. The particles are non-interfering, that is, the movement of any one particle is not influenced by the presence of others.
3. The particles are non-deformable spheres.
4. The level of macroscopic turbulence in the fluid is negligible.
5. The fluid medium is of such an extent relative to the particle dimensions that wall effects may be neglected.
6. The drag force acts always in the direction of the relative velocity vector between the fluid and particle.
7. The effects of Brownian motion are negligible.
8. Magnus forces are negligible.
9. Velocity profiles of the fluid are flat, that is, no velocity gradient in the z-direction is considered.

10. Body forces (gravity, magnetic, electrical) are negligible with respect to the centrifugal force.

The ratio of particle and fluid densities for the conditions of this study is always quite large, since, in order to achieve significant relative tangential displacements of particles the fluid must be of low density relative to that of the particle. Fortunately, this permits elimination of the "added mass" terms and the buoyancy portion of the centrifugal and Coriolis force terms. Upon elimination of these terms, equations (37) and (38) reduce to

$$\frac{dV_r}{dt} = \frac{V_\theta^2}{r} + \alpha C \overline{V} (u_r - V_r) \tag{39}$$

and

$$\frac{dV_\theta}{dt} = - \frac{V_\theta V_r}{r} + \alpha C \overline{V} (u_\phi - V_\theta) \tag{40}$$

If it is now assumed that the drag coefficient is defined by Stokes law, the equations simplify further to

$$\frac{dV_r}{dt} = \frac{V_\theta^2}{r} + a (u_r - V_r) \tag{41}$$

and

$$\frac{dV_\theta}{dt} = - \frac{V_\theta V_r}{r} + a (u_\phi - V_\theta) \tag{42}$$

The equations in this form indicate that the drag force acting in each component direction is independent of the total net relative velocity

term and depends only on the relative velocity component in that direction. The best previous calculations of particle trajectories in centrifugal fields were based on equations (41) and (42).

In many liquid clarifiers and centrifugal filters, the tangential velocities of the fluid and particles are very nearly equivalent and the assumption has frequently been made that all tangential forces are negligible. If Stokes law is still assumed valid, the resulting one-dimensional equation of motion is given by

$$\frac{dV_r}{dt} = \frac{V_\theta^2}{r} + a\,(u_r - V_r) \qquad (43)$$

The further assumption has frequently been made that inertial effects of the particle are negligible. With this assumption and the condition for zero radial fluid velocity with solid body rotation, equation (43) further reduces to

$$\frac{dr}{r} = \frac{1}{a}\left(\frac{d\theta}{dt}\right)^2 dt \qquad (44)$$

This highly simplified equation is frequently used to calculate feed rates and centrifugation times for rotary filters.

CHAPTER III

SOLUTIONS OF THE EQUATIONS OF PARTICLE MOTION

Background

Many investigators of particle motion in centrifugal fields have considered the particle motion in terms of a steady-state terminal velocity for reasons of mathematical simplicity. Because the centrifugal force varies with radius, a particle in a centrifugal separator is subjected to a continuously varying force and computation of its trajectory should include this factor Calculations based on both the assumption of a constant settling velocity and the equivalence of the tangential velocities of the fluid medium and the particle are of interest in predicting such values as the time for centrifugation and the optimum feed rate for centrifugal clarifiers. However, since all of these cases result in no relative tangential displacement of the particle with respect to the fluid, they are all meaningless insofar as particle classification predictions based on size-density relationships are concerned.

Previous best estimates of particle trajectories in centrifugal fields have been restricted to cases in which Stokes law was assumed to represent the particle drag force The objective of this portion of the study was to confirm or reject solutions obtained by previous investigators and, if possible, to extend the results to more general cases.

The equations of particle motion developed in Chapter II which are appropriate to this study are analyzed in this section for various particle

sizes and densities, initial conditions of motion for the particles, types and strengths of centrifugal fields and representations of the drag force exerted on the particles. Particular emphasis was placed on the implementation of solutions of the equations of particle motion with an electrical analog computer because of the utility of such a system for the solution of ordinary differential equations having one independent variable.

Analog Computer Solutions of the More General Forms of the Equations of Motion

An analog computer program was devised to solve the equations of particle motion in their most general form as they relate to the conditions of interest in this study. These equations, in standard polar coordinate form, are

$$\frac{d^2r}{dt^2} - \alpha C \bar{V} \left(\frac{dr_f}{dt} - \frac{dr}{dt}\right) - r \left(\frac{d\theta}{dt}\right)^2 = 0 \qquad (45)$$

and

$$\frac{d^2\theta}{dt^2} - \alpha C \bar{V} \left(\frac{d\phi}{dt} - \frac{d\theta}{dt}\right) + \frac{2}{r} \left(\frac{dr}{dt}\right)\left(\frac{d\theta}{dt}\right) = 0 \qquad (46)$$

They are identical with equations (39) and (40) developed in Chapter II except that they are here expressed explicitly in terms of r, θ and ϕ as second order equations for convenience in transforming them from real parameters into suitable machine parameters for solution with the analog computer. Time scaling of these equations to permit machine solution times of reasonably short duration presented some difficulties because of the

extremely wide range of dynamic conditions imposed. Although there are no fixed rules as to the optimum computing times for problems, it is generally true that computing times of from about 10 seconds to one minute consistently yield the most precise results. Very fast computing times frequently result in errors due to lags in the response of electro-mechanical components or as a result of exceeding the recovery time of electronic components, whereas, slow computing times may result in errors from drift of electronic multipliers and other non-linear equipment or from prolonged integration of small voltage errors, to mention only a few of the possible causes. To minimize these types of errors, three separate time scales were provided in the computer program so that computing time could be adjusted to within 10 to 30 seconds for each particle trajectory.

Provision was made in the computer program for the incorporation of any type vortex from free to forced for the angular velocity of the fluid, $d\phi/dt$. That is, the value of n in equation (23) was continuously variable from zero to minus two. The radial velocity of the fluid was assumed to vary inversely with radial distance as expreseed by equation (10).

To evaluate particle drag coefficients, the particle motion was assumed to obey Stokes law in all cases up to a particle Reynolds number of 0.10. For Reynolds numbers above 0.10, the drag coefficient was made to approximate the best experimental values available by a series of straight line approximations on a diode function generator. Figure 3 compares these straight line approximations obtained with the diode function generator to the experimentally determined values for the drag coefficient-Reynolds number product versus Reynolds number. To solve for special cases of

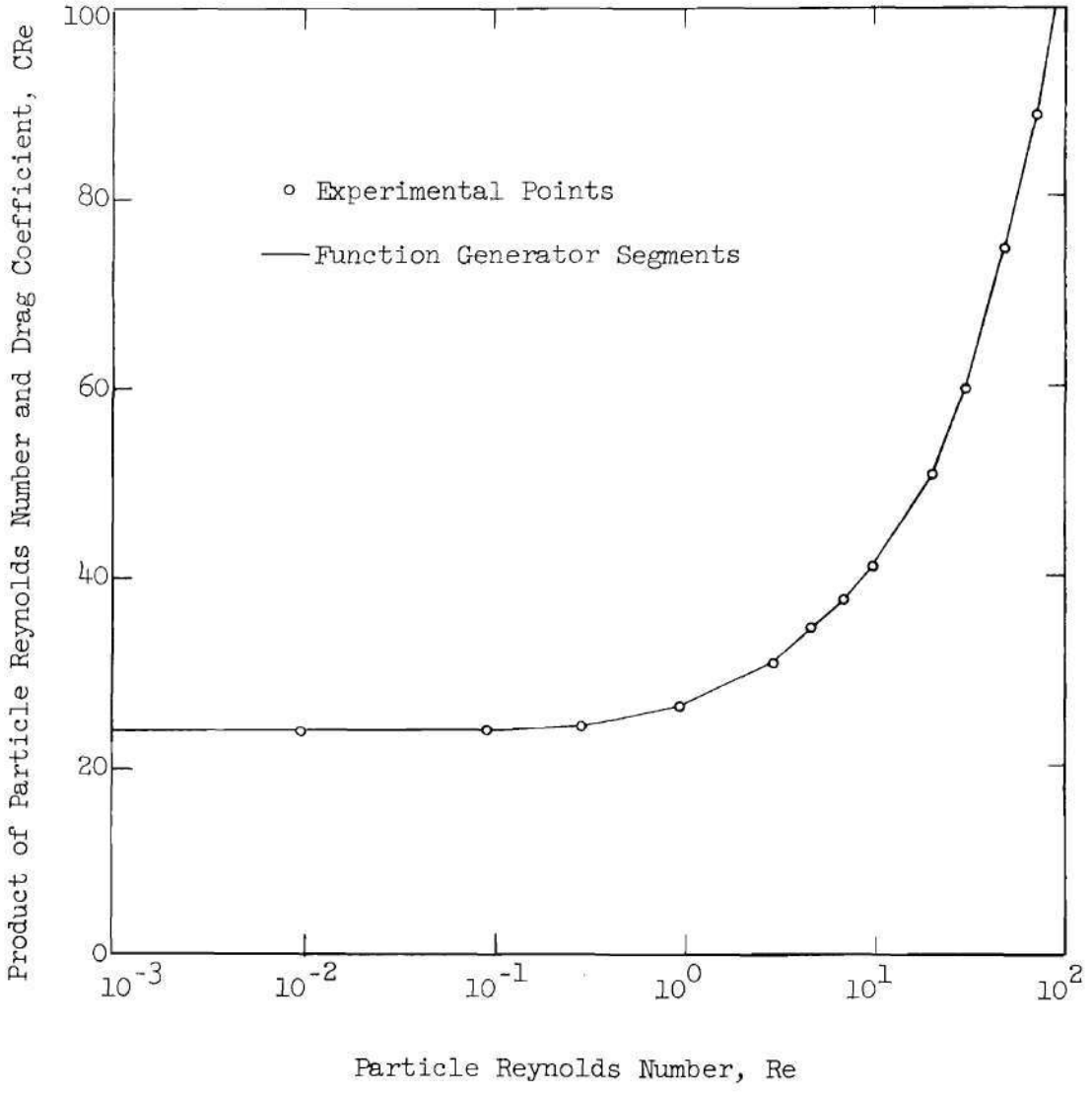

Figure 3. Function Generator Representation of Particle Drag Coefficients.

interest in which Stokes law was assumed for the entire range of Reynolds numbers, the voltage output of the drag coefficient function generator was held constant at 24 volts. This arrangement automatically adjusted the drag coefficient so that the product of the Reynolds number and drag coefficient was always 24, as predicted by Stokes law. Details of the analog computer program are presented in Appendix A.

Unfortunately, it was not possible to calculate a series of trajectories for fixed experimental conditions and subsequently derive other trajectories from these because of the additional mathematical complexities added when using drag force approximations other than Stokes law. For simplicity and brevity, particle trajectories calculated by the analog computer from equations (45) and (46) in which the diode function generator approximations of drag coefficients were used are hereafter referred to as "$\overline{V}$ curves" and those calculated using Stokes law are called "Stokes curves". Computers results were generally expressed as trajectories of particles relative to a set of axes rotating at the same angular velocity as the rotor. Results plotted in this manner show immediately where each particle size intersects the rotor periphery or any internal boundary.

The volumetric flow rate of fluid through the centrifuge rotors in this study was quite small. Because of this and the fact that the radial fluid velocity always decreased inversely with increasing radial displacement, it was believed that the effects of the radial velocity of the fluid on particle trajectories would be slight. Subsequent particle trajectory calculations with the analog computer revealed that trajectories calculated using the radial fluid velocity term were identical with those calculated without this term except for particle densities of 1.25 gm/cm^3

and less and diameters below about two microns at rotor speeds of 12,000 rpm and above in a forced vortex. Deviations noted in the results for these low density, small diameter particles were only about three degrees at the rotor periphery. Since these differences are comparable to the uncertainty in the initial location of the individual particles, it was decided that the radial fluid velocity term could be justifiably omitted from further trajectory calculations.

Forced Vortex Solutions

The theoretical conditions necessary for efficient particle classification in a device of the type used in this study were intuitively shown by the fluid flow considerations of Chapter II to be those of a perfect or near-perfect forced vortex of fluid. Therefore, extensive study was made of the relative trajectories of a wide range of particle densities and diameters in forced vortices of several intensities. Specifically, particle densities of 1.25, 2.50, 3.00 and 7.00 gm/cm^3 and diameters from two to 50 microns in forced vortices of air corresponding to rotor speeds of 2,400; 4,800; 7,200; and 9,600 rpm were investigated. Figures 4 and 5 illustrate the type of results obtained for typical operating conditions when Stokes law and the more general drag force relationship were used, respectively. These results are shown as the relative trajectories of the various particles on a polar coordinate grid which corresponds exactly to one classification chamber of the rotor used in the experimental portion of this study. To calculate each trajectory, four initial conditions were specified as follows:

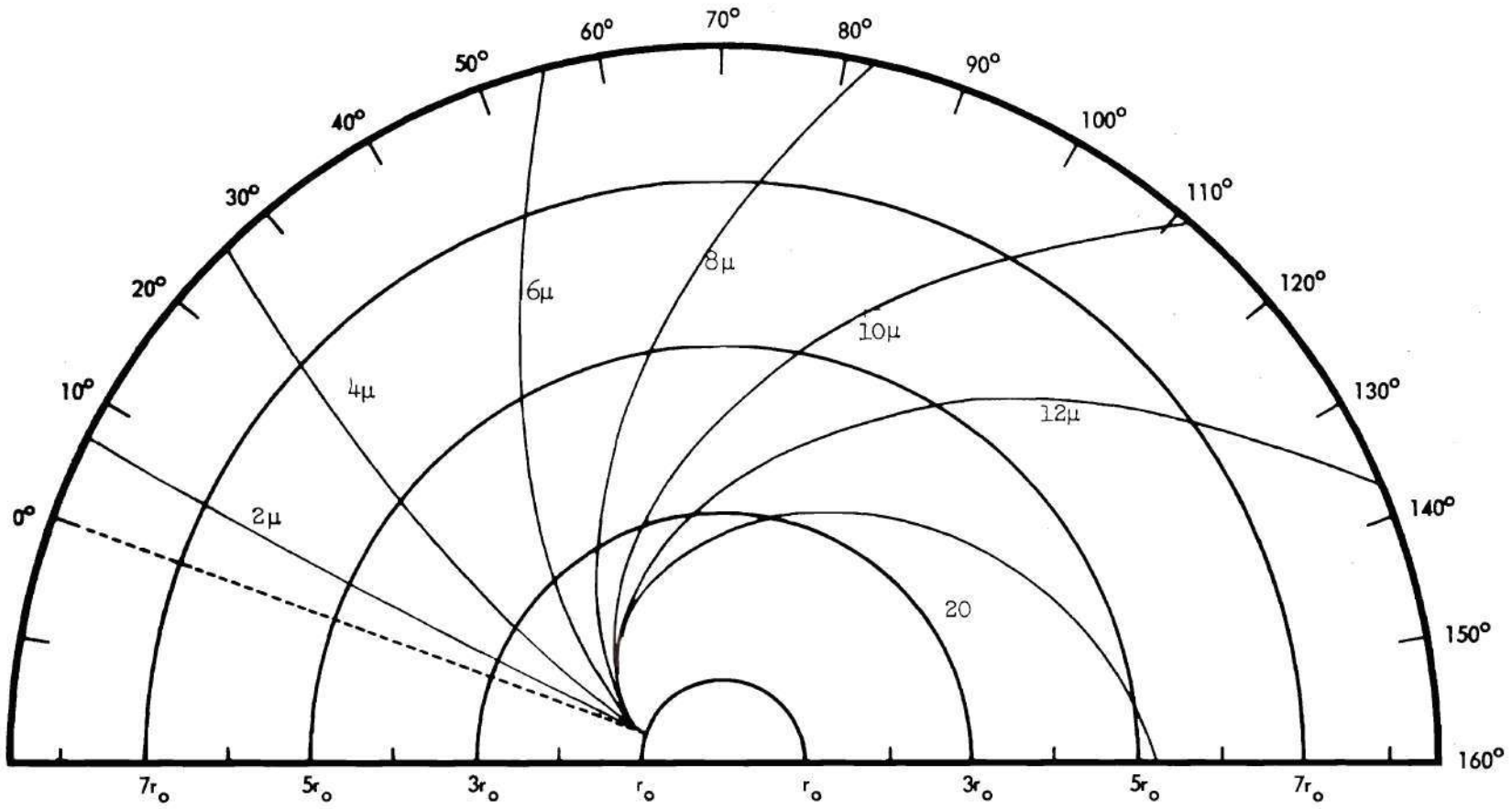

Figure 4. Analog Computer Solutions for the Trajectories of Spherical Particles having a Density of 3.0 gm/cm^3 Relative to a Constant Speed Rotor for Forced Vortex Conditions in which Stokes Law is Assumed Valid. (Rotor Speed: 7200 rpm).

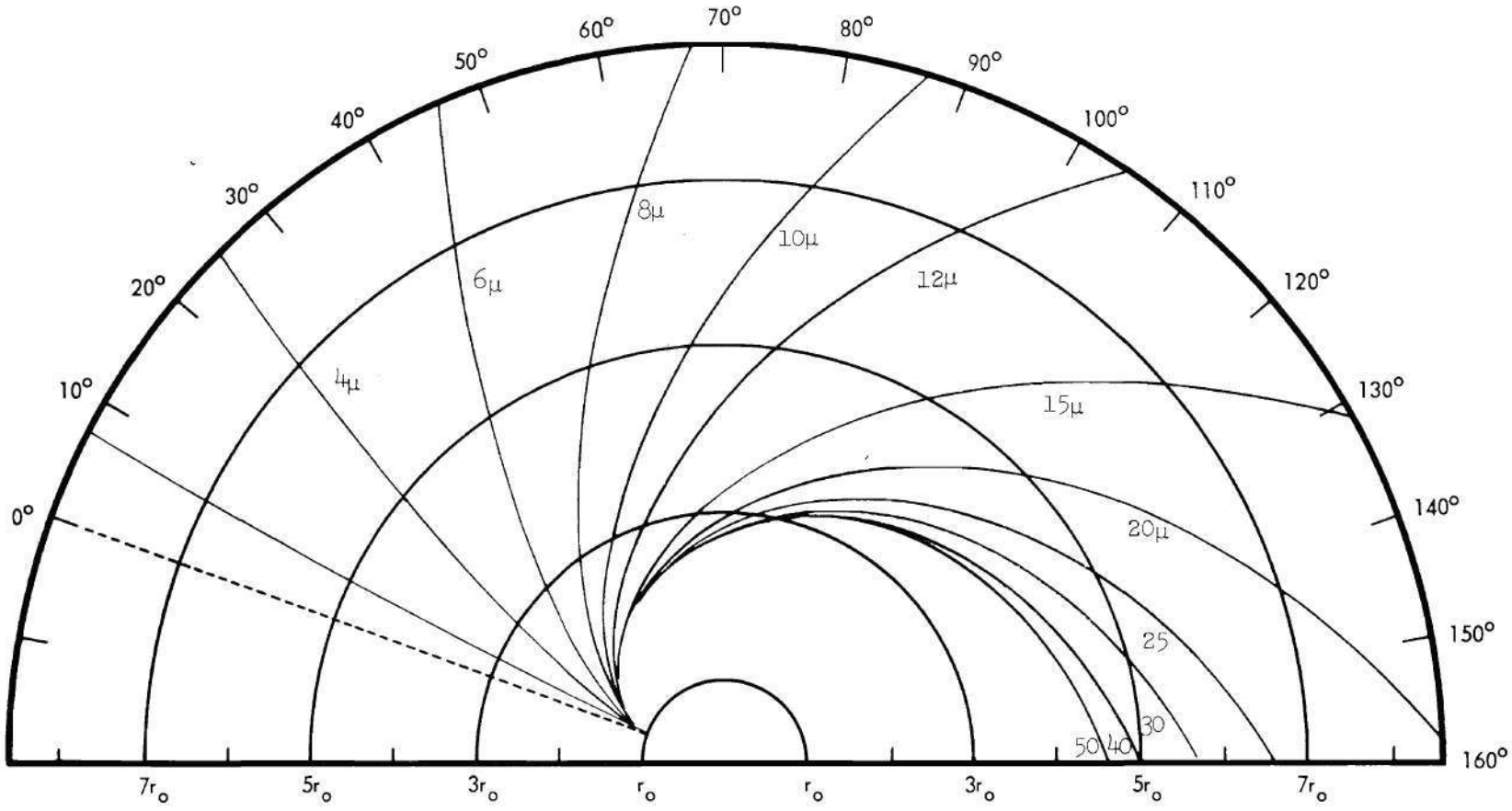

Figure 5. Analog Computer Solutions for the Trajectories of Spherical Particles having a Density of 3.0 gm/cm^3 Relative to a Constant Speed Rotor for Forced Vortex Conditions in which a General Drag Relationship is Assumed Valid. (Rotor Speed: 7200 rpm).

$\left(\frac{dr}{dt}\right)_{t=o}$ = initial radial velocity of the fluid ; $r)_{t=o} = 1$

$\left(\frac{d\theta}{dt}\right)_{t=o}$ = angular velocity of the fluid ; $\theta)_{t=o} = 0$

Subsequent Stokes law results were all derived from the trajectories of Figure 4. The "$\overline{V}$ curves" for the remaining conditions of interest are given in Appendix B.

Free Vortex Solutions

To illustrate differences in particle trajectories in a free vortex of air as compared to a forced vortex, Figure 6 presents relative trajectories of particles with the same density and diameter and with identical initial conditions as for those shown in Figure 5 except in this case $d\phi/dt = \text{constant}/r^2$, i.e., n= -2 in equation (25). In a free vortex, the centrifugal force acting on a particle decreases inversely as the cube of the radial displacement. Because of this, each particle attains a maximum velocity shortly after entering the centrifugal field and thereafter decelerates rapidly. This behavior is demonstrated in Figure 7 which shows the analog computer results for the variation of particle Reynolds number with radial displacement.

Analytical Solutions of the Equations of Motion for Forced Vortex Conditions

When the particle drag force is assumed to obey Stokes law, equations (41) and (42) which were developed in Chapter II were shown to describe the motion of a particle. Kriebel[32] solved analytically these simplified equations by use of Laplace transforms for the case of a forced vortex of

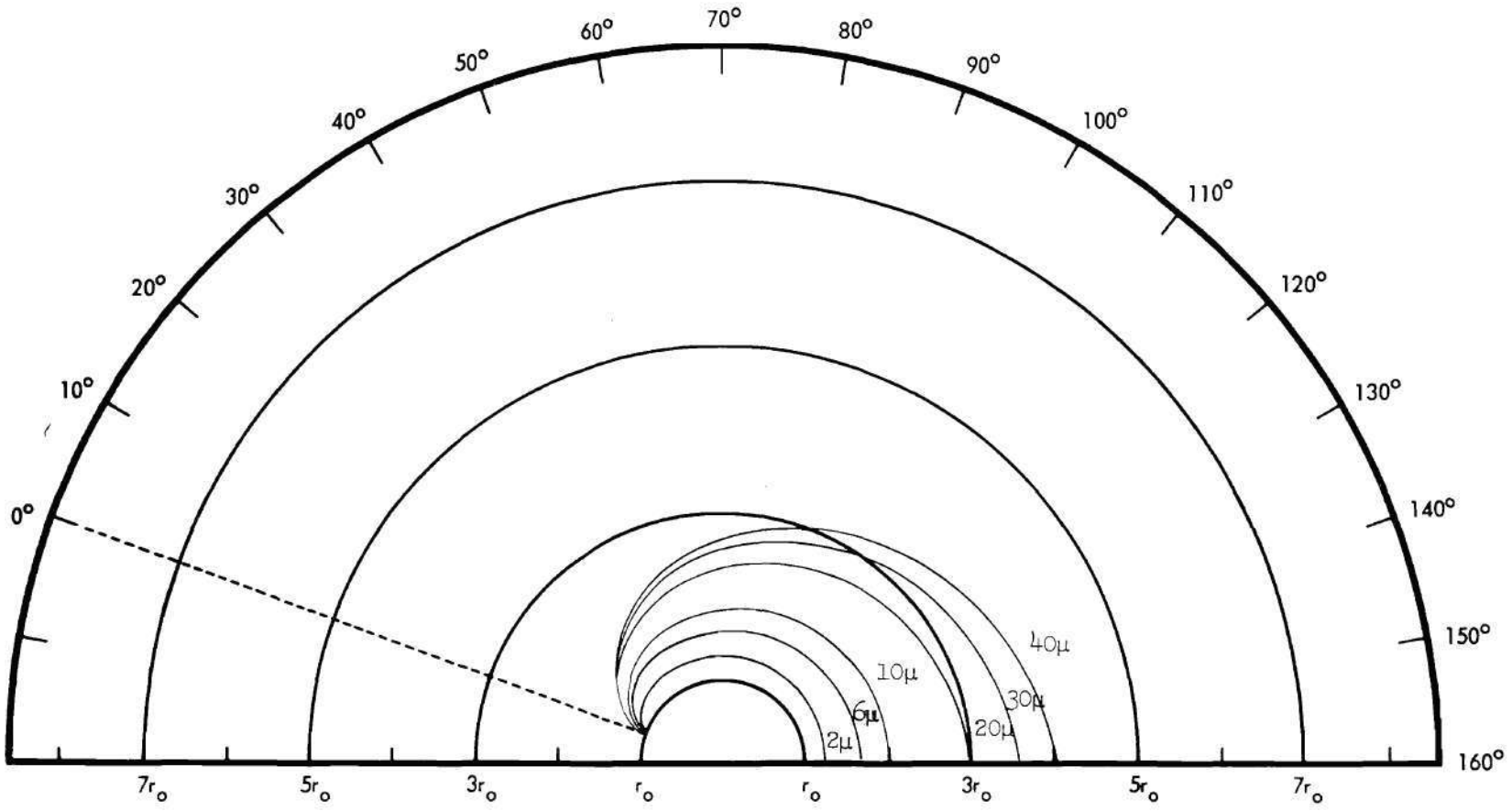

Figure 6. Analog Computer Solutions for the Trajectories of Spherical Particles having a Density of 3.0 gm/cm^3 Relative to a Constant Speed Rotor for Free Vortex Conditions in which a General Drag Relationship is Assumed Valid. (Rotor Speed: 7200 rpm).

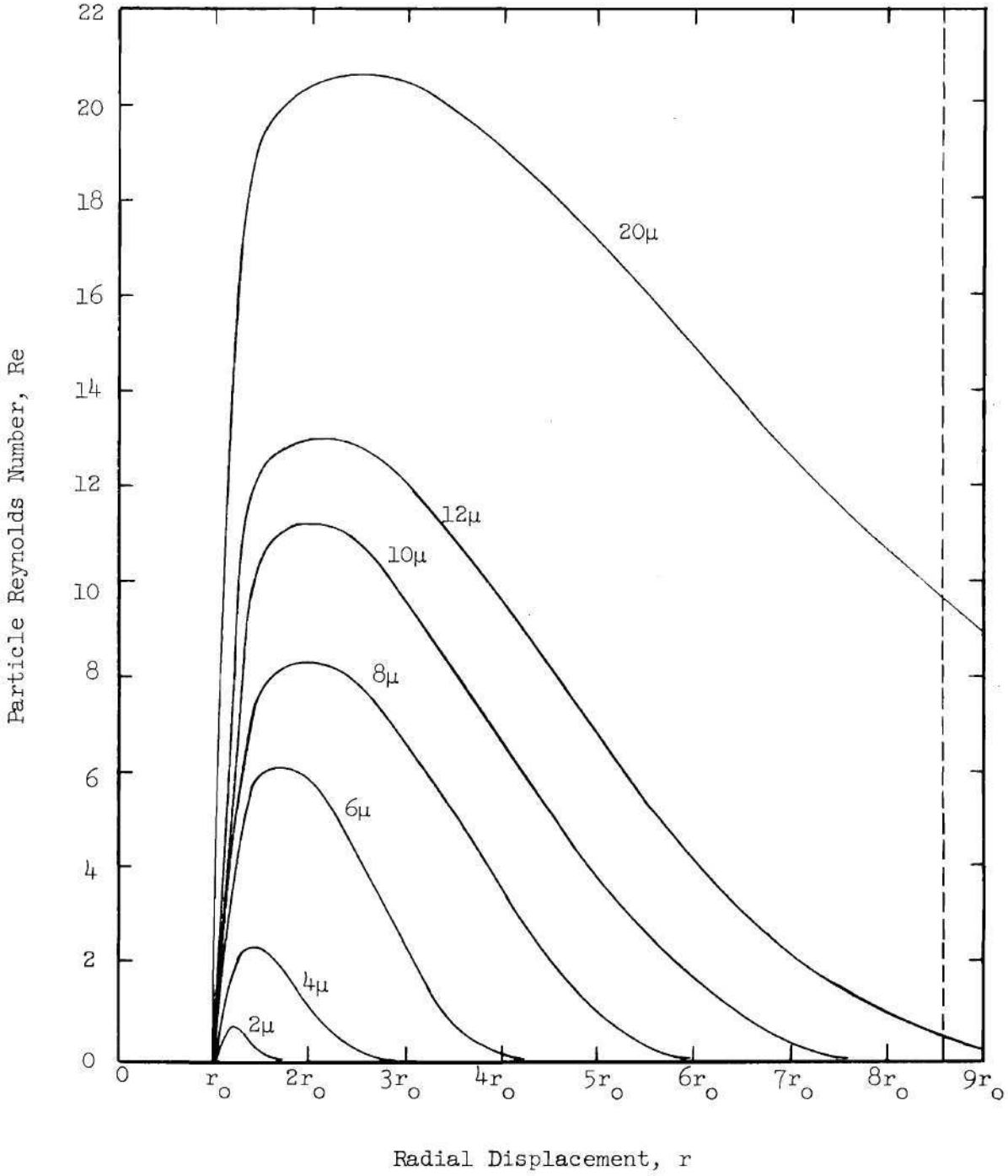

Figure 7. Variation of Particle Reynolds Numbers with Radial Displacement in a Free Vortex of Air.

fluid and no radial fluid flow. The analytical solutions obtained are

$$X(D, G, \epsilon) = \exp(-\epsilon/2D) \cos g\epsilon\, 2D \left\{ \cosh d\epsilon/2D + \left[\frac{d(1 + 2DG) + 2Dg}{j^2} \right] \sinh d\epsilon/2D \right\}$$

$$+ \exp(-\epsilon/2D) \sin g\epsilon/2D \left[\frac{g(1 + 2DG) - 2Dd}{j^2} \right]$$

$$\cosh d\epsilon/2D \tag{47}$$

and

$$Y(D, G, \epsilon) = \exp(-\epsilon/2D) \left[\frac{d}{2} + \frac{d}{2j^2}(1 + 4DG) \right]$$

$$\sin g\epsilon/2D \cosh d\epsilon/2D + \exp(-\epsilon/2D) \sin g\epsilon/2D$$

$$\sinh d\epsilon/2D + \exp(-\epsilon/2D) \left[\frac{g}{2} + \frac{g}{2j^2}(1 + 4DG) \right]$$

$$\cos g\epsilon/2D \sinh d\epsilon/2D \tag{48}$$

CHAPTER IV

EQUIPMENT DESIGN AND EXPERIMENTAL PROCEDURE

Description of Apparatus

Determining the trajectories of small particles in centrifugal force fields requires accurate specification of the initial conditions of motion for each particle as it enters the field; production of a centrifugal field with known characteristics; and provision for a particle deposition region which is amenable to detailed microscopic study. The centrifugal particle classifier described in this section was thus designed with these as the primary criteria plus the desire for a compact, self-pumping unit which would be easy to operate. It was constructed and evaluated with a wide variety of materials and under various operating conditions.

The main rotor component was machined from a hand-forged billet of high strength aluminum alloy, type 7075-T6, which has an average yield strength of 66,000 psi. Two small holes were drilled in the rotor wall every ten degrees. The flow within the rotor could easily be varied from forced to almost free vortex conditions and from laminar to quite turbulent flow by sealing or opening the desired holes in the rotor wall.

Several plexiglass covers were designed to fit snugly on the main rotor component. Each was of a different thickness, so these provided a means of varying the height of the classification chamber within the rotor and, consequently, another means of varying the radial velocity of the gas

passing through the centrifuge. An O-ring seal was provided between the main rotor component and the rotor top so that the classification chamber could be sealed off completely except for the holes open on the rotor wall. To assure dynamic and static balance during operation, the classification chamber within the rotor assembly was divided into two symmetrical regions of 180 degrees each by plastic webs extending from the rotor top to the bottom of the chamber along a radius from the rotor shaft to the rotor wall. Each region was sealed from the other except for the central entrance slots for the incoming aerosol. Thus each classification chamber was operated essentially independently of the other.

A non-rotating, stainless steel tube located inside of and coaxial with the rotor shaft led particles from an aerosol generator to the classifying chambers. The incoming aerosol was drawn down this feed tube by the pumping action of the rotor and, upon emerging into the area of the rotor shaft feed slots, was subjected to a high rate of fluid shear from the rapidly turning shaft. This additional shearing action was designed to assure a high degree of dispersion just prior to entry of the aerosol into the classification chambers. The aerosol progressed from the feed tube through a plastic insert in the rotor shaft and emerged through two narrow feed slots into the classification chamber. Figures 8 and 9 show photographs of the component parts of the rotor and the assembled rotor. Constructional details are given in Appendix C.

The rotor assembly was mounted with its axis of rotation vertical and driven by a 2-1/2 H.P. electric motor. The driving motor was controlled by a variable rheostat and capable of speeds from zero to 18,000 rpm. An observation port was provided in the rotor case so that motion of

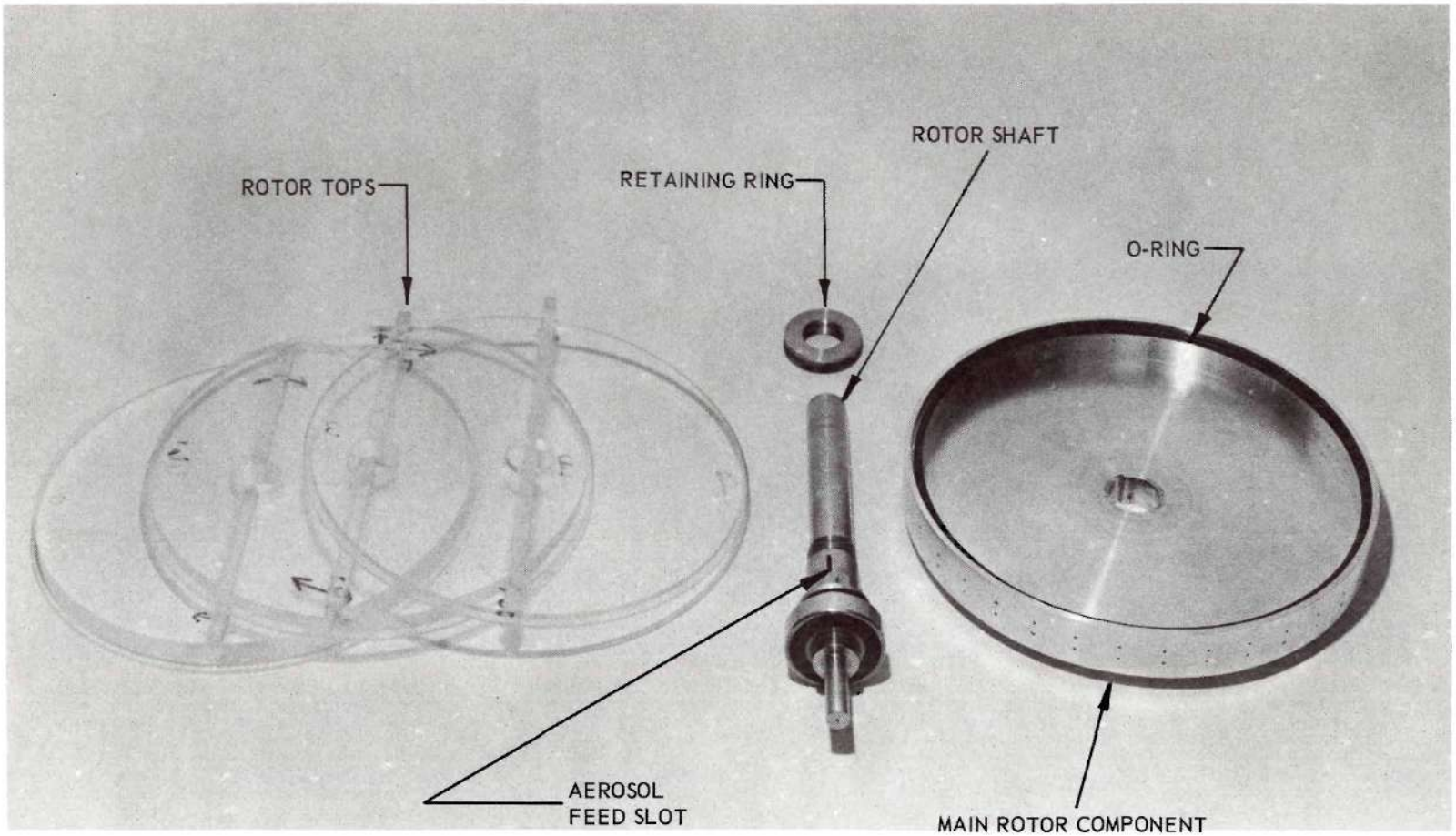

Figure 8. The Centrifugal Classifier Rotor Components.

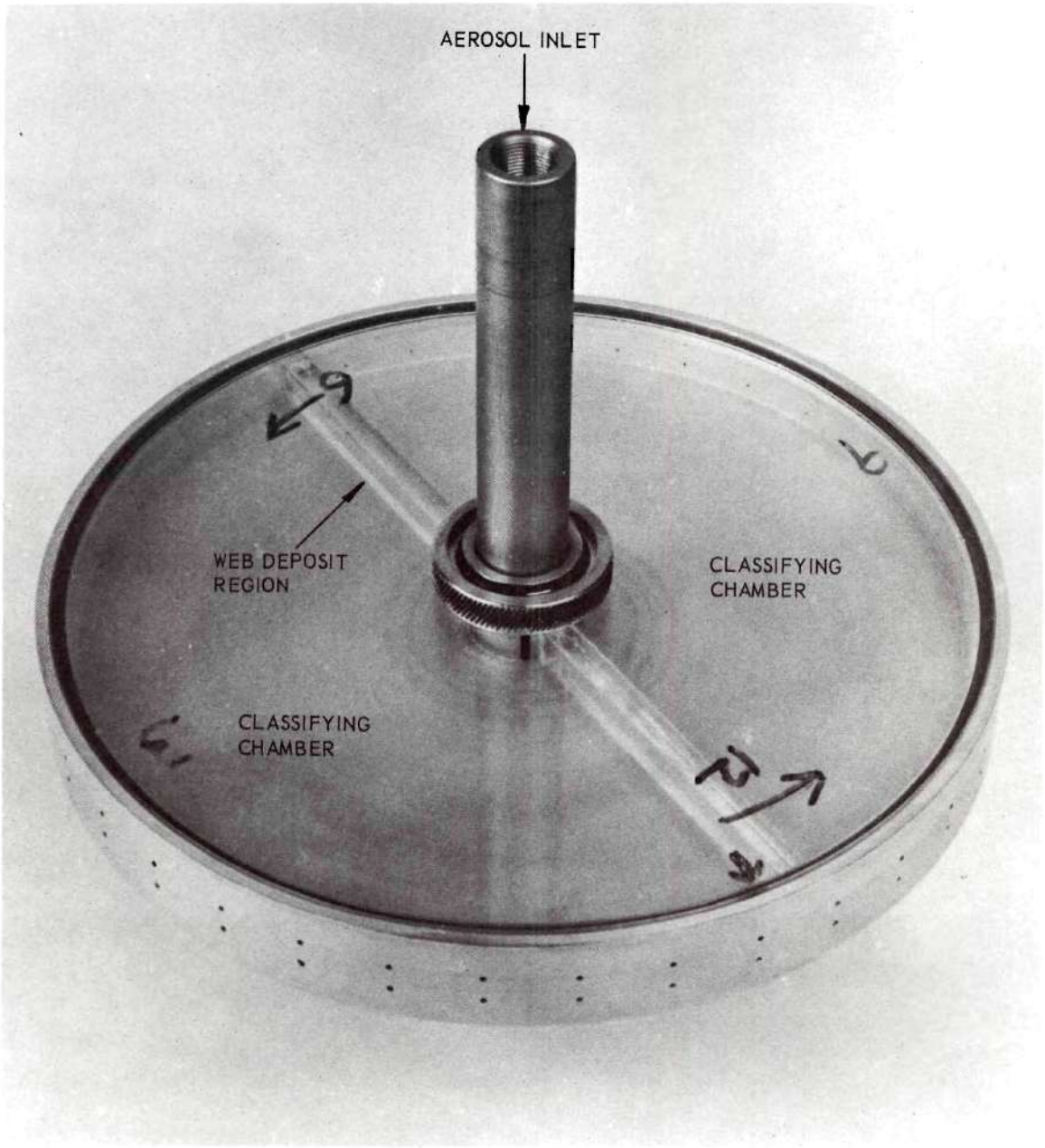

Figure 9. The Centrifugal Classifier Rotor Assembly.

the rotor and aerosols contained therein could be examined stroboscopically. Figure 10 shows an overall view of the entire apparatus with a stroboscope positioned for studies of smoke flow patterns.

The entire rotor assembly was designed to operate at speeds to 20,000 rpm with an adequate safety factor. The rotor was electronically balanced for speeds to 15,000 rpm. It would operate at speeds to about 18,000 rpm with only slight vibration, most of which probably originated in the bearings.

Experimental Procedure

A well-dispersed aerosol of the powder to be classified was generated by ordinary atomizers, such as the "Wright Dust Feed Mechanism"[44], or by several others of special design. The type used depended upon the size, shape and other physical characterisitics of the material to be classified. The maximum particle concentration in an aerosol to be classified according to settling diameter in a gravitational or centrifugal field must be quite low to prevent hindered settling and other particle-to particle interactions. The most suitable generation technique and particle concentration weredetermined experimentally for each of the materials used in this study.

The aerosol upon generation was directed to an aerosol chamber which consisted on a three-liter, inverted filter flask connected by plastic tubing to the aerosol feed tube. A pressure-bleed arrangement was provided in the aerosol chamber to prevent a pressure build-up within the chamber during the course of a run. The aerosol to be classified was generated continuously throughout a run to assure that aggregation and

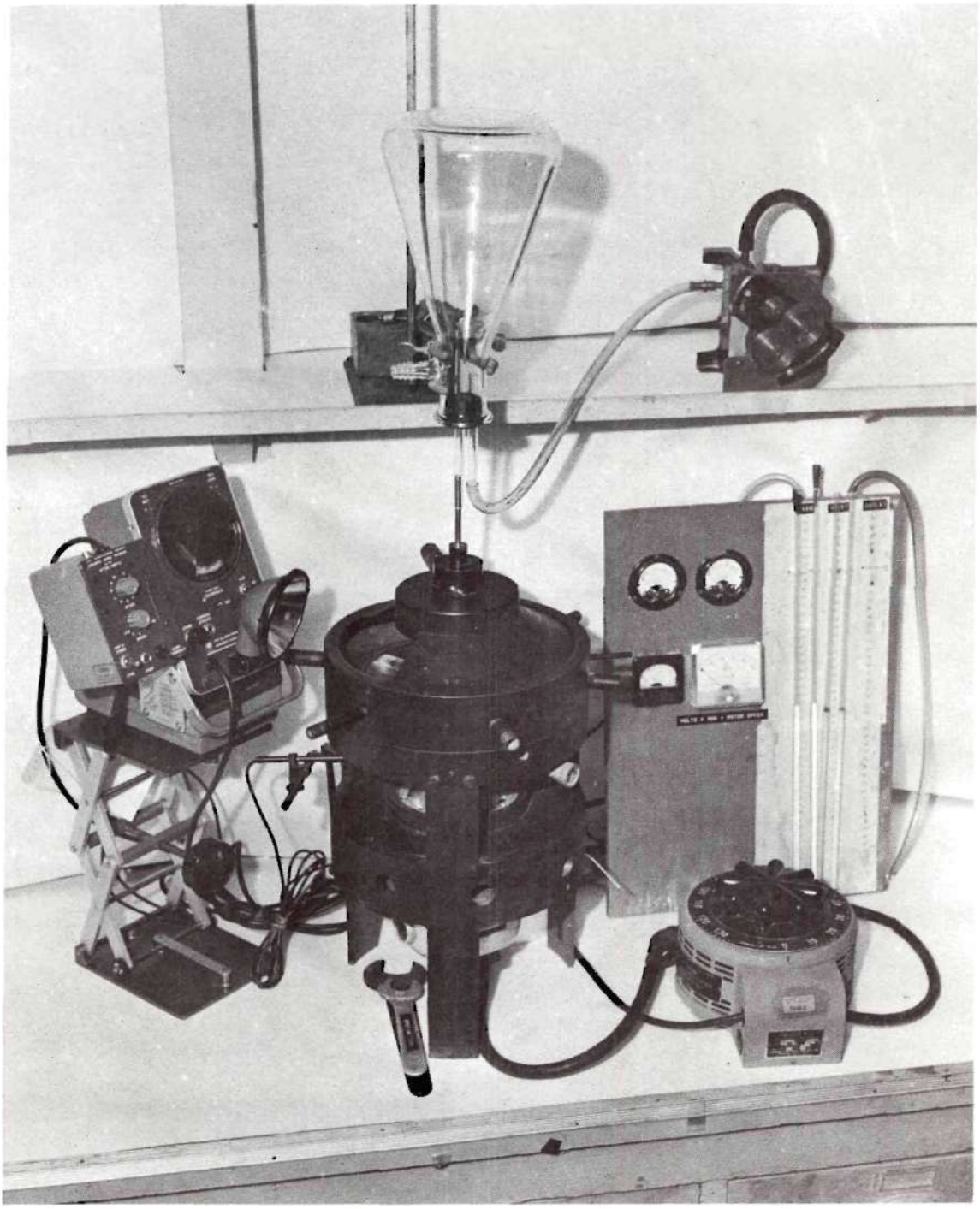

Figure 10. The Centrifugal Classifier and Associated Equipment.

settling of the larger particles did not change the aerosol's characteristics during the run.

The rotor was brought to the desired speed for the test while aerosol was being generated. To control the rotor speed, the stroboscope was set for the desired rate, and slight adjustments of the motor rheostat were made to keep the speed as nearly constant as possible throughout a test. This type of control arrangement limited speed variations to within about $\pm$ 5 rpm. When the rotor speed became constant, a clamp connecting the aerosol chamber and the feed tube was opened and aerosol was drawn into the rotor. The aerosol entered at essentially atmospheric pressure because of the pressure-bleed system on the aerosol chamber. The volumetric flow rate of the aerosol was therefore determined by the rotor speed, thickness of the rotor top used and the number and diameter of holes open in the rotor's periphery. All of the experimental tests from which quantitative size data were obtained were made with rotor top number 3 which fixed the depth of the classification chamber at 9.0 mm. The angular designation of the hole in the rotor periphery that was directly opposite the aerosol entry slot was zero degrees. Positive angles were measured clockwise to the plastic webs dividing the classification chamber and negative angles counter-clockwise to the opposite web. The reason for this arrangement was to offset the aerosol entry slots from the plastic webs by a sufficient amount (20 degrees) to avoid wall effects on the incoming aerosol and still provide a large classification region (160 degrees).

The classified particles were collected on thin, transparent plastic strips placed along the rotor wall. When a quantity adequate for size

distribution measurements had been collected on the plastic strips, the clamp on the aerosol feed tube was closed. The rotor was slowly stopped after several more minutes of operation at constant speed to collect and classify those particles remaining in the aerosol feed tube. The plastic rotor top was carefully removed and the two plastic strips containing the classified material then removed. To mount the strips for microscopic examination, a film of transparent, pressure-sensitive tape with adhesive on both sides was placed on a microscope slide and one of the plastic strips on which the particles were collected was placed upon the pressure sensitive tape. This microscope slide was placed on the mechanical stage of a microscope and examined with transmitted light. Vertical traverses at specified angular locations were made and the number and size of particles present were determined with the aid of a filar eyepiece. At least 50 particles were measured at each angular position specified where possible; however, in some cases the number of particles present was not sufficient for 50 counts, and in these instances all of the particles present were measured and counted. At least 400 particles were measured in determining the original size distribution of each of the materials to be classified.

Materials Used in the Experimental Studies

Glass Spheres

A sample of spherical glass particles of density 2.5 gm/cm^3 and having particle diameters from about two to 40 microns was used as one of the test materials. Preliminary tests in the classifier with this material yielded anomalous results in that there were mixtures of large

and small particles at certain angular locations on the rotor wall. Careful microscopic examination revealed that there were significant quantities of hollow particles present. This, of course, created a variation in the actual densities of particles which explained the disparities noted in the results. To circumvent this difficulty, all particles having densities less than 2.45 gm/cm^3 were separated by a flotation technique. The flotation technique used a mixture of acetone and 1,1,2,2, - tetrabromoethane, the density of which was adjusted to 2.45 gm/cm^3, as the separating medium. The glass spheres were stirred in this mixture for five minutes and centrifuged in a standard laboratory centrifuge for 30 minutes. The solid glass particles were collected from the bottom of the centrifuge tube, washed several times with acetone and distilled water and finally dried for three hours at 105°C. The density of the recovered matter was determined to be 2.49 gm/cm^3 in a Beckman air comparison pycnometer. The size distribution of the glass beads before classification and at specified angular locations from a typical experimental determination are shown in Figure 11. Additional data for glass beads are given in Appendix D. An estimate of the average diameter particle present was made for those cases at small angular displacements in which there were insufficient particles for statistical analysis. The result is shown on the figure by a single point as the 50 per cent value.

Plastic Spheres

A sample of plastic molding powder was used as a test material primarily because of the tendency for this material to accumulate static charges, thereby making size separations especially difficult. The

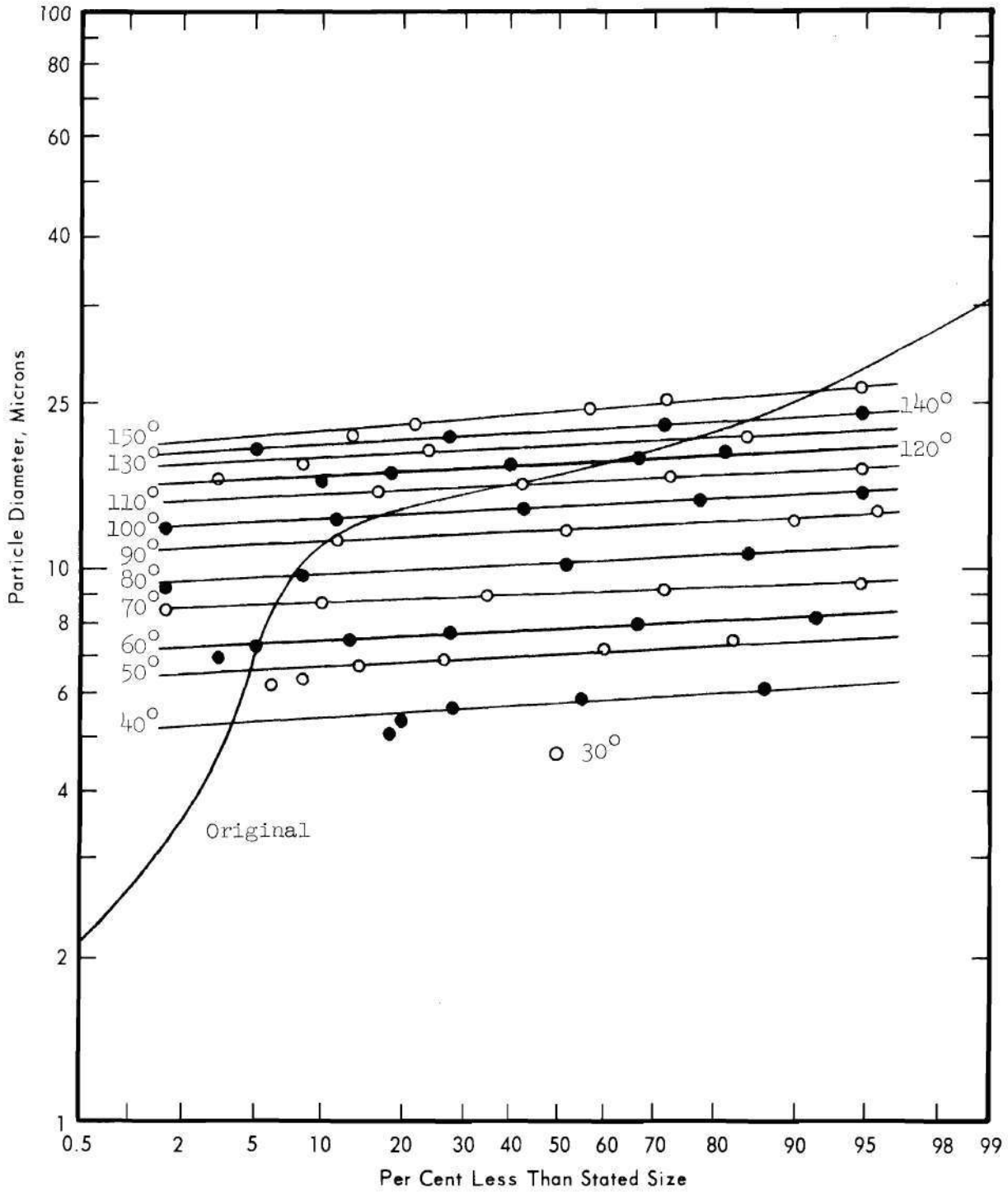

Figure 11. Size Distribution of Glass Spheres before Classification and as Deposited at Specified Angular Locations on the Rotor Wall. (Rotor Speed: 7200 rpm).

powder of this study had a density of 1.25 gm/cm^{3}as determined with the Beckman pycnometer. Microscopic examination showed the particles to be quite smooth and spherical except for some doublets larger than about 50 microns in diameter. The powder was wet sieved to remove these larger particles, rinsed several times with distilled water and dried for three hours at 105°C. Size distributions before separation and at specified positions on the rotor wall for various operating conditions are shown in the Figures of Appendix D.

Aluminum Spheres

Spherical aluminum powder was used as a test material primarily because of its ease of dispersability. The theoretical density of aluminum is 2.70 gm/cm^3; however, because of oxidation, the density of the material actually used in this study was 2.83 gm/cm^3 as determined with the Beckman pycnometer. The size distribution before separation and at specified angular positions on the rotor wall are shown in the Figures of Appendix D for the various operating conditions of interest.

Zinc Spheres

To assure that experimental conditions covered a wide range of densities, a sample of zinc powder was also used. This material, although originally non-spherical, had been spherodized by repeatedly passing it through a radiant heat transfer apparatus. The resulting material was quite spherical and its original size distribution as well as those distributions of material collected at specified points on the rotor wall for the various conditions of interest are given in the Figures of Appendix D. Because of oxidation again, the density was taken to be 6.81 gm/cm^3 as determined with the Beckman pycnometer instead of

the theoretical value of 7.13 gm/cm^3.

Flow Visualization Studies

A flow visualization study was made to provide qualitative information on the characteristics of the fluid flow within the rotor during actual operation. To perform a flow visualization test, an aerosol consisting of tobacco smoke with an average particle diameter of between about 0.1 and 0.2 micron was introduced into the rotor in the same manner as was an aerosol consisting of larger particles to be classified. The tobacco smoke, because of its very small particle size, should follow very closely the fluid streamlines.

A viewing port was provided in the outer case of the centrifugal separator and a stroboscope was mounted so the movement of the rotor could be "frozen" and the flow pattern of a tobacco smoke aerosol observed. The stroboscope was electronically triggered each time the rotor made one revolution by placing a narrow strip of reflective tape on the rotor shaft and directing a narrow beam of light and a photocell at the rotating shaft. This type of photoelectric pickoff operated the stroboscope in near-perfect synchronism with the rotor and eliminated the adjustments that are otherwise needed for slight variations in angular speed. An electronic flash delay permitted a controlled lag of the flash time after the pickoff time, thus all portions of the rotor could be examined by varying the flash delay time.

A trial and error method determined that a single hole of 0.25 mm diameter directly opposite the aerosol entry ports on each side of the classifier rotor gave very stable flow patterns that closely approximated

a forced vortex from speeds of 1,600 to 12,000 rpm. The remaining holes were sealed by a thin film of pressure sensitive tape. Figure 12a shows a smoke streamer at a rotor speed of 7,200 rpm moving directly from the aerosol entry port of one side of the rotor to the small hole at zero degrees in the periphery. The dark streaks on the bottom of the rotor are condensed tars from the tobacco smoke. The flow pattern in Figure 12a is actually the relative trajectory of the sub-micron smoke particles within the rotor and closely resembles the relative trajectory for a fluid under perfect forced vortex conditions as was predicted in Chapter II. When the diameter of the hole in the rotor periphery was increased to 0.50 mm and the rotor speed was maintained constant at 7,200 rpm, the smoke streamer began to spiral relative to the rotor as is shown in Figure 12b. A further increase in the hole diameter to 0.78 mm still at a rotor speed of 7,200 rpm tightened the spiral as is shown in Figure 12c. Comparison of the smoke patterns in Figures 12a, 12b, and 12c with predicted flow patterns of Figure 1 in Chapter II confirms that, under conditions of increased gas flow rate and decreased torque transfer from rotor to fluid, the fluid flow characteristics deviate from a forced vortex and begin to approach those of a free vortex, i.e., $n < 0$. It is also intuitively evident from the photographs of smoke flow patterns that efficient particle classification in a centrifugal classifier of this design can occur only under near-perfect forced vortex conditions.

Figure 12d shows the onset of turbulence when the O-ring seal at the rotor periphery ruptures. This photograph was taken at about 12,000 rpm rotor speed with one 0.25 mm diameter hole open on each side of the rotor. The character of the flow changes abruptly at about 12,000 rpm

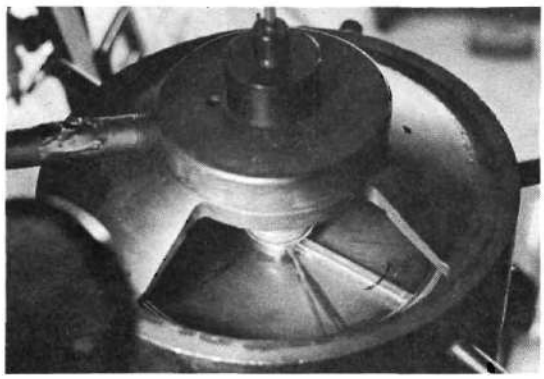

(a) ROTOR SPEED = 7200 rpm
HOLE DIAMETER = 0.25 mm

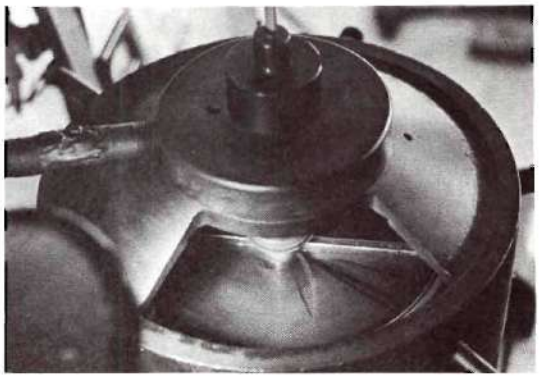

(b) ROTOR SPEED = 7200 rpm
HOLE DIAMETER = 0.50 mm

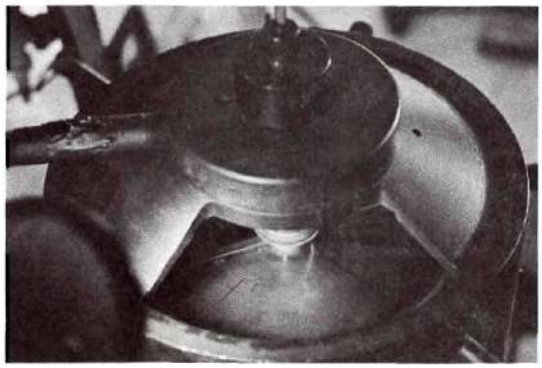

(c) ROTOR SPEED = 7200 rpm
HOLE DIAMETER = 0.78 mm

(d) ROTOR SPEED = 12,000 rpm
HOLE DIAMETER = 0.78 mm

Figure 12. Smoke Flow Patterns in the Centrifugal Classifier Rotor for Various Aerosol Flow Rates.

from the laminar striae shown in Figures 12a, 12b, and 12c to the turbulent eddies seen in Figure 12d.

Flow Rate Measurements

Theoretical estimates of the flow rate of gas through the centrifuge were obtained from the relation for the flow of an incompressible fluid through a sharp-edged orifice, viz.

$$Q = 0.6A_h \left[\frac{2 \Delta p}{\rho} \right]^{1/2}$$

The expression for the pressure drop was evaluated from the pressure rise for a forced vortex as given by equation (20) of Chapter II. Figure 13 shows theoretical values obtained by this method and experimental values measured under conditions identical with those assumed for the theoretical calculations.

Because of the extremely low flow rates at low speeds, conventional flow rate devices such as rotameters were of limited value due to the large pressure drops created across the measuring device itself. The experimental flow rate values were obtained by forming a soap film in a calibrated glass tube and timing the excursion of the soap film over a measured distance. With this technique, very low flow rates can be readily measured because of the almost negligible pressure drop associated with the movement of the film.

Significant deviations of the experimental values from the theoretical predictions were noted for rotor speeds in excess of about 12,000 rpm. The cause of this discrepancy was found to be a leak in the O-ring seal between the lower rotor component and the plastic rotor top. At speeds

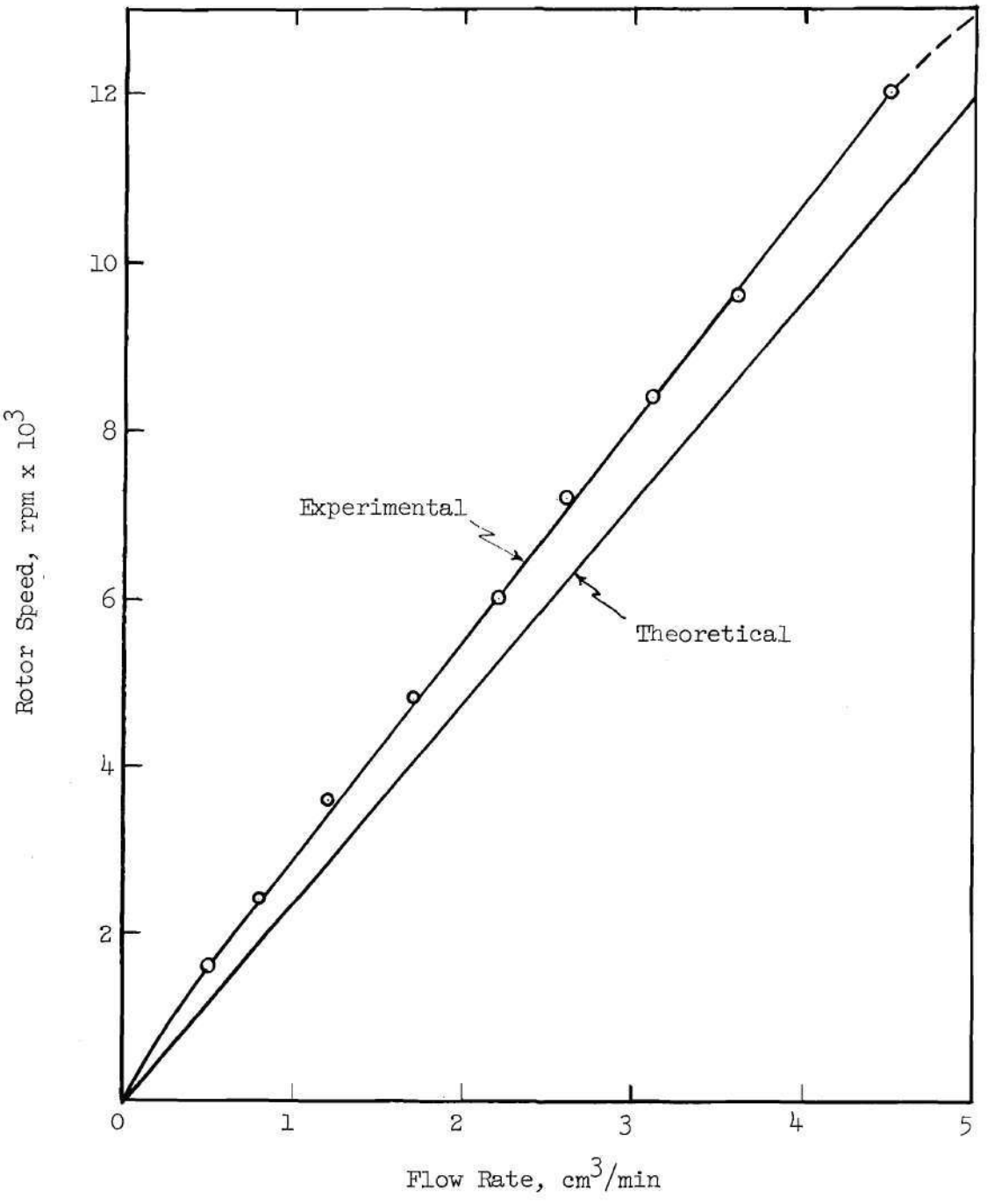

Figure 13. Variation of Aerosol Flow Rates Through the Centrifugal Classifier with Rotor Speed.

to 12,000 rpm, the seal was adequate; however, at higher speeds the expansion of the outer wall of the rotor combined with the tendency of the plastic to bend upward ruptured the seal. The breaking of the seal was readily noted by a sudden increase in the gas flow rate through the centrifuge and the resulting onset of turbulent flow when tobacco smoke was used as the aerosol. The effect is clearly shown in Figure 12d.

CHAPTER V

RESULTS AND DISCUSSION

Fluid Flow Studies

Analyzing the transport of momentum to a fluid in an enclosed rotor is necessary in any study of the dynamic behavior of particles within that fluid. Recourse was made to approximate solutions for simplified flow models in this study because of the complexities of the fluid motion under typical operating conditions. To have been more exact in the mathematical models describing the fluid flow, provision might well have been made to allow for asymmetry effects due to the division of the rotor into two chambers, compressibility and wall effects, and the possibility of turbulent flow. Furthermore, the radial flow model could have been improved considerably by using a model for a rectangular jet emerging into a semi-infinite chamber. To test the general validity of these simplifying assumptions, however, comparisons were made of theoretically predicted results using the simplified flow models developed in Chapter II with the experimental observations of the flow visualization and flow rate studies of Chapter IV. The predicted and experimental results were found to be in reasonably good agreement. Thus they indicated that these models furnish at least a qualitatively correct description of the fluid flow in a centrifuge rotor of the type involved here. Consequently, it is believed that the mathematical simplifications in the fluid flow analysis were justified in arriving at suitable fluid velocity components.

Most of the fluid within the rotor during ideal operating conditions, as shown by the flow visualization studies, actually moves as a solid body. Only a relatively small segment, from approximately one to five degrees from the aerosol entry slots, has appreciable radial flow components. Thus the larger diameter particles settle for the most part in a fluid which is not moving relative to the rotor and only the smallest particles, generally less than about two microns diameter, are affected by the radial flow components. The effect of the radial velocity of the fluid on the small particle trajectories under these conditions is to cause particle deposition at smaller angles. The effects of the radial velocity become considerably more important at higher flow rates during which the fluid motion departs from near-perfect forced vortex conditions.

Initial Condition Effects

The particle trajectory calculations made in this study were all initial condition solutions of two independent, second-order, ordinary differential equations. That is, the trajectory of each particle was specified primarily by the initial conditions imposed on it. The resulting solutions were allowed to proceed from specified initial conditions for the desired time-distance interval. The initial radial position for each particle was taken as the outer radius of the rotor shaft since each particle emerged from entry slots of this shaft into one of the two classification chambers of the rotor. The initial angular location of each particle was defined as zero degrees at the center line of each of the aerosol entry slots of the rotor shaft. Because of the finite width of these slots, there exists an uncertainty of $\pm$ three degrees in the

actual angular location of each entering particle. The tortuous path of each particle through the narrow confines of the rotor shaft and the aerosol entry slots virtually assures that the angular velocity of the entering aerosol particles will be equal to, or very nearly equal to, that of the rotor. The initial radial velocity of the fluid is readily calculated from the cross-sectional area of the aerosol entry slots and the volumetric flow rate corresponding to the specified rotor speed. Figure 13, which was shown in Chapter IV, supplies aerosol flow rates as a function of rotor speed for the experimental conditions of this study. The initial radial velocity of each particle entering the classification chambers was taken as equal to, or very nearly equal to, that of the incoming fluid since their masses were very small.

Large initial radial velocities for particles cause intersection of the trajectories of the larger and smaller particles and thus must result in poorer size classification. Kriebel[32] showed that this was true when Stokes law applies, and the analog computer results of this study for the more general equations of motion confirmed this behavior for the conditions of this study. Examination of Figure 14, which shows the analog computer calculated trajectories of particles in a forced vortex of air corresponding to a rotor speed of 4800 rpm with initial radial velocities of particles equal to 500 cm/sec, reveals intersections of many of the trajectories and a reversal of deposition angles for particles larger than about 40 microns in diameter. Consequently, for best size classification, particles should enter the rotor with the lowest feasible radial velocities. Fortunately, these same criteria yield the most favorable fluid flow patterns in a centrifugal separator of the type

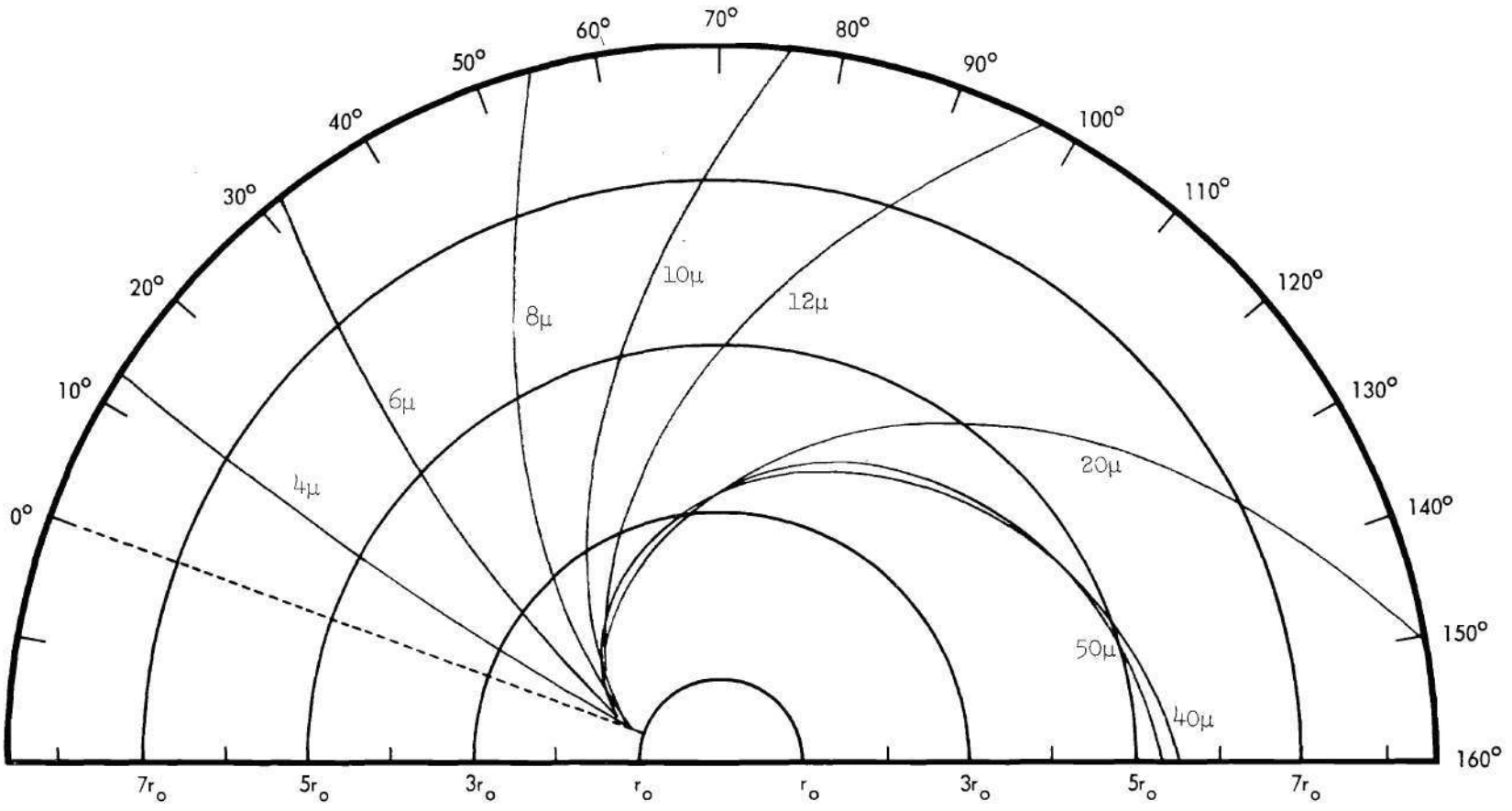

Figure 14. Analog Computer Solutions for the Trajectories of Spherical Particles having a Density of 3.0 gm/cm^3 Relative to a Constant Speed Rotor for Forced Vortex Conditions in which a General Drag Relationship is Assumed Valid and when Injected at High Velocity. (Rotor Speed: 4800 rpm).

used in this study. Although these conditions are the most favorable for size classification, they also limit the capacity of the classifier since only small quantities of aerosol can be classified per unit time.

Solutions for Limiting Cases

Examination of solutions for the equations of particle motion believed to be most appropriate reveals that significant separation of particles is possible for only a limited size-density range. Numerical values of the size-density product in the denominator of the α-term of equations (45) and (46) rapidly become quite small, for small diameters and low particle densities and the particle drag force far outweighs the effects of the other terms of the equations. Thus the relative trajectories of the small-diameter, low-density particles approach more closely the relative trajectory of the fluid. Practically speaking, this means that particles of average densities with diameters less than about one or two microns are all deposited at approximately the same angular location on the rotor, i.e., zero degrees. For high values of the size-density product, the α-term becomes insignificant with respect to the inertial terms, and these larger particles all traverse roughly the same trajectory. The trajectory curves of Appendix B verify this behavior for the large, dense and the small, light-weight particles.

Free Vortex Studies

The results of the free vortex studies clearly indicate that efficient particle classification is not possible for these conditions in the type of experimental rotor used in this investigation. Qualitative studies of classification were obtained when an aerosol of glass beads

was admitted to the experimental rotor under conditions approximating those of a free vortex, i.e., all holes were open in the rotor periphery. Highly turbulent flow resulted and no separation of particles according to size was evident.

Theoretical and Experimental Results

Figures 15, 16, 17, and 18 illustrate typical results by both theoretical and experimental methods for each of the four materials used in this study. The two curves on each figure represent, respectively, theoretical results obtained for forced vortex conditions using Stokes law and the diode function generator approximation for the particle drag coefficients. The upper curve on each figure represents values from the "Stokes curves" analog computer results and the lower curve represents values from the "$\overline{V}$ curves" analog computer solutions of equations (45) and (46). Comparison of these theoretical results reveals that the two mathematical models yield the same results for the smaller particle diameters. For larger particle diameters however, the Stokes law solution always predicts deposition at larger angles than does the more general model. The reasons for these deviations are, of course, due primarily to differences in the drag coefficients used in the two models. The upper limit of applicability of Stokes law is generally accepted as a particle Reynolds number of one. To assess the validity of the Stokes law assumption, particle Reynolds numbers were calculated for a typical case at increasing radial displacements assuming a particle of 3.00 gm/cm^3 density in a forced vortex field and a rotor speed of 7200 rpm. The results are presented in Figure 19 for various particle diameters. The

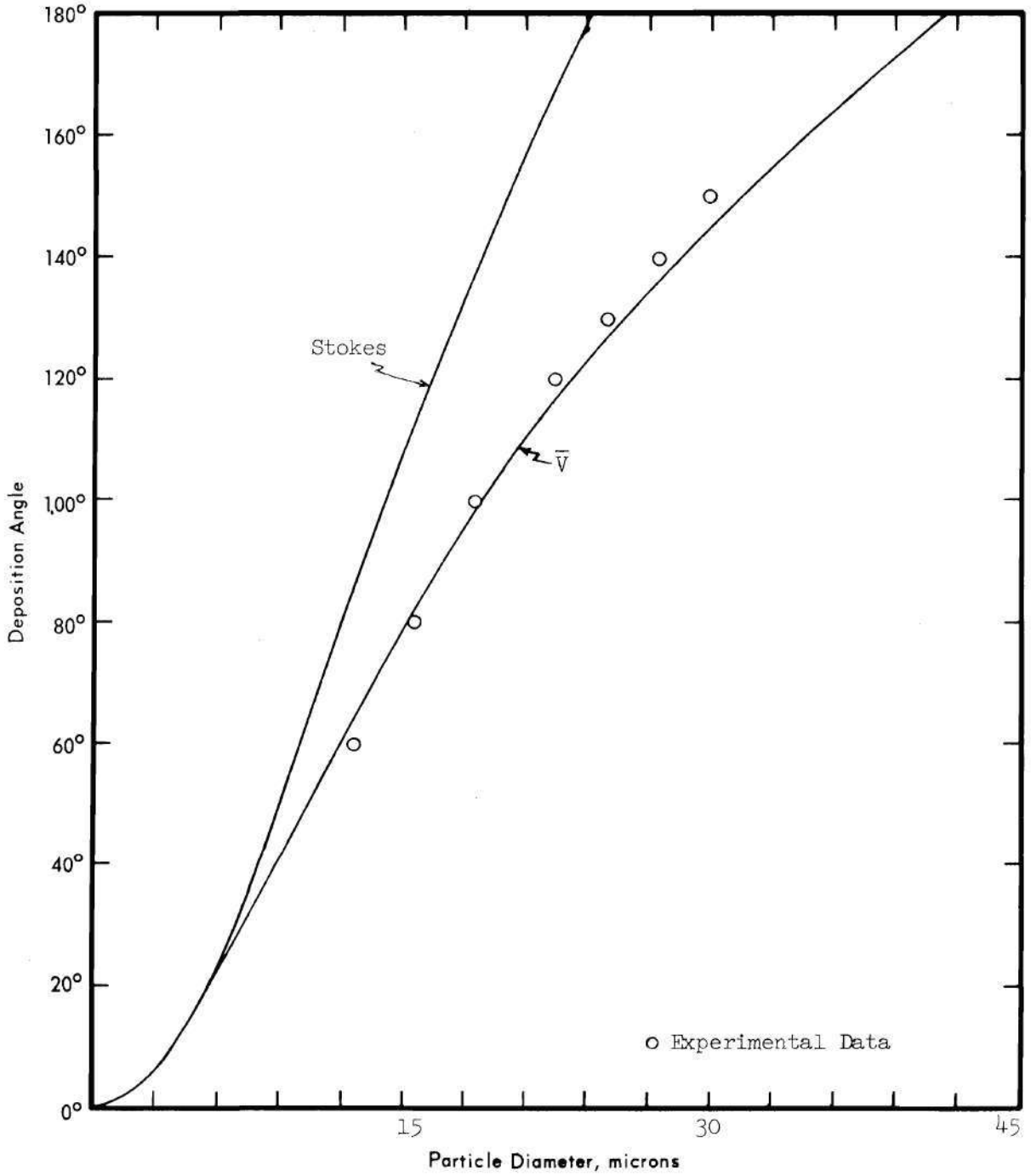

Figure 15. Comparison of Analog Computer Solutions Obtained Using Stokes Law and a More General Drag Relation with Experimental Data for Plastic Spheres. (Rotor Speed: 7200 rpm).

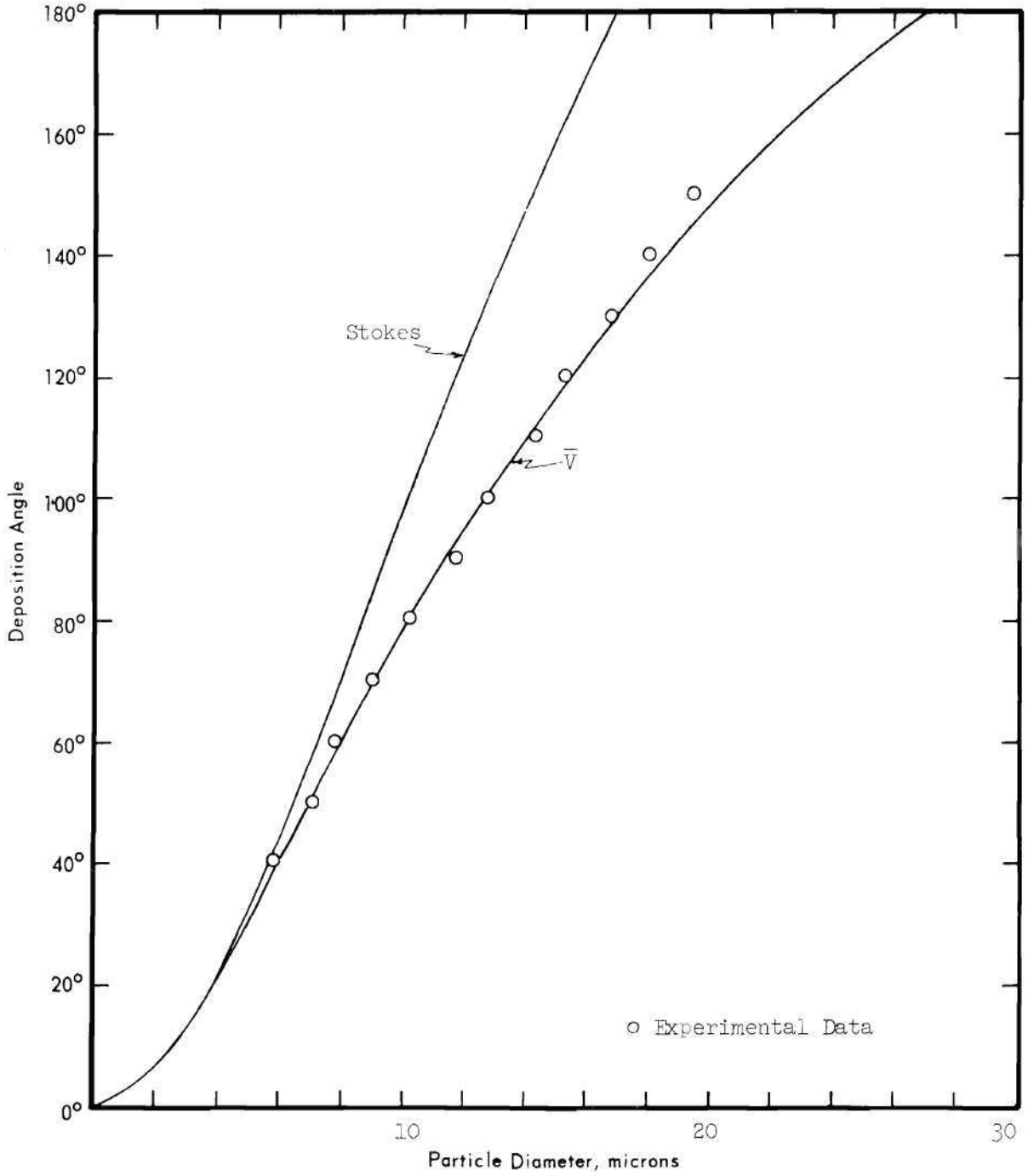

Figure 16. Comparison of Analog Computer Solutions Obtained Using Stokes Law and a More General Drag Relation with Experimental Data for Glass Spheres. (Rotor Speed: 7200 rpm).

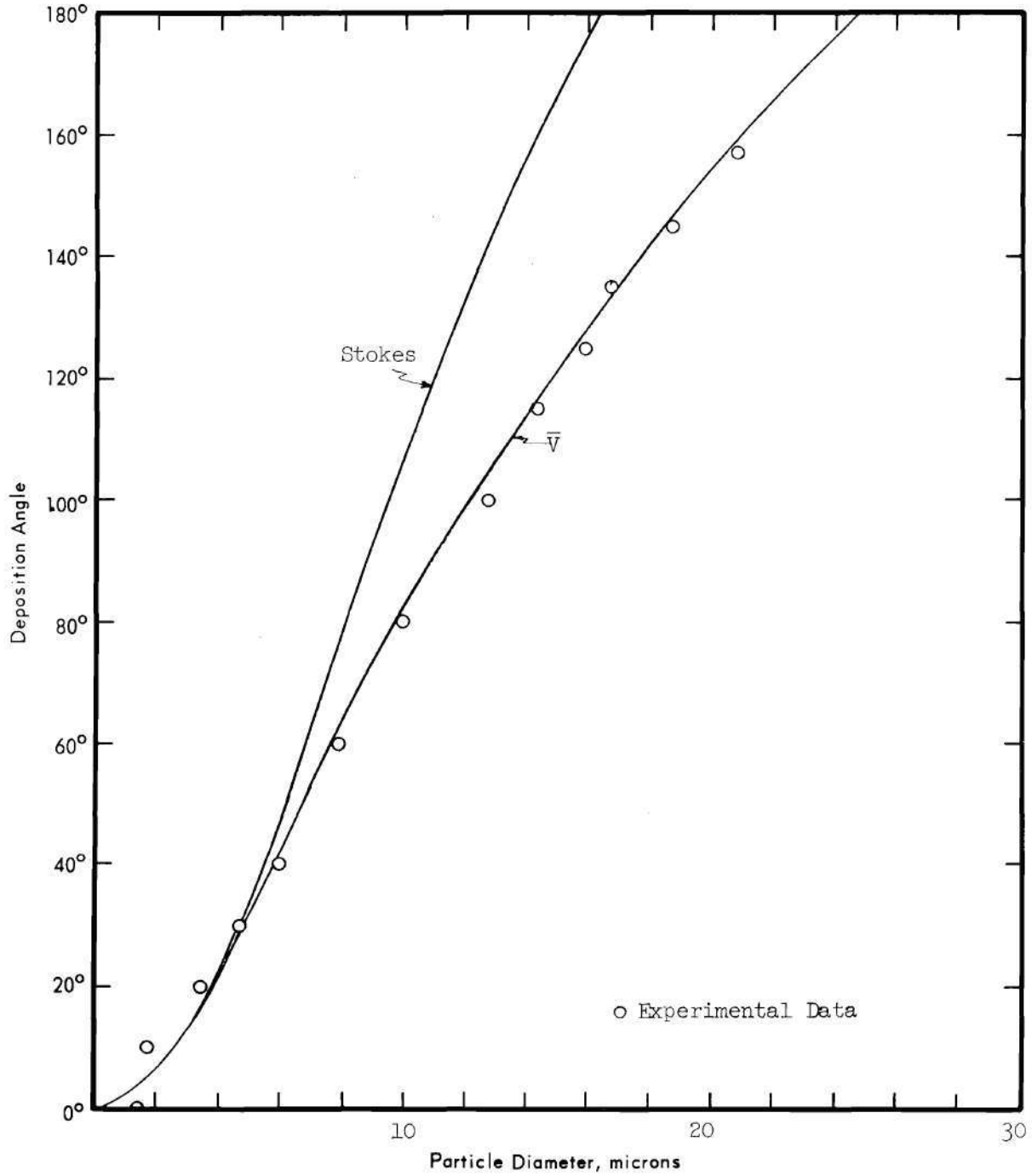

Figure 17. Comparison of Analog Computer Solutions Obtained Using Stokes Law and a More General Drag Relation with Experimental Data for Aluminum Spheres. (Rotor Speed: 7200 rpm).

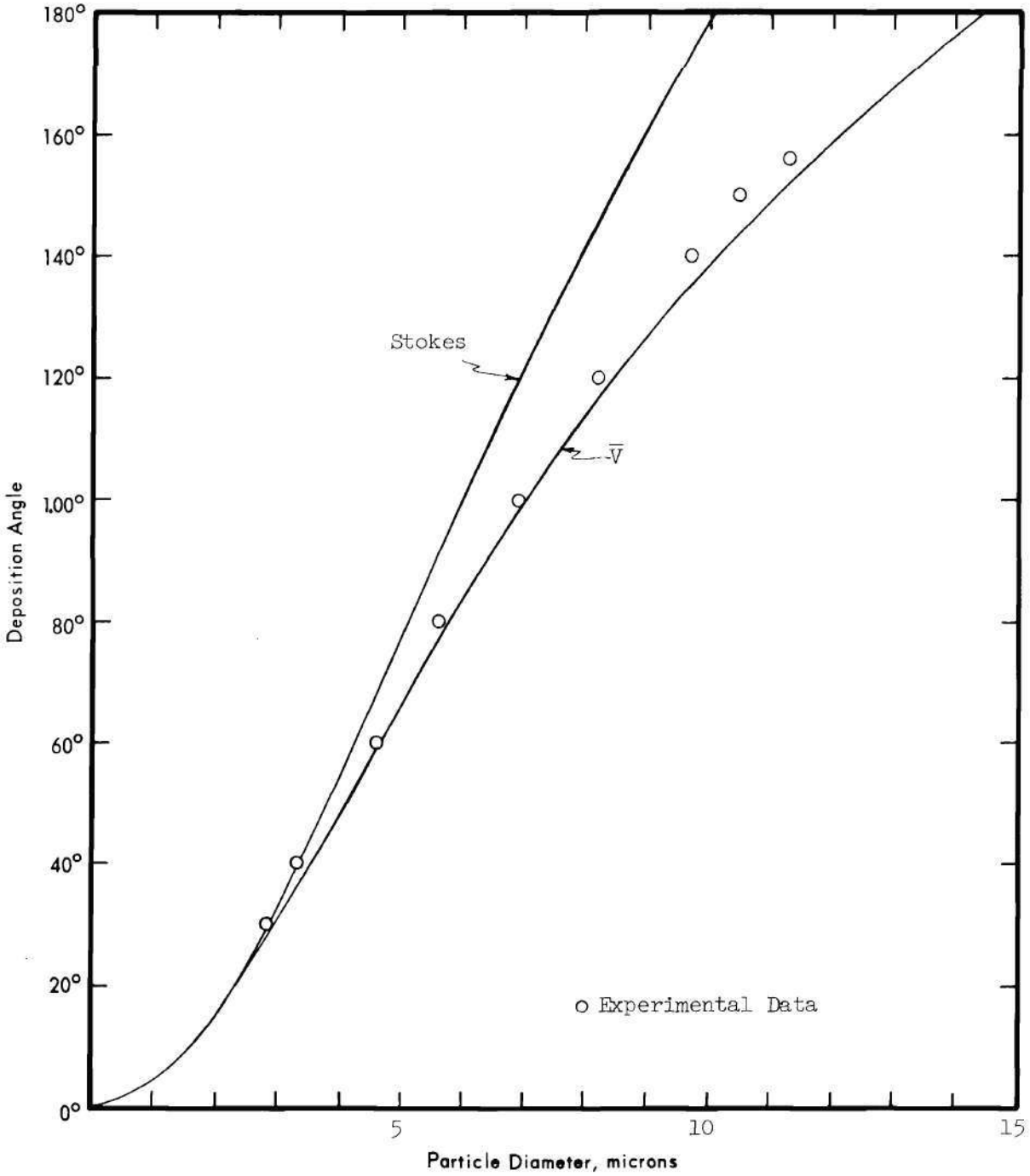

Figure 18. Comparison of Analog Computer Solutions Obtained Using Stokes Law and a More General Drag Relations with Experimental Data for Zinc Spheres. (Rotor Speed: 7200 rpm).

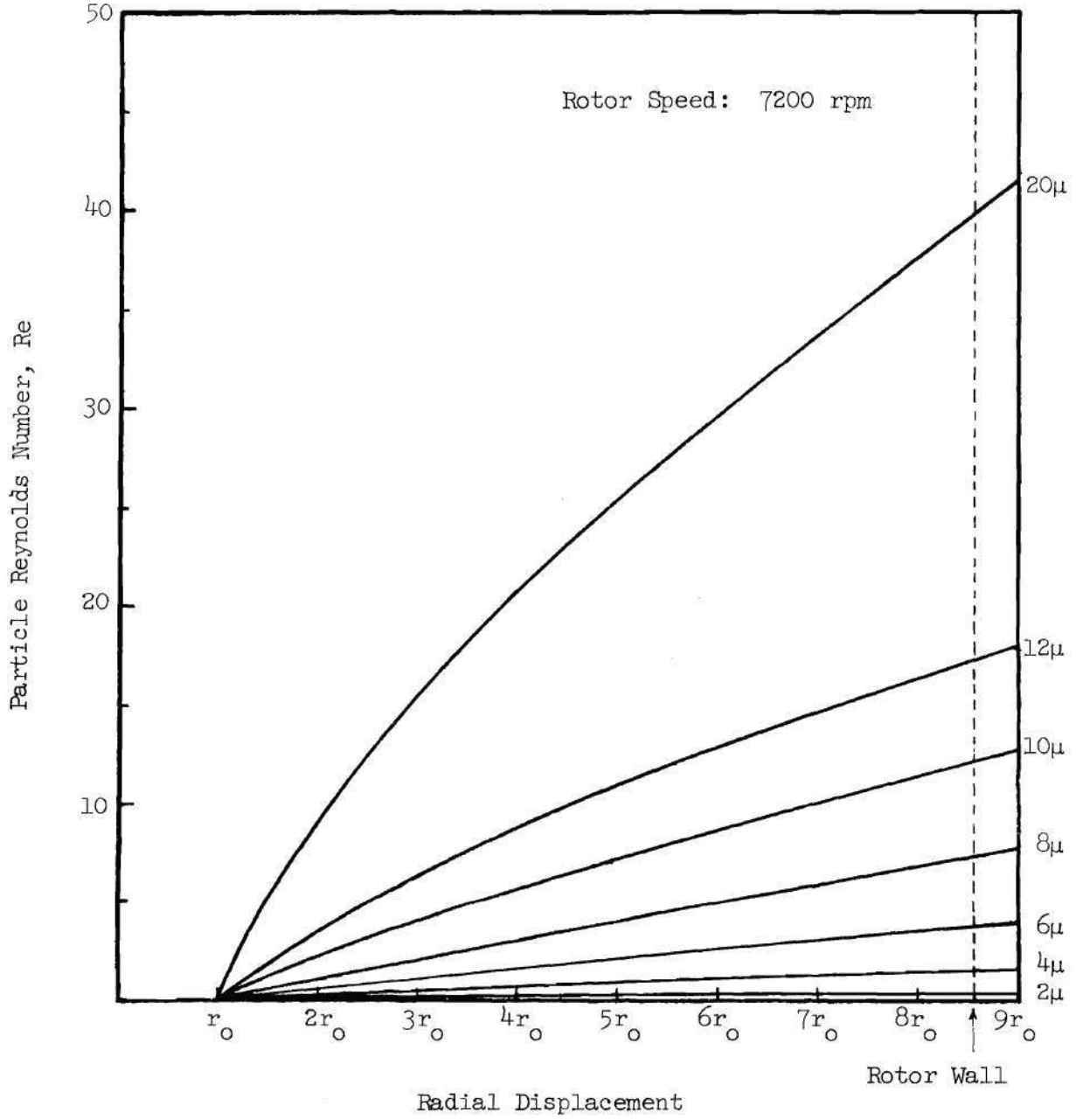

Figure 19. Variation of Particle Reynolds Number with Radial Displacement in a Forced Vortex of Air.

calculations indicate that all particles with diameters larger than about four microns had attained Reynolds numbers greater than one when they had reached radial displacements equivalent to the periphery of the rotor. Re-examination of Figure 17, which shows the "Stokes" and "$\overline{V}$" analog computer results for the same conditions as the Reynolds number plot of Figure 19, reveals that significant divergence in calculated results also begins to appear at a particle diameter of about four microns. Larger particle diameters with corresponding larger Reynolds numbers show much greater deviations from the Stokes law solution.

To obtain good separation of particles on a classifier rotor, it is evident from the relative trajectory curves shown in Appendix B that a large radial displacement is desirable. Unfortunately, this also leads to large particle Reynolds numbers and renders the Stokes law assumption inadequate. Thus it is apparent from theoretical considerations that Stokes law is not a valid assumption for the calculation of particle trajectories in a centrifugal classifier of the general type employed here.

The open circles shown on Figures 15, 16, 17, and 18 are experimental values obtained from the size distribution curves of Appendix D. Each experimental point represents the number mean diameter for the size distribution measured at that particular angular location. Agreement between experimental data and theoretical results predicted by analog computer solution of equations (45) and (46) in their more general form is thus shown to be excellent. This agreement therefore indicates that the mathematical model represented by equations (45) and (46) when using linear approximations for the best experimental values of drag coefficients describes the trajectories of particles in the centrifugal classifier of

this study and very closely predicts the actual size separations achieved. The experimental results furthermore confirm the theoretical prediction of the inadequacy of Stokes law for these conditions. Comparisons of theoretical and experimental results for the remaining conditions of operation are presented in Appendix E. Generally excellent agreement was obtained for all cases considered.

To indicate the reproducibility of the experimental data, Figure 20 shows experimental results for two entirely separate classifications of zinc particles under forced vortex conditions at 4800 rpm. The variation from run to run in experimentally measured number mean diameters of size distributions is here shown to be generally less than one micron at each angular position.

The size distributions measured at specified angular locations are shown in Appendix D. A perfect separation, i.e., an absolutely monodisperse system at each angular position, would be represented by a horizontal line on the log-probability size distribution plots. For angular locations larger than about 20 degrees, most of the size distributions of Appendix D appear as very nearly horizontal lines with quite small geometric standard deviations. Poorer results at the smaller angles (below 20 degrees) are probably due to flow irregularities in this region and the effects of the radial velocity of the fluid.

According to Figure 20, zinc particles larger than about 14 microns diameter in forced vortices equivalent to 4800 rpm and higher are not deposited on the rotor wall, instead they are deposited on one of the plastic webs which separate the rotor into two separate compartments. Figure 21 shows the calculated deposition points on this web for various

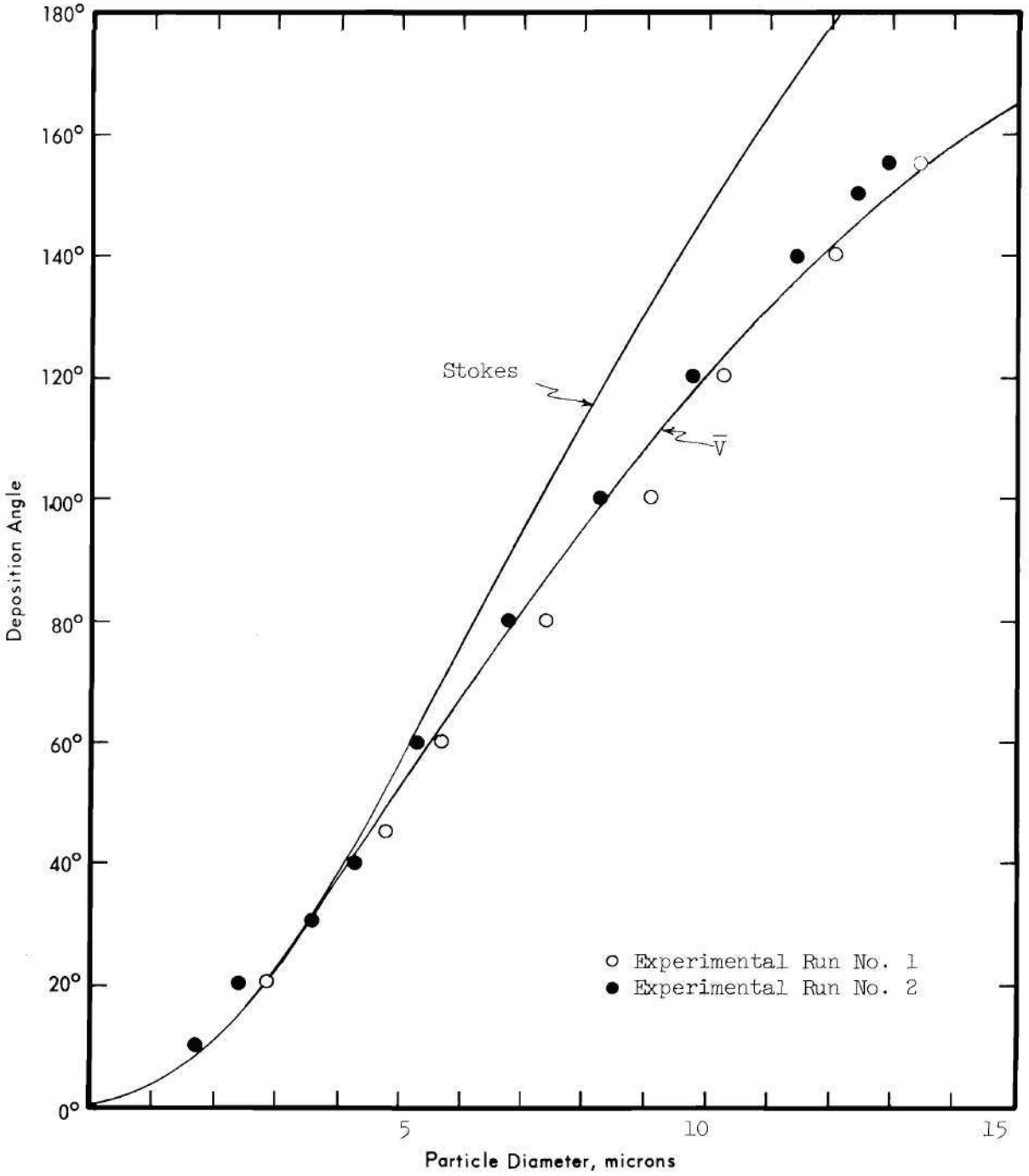

Figure 20. Comparison of Analog Computer Solutions Obtained Using Stokes Law and a More General Drag Relation with Experimental Data for Zinc Spheres for Two Separate Experimental Determinations. (Rotor Speed: 4800 rpm).

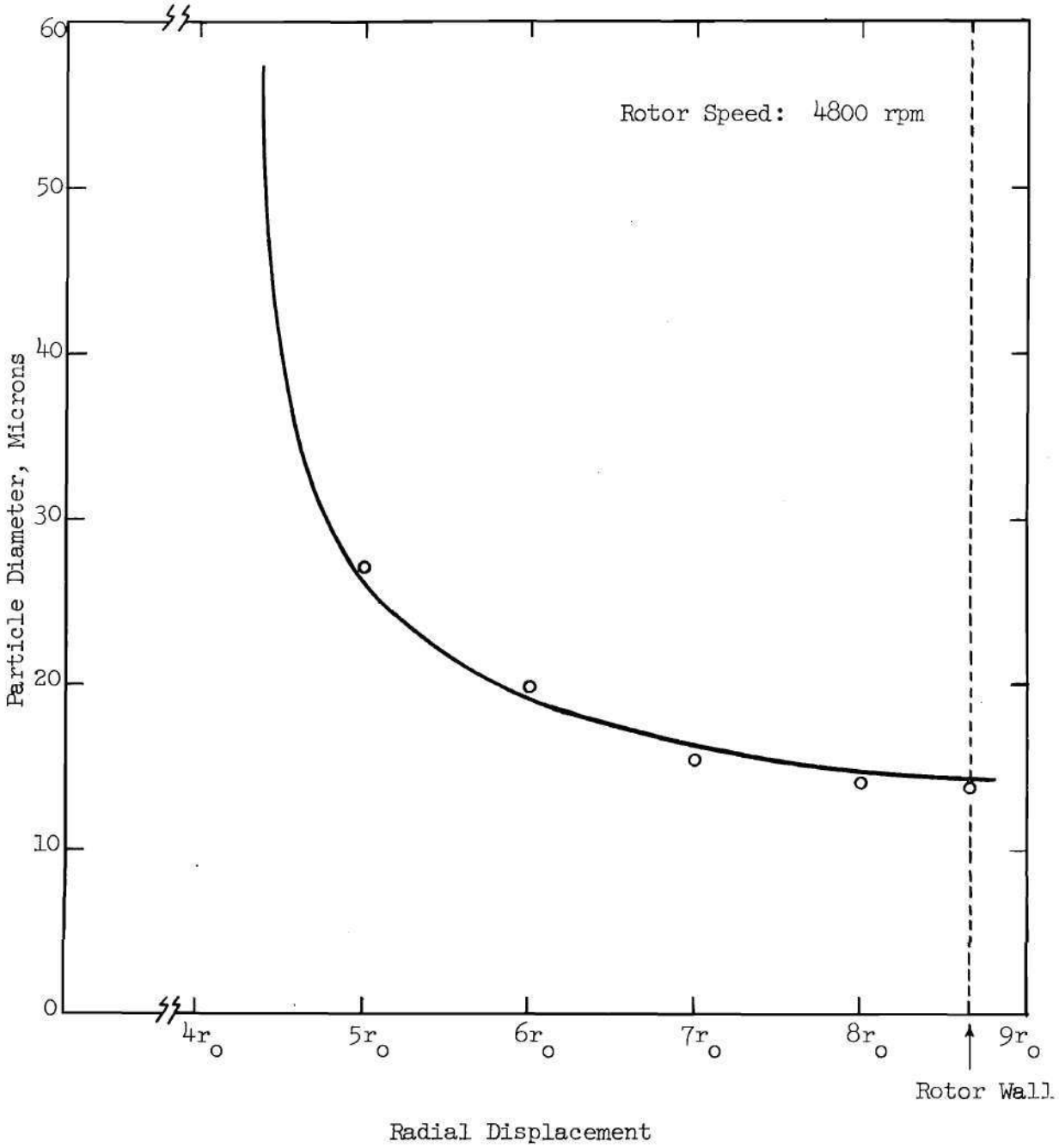

Figure 21. Calculated and Experimental Results for Various Diameter Zinc Spheres Deposited on the Rotor Web (Deposition Angles Greater than 160 Degrees).

particle diameters as determined from analog computer solutions of the more general forms of equations (45) and (46). The experimental points were obtained by placing a strip of pressure sensitive plastic tape with adhesive on both sides onto the plastic web. The larger particles striking the adhesive coated web adhered to the strip and later their diameters and relative positions on the strip were measured. Agreement between calculated and measured results was excellent for this case. However, in most cases significant classification could not consistently be achieved on the web because, after a single layer of particles adhered to the tape, those particles subsequently arriving at the web surface would slide outward along the web and collect at the intersection of the web and the rotor wall.

Figure 22 shows photomicrographs of the various angular deposition points for zinc particles collected at 9600 rpm. Examination of these photomicrographs confirms that the separations achieved were very clean; that is, there were essentially no small particles present in the large particles and vice versa. Probably the most signigicant feature of these photomicrographs is the absence of small particles among the larger particles. To isolate small particles from a distribution of particle sizes is generally not particularly difficult. However, none of the previous size classification techniques has been able to separate quantitatively the smaller particles when they are intermixed with large particle fractions. This difficulty arises from particle interactions such as small particles settling in the wake of large particles, inadequate particle dispersion, and electrostatic effects. Apparently the methods of aerosol generation, the low particle concentrations, and the

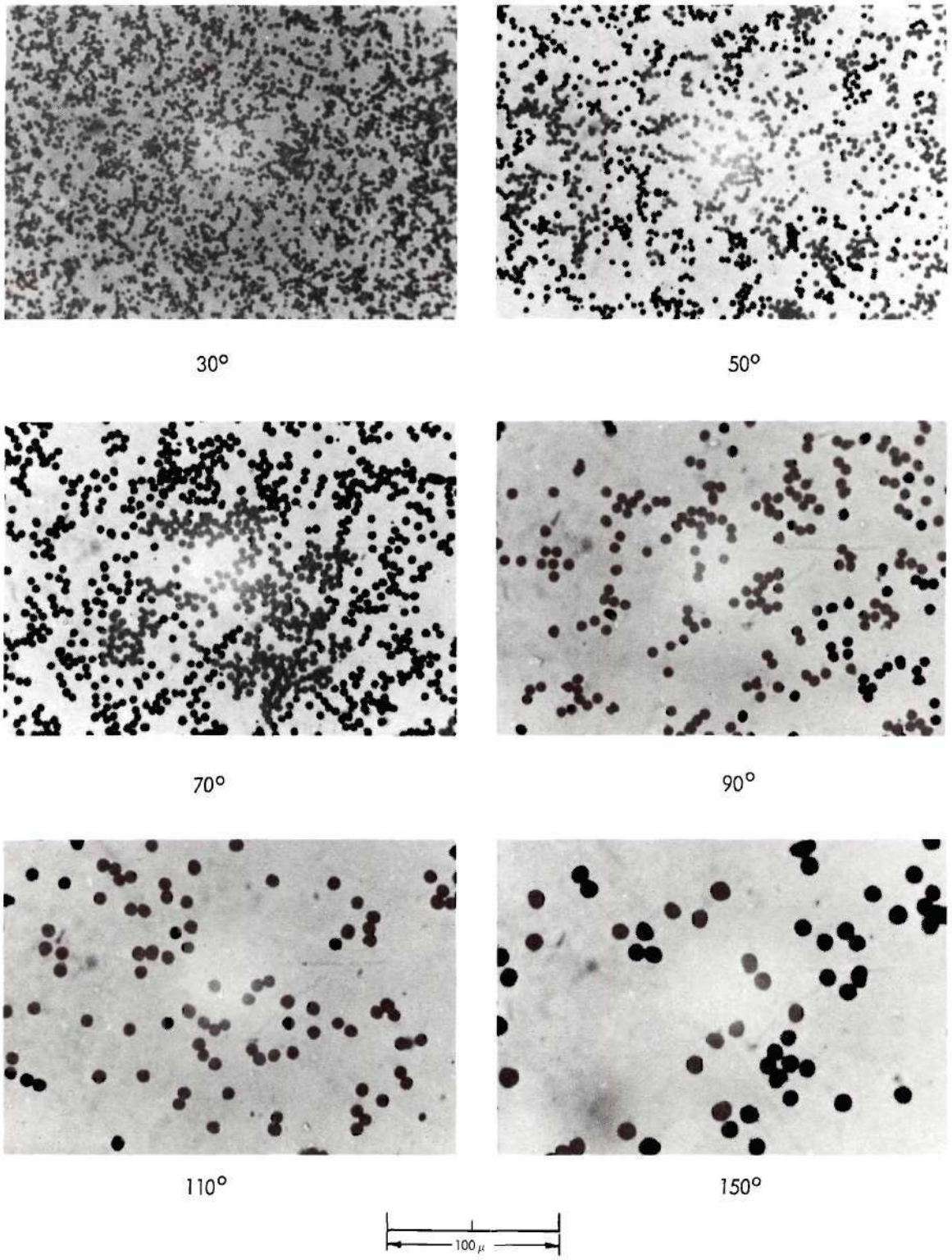

Figure 22. Photomicrographs of Zinc Particles Collected at Specified Locations in the Centrifugal Classifier Rotor. (Rotor Speed: 9600 rpm).

general separation procedure used in this study have eliminated many of these previous limitations and have resulted in exceptionally good separations at all size ranges. To illustrate further the separations achieved for the other materials of this study, Figures 23, 24, and 25 present photomicrographs at indicated angular locations and specified operating conditions. The extraneous materials evident on some of the photomicrographs are due primarily to irregularities in the adhesive on the pressure sensitive tape, dirt on the microscope lenses, air bubbles underneath the adhesive, etc.

Figure 26 illustrates by photomicrographs the separation according to settling diameters achieved for irregular shaped nickel oxide particles. Although it is difficult to arrive at meaningful size distributions for irregular particles and thus attach quantitative significance to the size separations, it is readily apparent that at least qualitatively significant size separation was achieved.

Figures 27, 28, 29, and 30 which were derived from the trajectory curves of Appendix B, show the variation of deposition angles with rotor speed for specified particle diameters. It is possible to determine from these curves what rotor speed should be used for particles of known density in order to achieve the best separation. Similar curves could also be prepared to illustrate the variation of deposition angle with varying particle densities and rotor speeds. Since all of these cross-plots merely represent methods to extrapolate and smooth theoretical calculations, only those of Figures 27-30 are presented to illustrate the procedure. Cross-plots of these types were used to correct theoretical results for assumed particle densities of 7.00 gm/cm^3 and 3.00 gm/cm^3 to

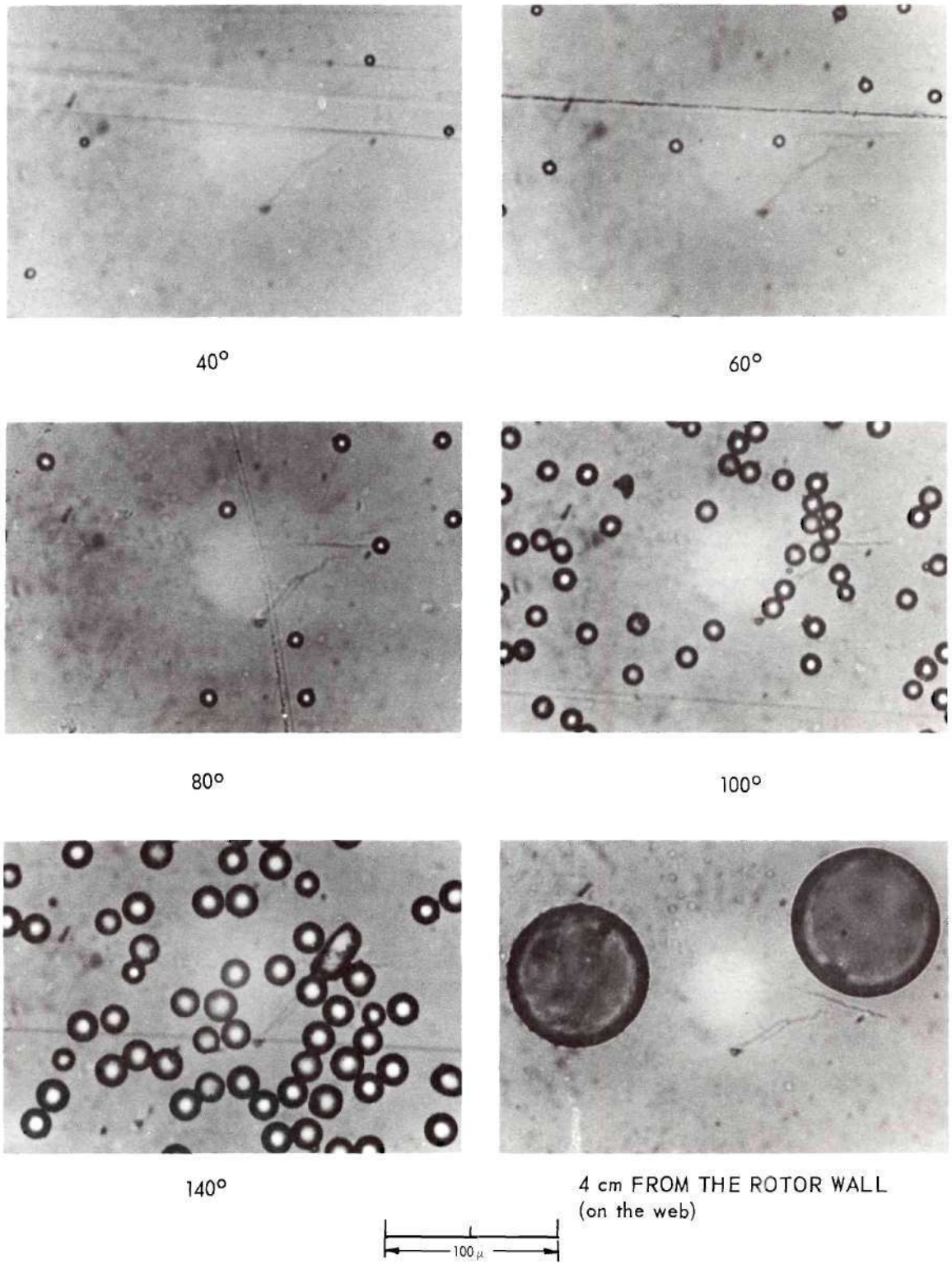

Figure 23. Photomicrographs of Glass Particles Collected at Specified Locations in the Centrifugal Classifier Rotor. (Rotor Speed: 7200 rpm).

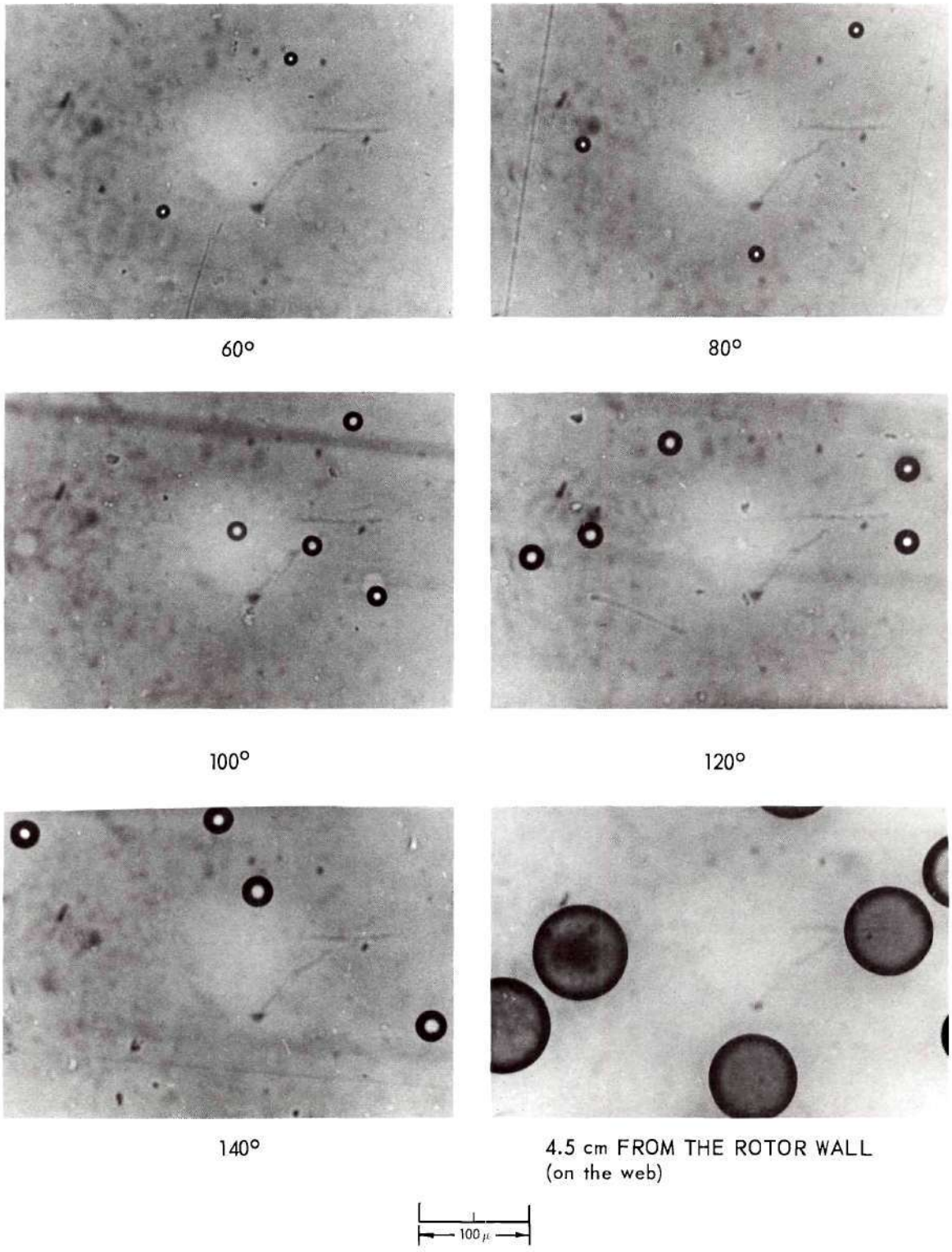

Figure 24. Photomicrographs of Plastic Particles Collected at Specified Locations in the Centrifugal Classifier Rotor. (Rotor Speed: 7200 rpm).

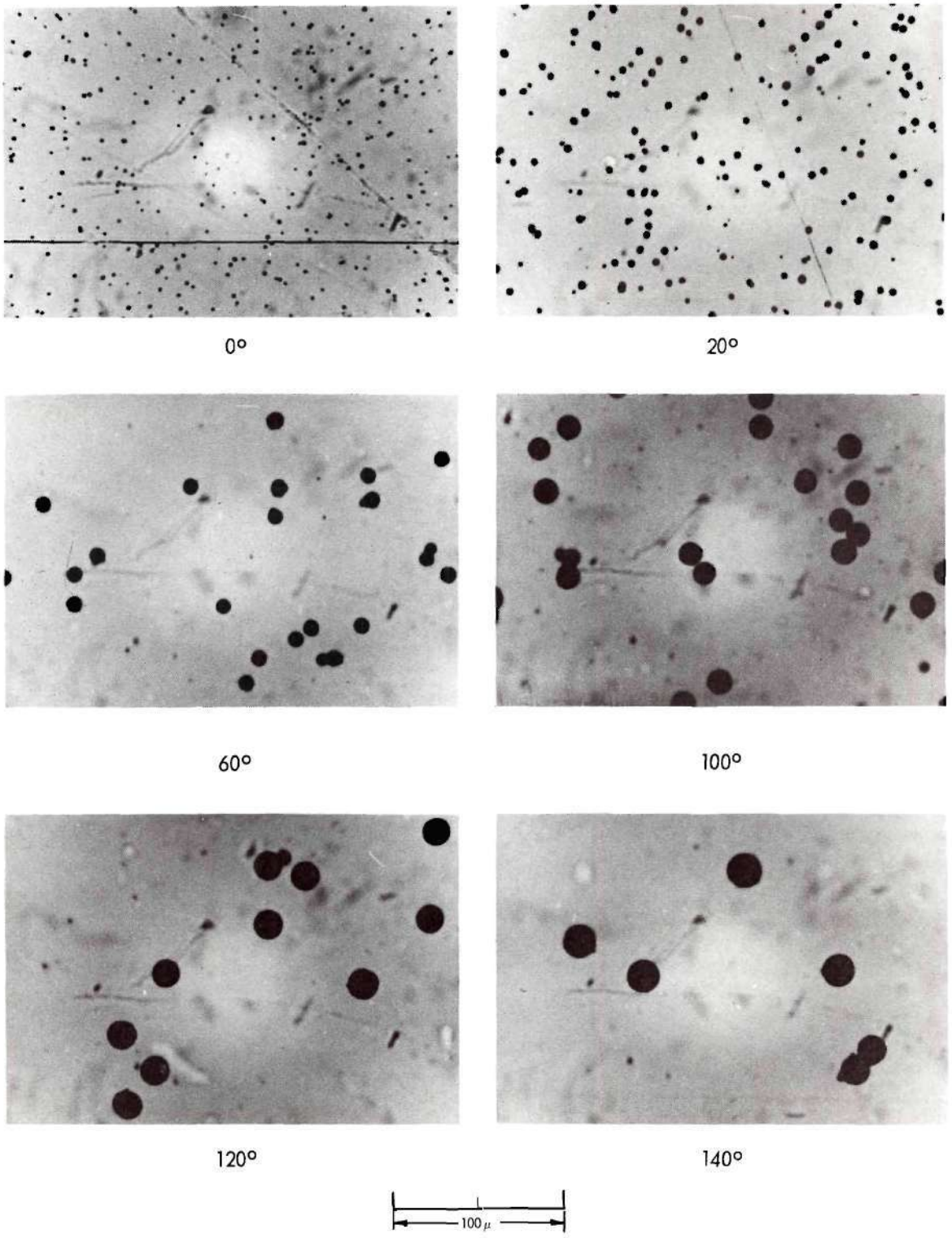

Figure 25. Photomicrographs of Aluminum Particles Collected at Specified Locations in the Centrifugal Classifier Rotor. (Rotor Speed: 7200 rpm).

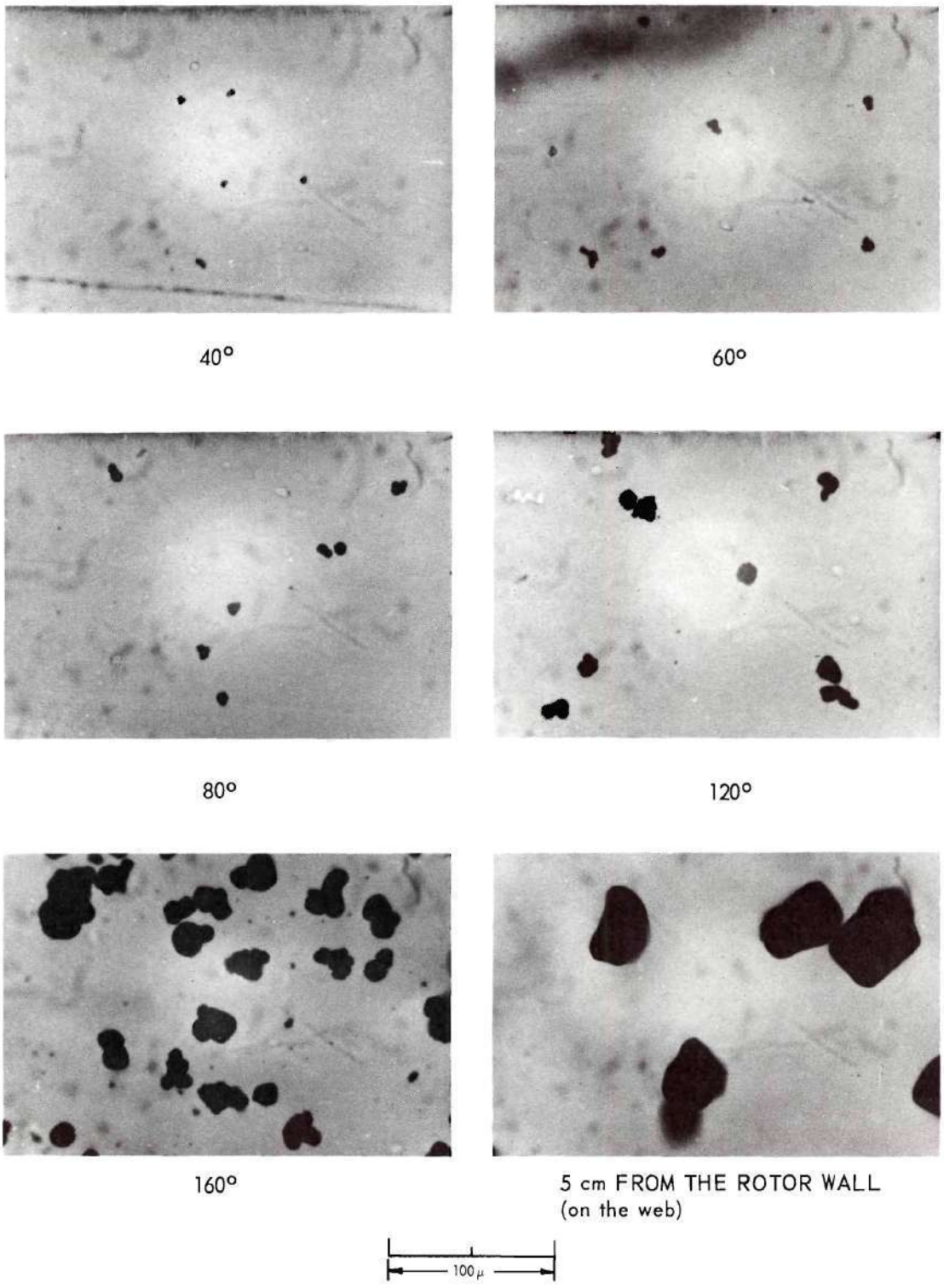

Figure 26. Photomicrographs of Nickel Oxide Particles Collected at Specified Locations in the Centrifugal Classifier Rotor. (Rotor Speed: 4800 rpm).

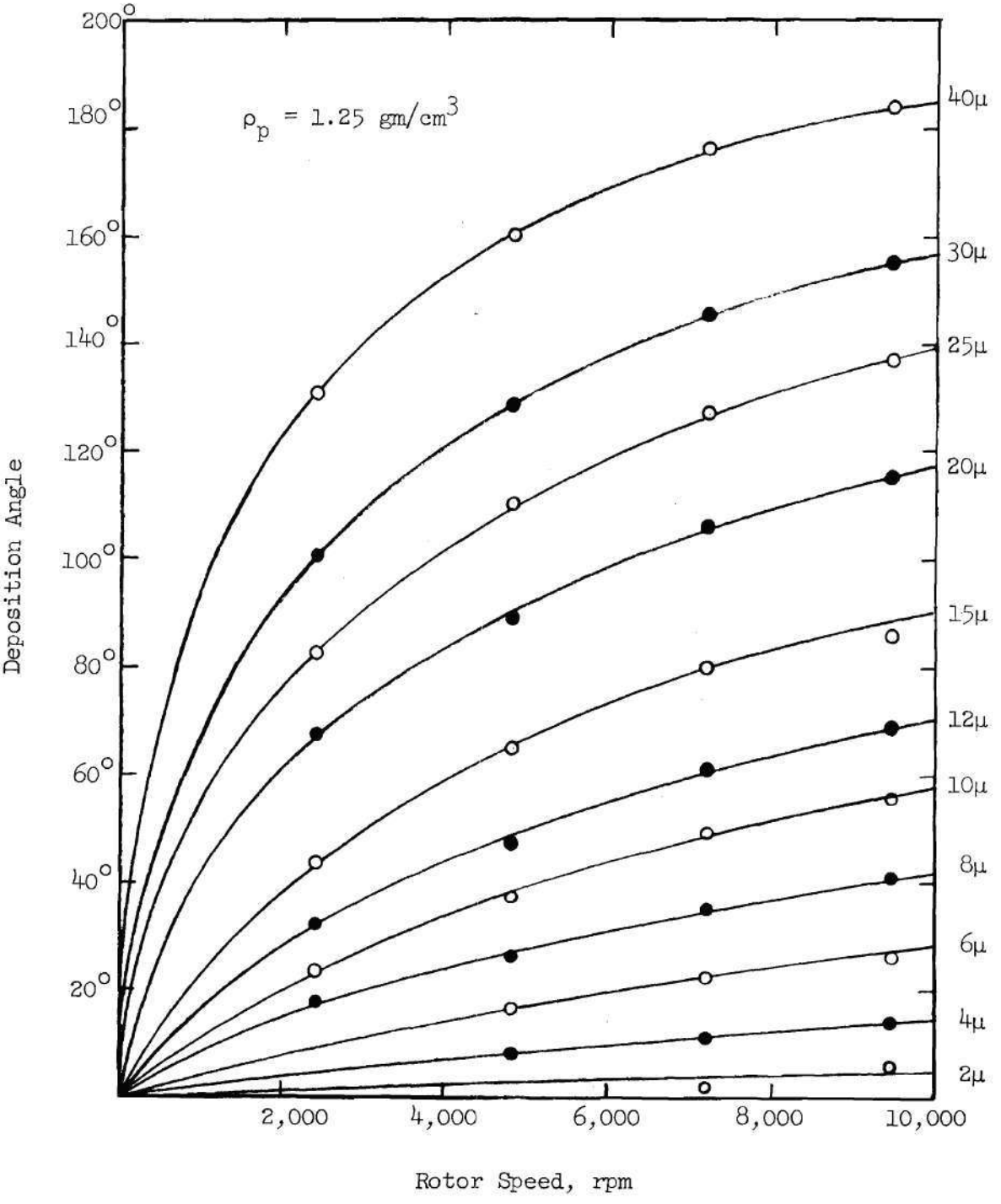

Figure 27. Variation of Deposition Angle with Rotor Speed for Spherical Particles with Density 1.25 gm/cm^3 in a Forced Vortex of Air.

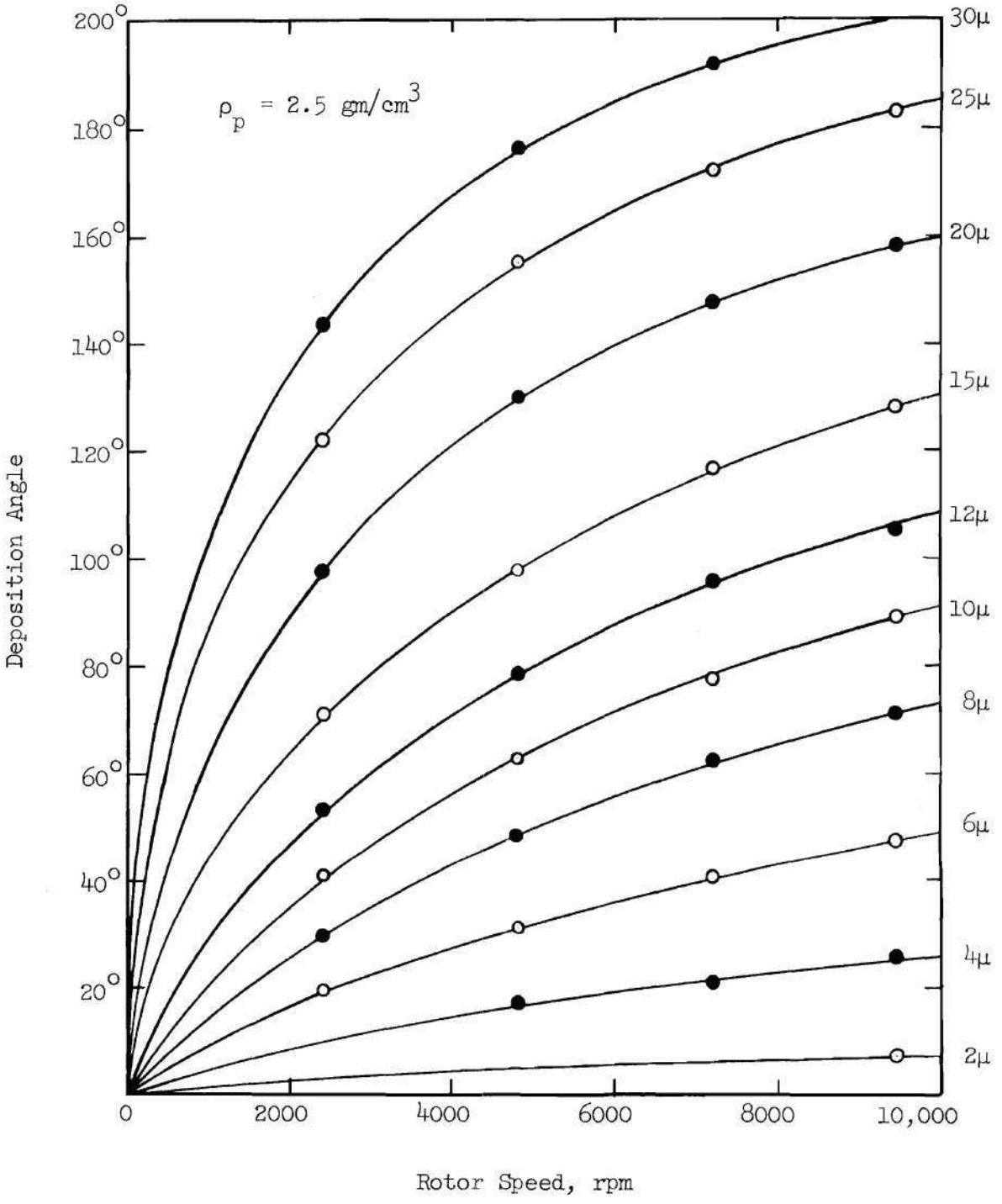

Figure 28. Variation of Deposition Angle with Rotor Speed for Spherical Particles with Density 2.5 gm/cm^3 in a Forced Vortex of Air.

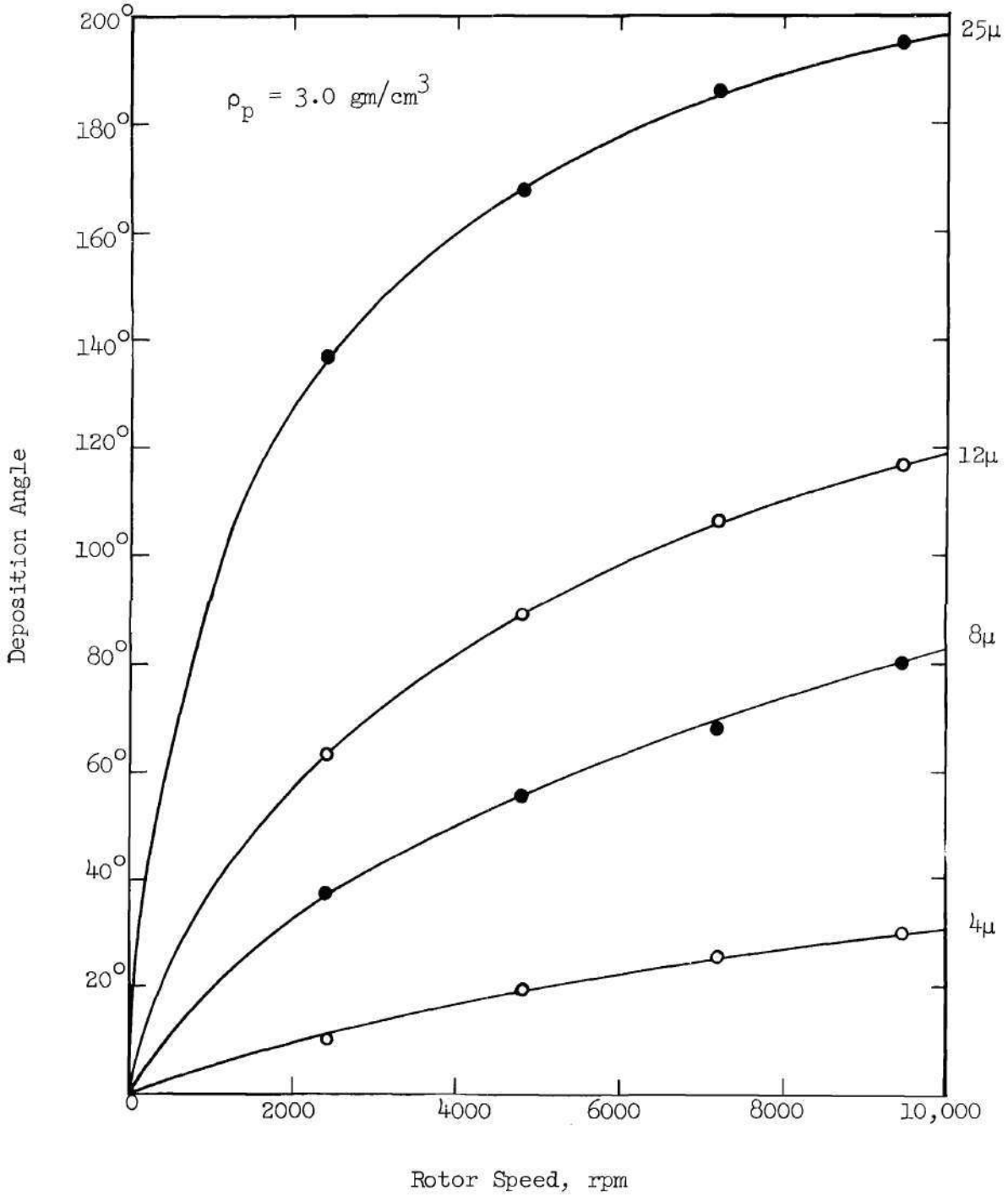

Figure 29. Variation of Deposition Angle with Rotor Speed for Spherical Particles with Density 3.0 gm/cm^3 in a Forced Vortex of Air.

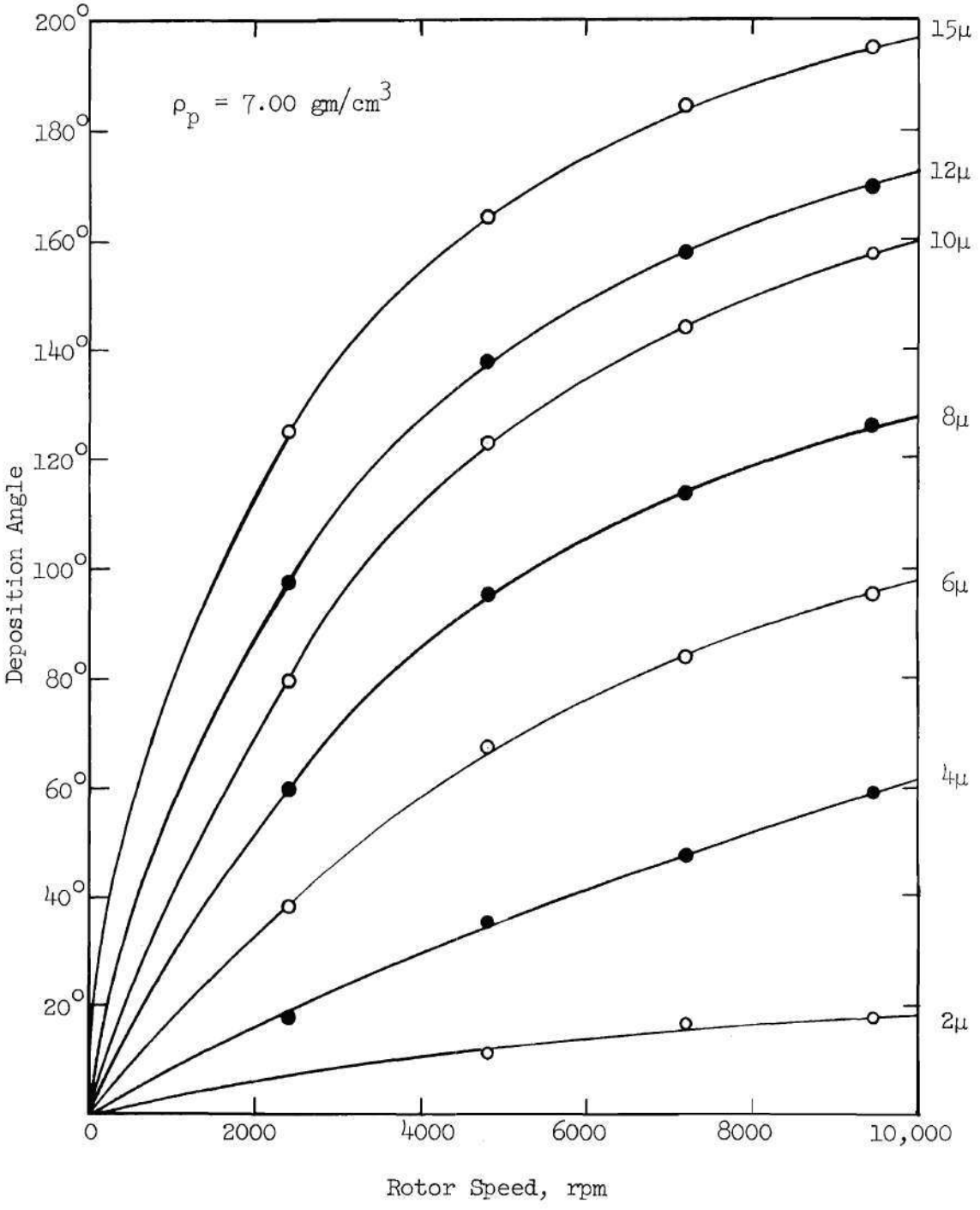

Figure 30. Variation of Deposition Angle with Rotor Speed for Spherical Particles with Density 7.00 gm/cm^3 in a Forced Vortex of Air.

the measured experimental values of 6.81 and 2.83 gm/cm^3 for zinc and aluminum, respectively.

Precision and Accuracy of Computer Solutions

Solution of ordinary differential equations is possible with digital computing equipment by the methods of numerical analysis. The accuracies of solutions thus obtained are limited primarily by practical considerations since compromises between step intervals and solution times required are usually necessitated. A digital computer program was written in "Algol" lanquage for use on the compiler of the Burroughs B-220 computer to solve equations (45) and (46) in their more general form. Extremely short step intervals were required for most of these solutions to proceed in a stable manner. This resulted in long computer times for each trajectory and rendered the numerical analysis scheme undesirable for this problem. Undoubtedly, refinements in the numerical analysis scheme are possible to allow satisfactory solution of these equations with digital computers. However, the analog computer was determined to be better suited for these solutions because of its general ease of programming, flexibility of operation insofar as changes of equation parameters are concerned, and the method of expressing solutions as a continuous curve directly analgous to the physical problem.

The accuracy characteristics of the digital computer are influenced primarily through the numerical methods used in solutions and in round-off errors. The judicious selection of numerical methods and step intervals generally produces results of the desired accuracy. The analog method of solution, however, represents a physical system by an

electrically analogous system and usually represents the differential equations within a small error. Additional errors are introduced by the physical limitations of precision resistors and capacitors, limitations of linear amplification, and drift of non-linear components. The overall accuracy of the solutions obtained with the analog computer is thus dependent on all of these factors plus cancellation of error effects, the precision to which adjustments are made, and the overall state-of-repair of the instrument. The precision of solutions obtained is primarily dependent upon the number and type of non-linear components, such as electronic multipliers, present in the program circuit. The precision of the solutions obtained with the analog program shown in Appendix A for solution of equations (45) and (46) was quite good, generally repeating solutions within the width of the recorder pen line.

The overall accuracy of the analog computer is obviously quite dependent on the complexity of the program circuity and no exact figure can be quoted. This can be determined to some extent, however, by comparison of computer results with test cases for which solutions are known. Fortunately, an analytical solution is available for equations (45) and (46) when Stokes law is assumed to describe the drag force. These same equations are also solvable with the computer program described in Appendix A for identical conditions when the output of the drag coefficient function generator is fixed at 24 volts. Table I shows deposition angles for various particle sizes as determined from the analytical and computer solutions of the same equations. Agreement between results was within $\pm$ 2 degrees, indicating that the overall accuracy for this case was very good.

Table 1. Comparison of Analytical and Analog Computer Results for the Trajectories of Spherical Particles having a Density of 3.0 gm/cm^3 in a Forced Vortex of Air When Stokes Law is Applicable (Radial Displacement = $4r_o$).

Particle Diameter, Microns	Analytical Value	Analog Computer Value
2	4.5^o	4.5^o
4	16.2^o	16.0^o
6	23.8^o	24.0^o
8	51.5^o	51.5^o
10	68.0^o	68.0^o
12	86.3^o	85.5^o
15	122.3^o	121.0^o

Rotor Speed = 7200 rpm
Initial Particle Radial Velocity = Zero
Initial Particle Angular Velocity = Angular Velocity of Rotor

The more general solutions of equations (45) and (46) introduce more non-linear components in the drag coefficient approximation and the $\bar{V}$ circuits. However, these components were generally quite stable in operation and in all probability only slight errors were introduced by them. Thus, if it is true that these additional components did not unduly affect the solutions, then the accuracy of the analog computer results of this study were generally quite high, probably within one or two per cent of actual values.

CHAPTER VI

CONCLUSIONS

The following statements summarize some of the more important conclusions reached in this investigation.

(1) An analysis involving the interaction of vortex and radial flow from a source at the axis of rotation provided a qualitatively correct description of the flow field in a newly designed particle classifier.

(2) Non-steady drag components and the slip correction were negligible for the range of particle sizes and fluid densities pertinent to this study. The lift force was also negligible since there were no strong shear gradients.

(3) The general equations of motion were developed for two-dimensional, non-steady motion of particles in a plane perpendicular to the axis of rotation within a viscous fluid. Simplified forms of the equations were developed for certain special cases.

(4) An analog computer program was developed which was capable of solving the equations of particle motion in their general and simplified forms for a wide range of vortex types, particle densities and diameters, and other operating conditions.

(5) Theoretical and experimental results indicate that particle classification under free vortex conditions in a rotor of the type used in this study is not feasible.

(6) The volumetric flow rate of aerosol into the classifier rotor must be low enough that near-perfect forced vortex conditions exist in order to achieve the best size separations.

(7) Optimum size classification results when particles enter a forced vortex centrifugal field with the same tangential velocity as the fluid and with zero initial radial velocity. Injection of particles into the rotor at large radial velocities causes standing vortices near the entry region and further causes intersections of large and small particle trajectories.

(8) A very narrow entry slot must be provided to minimize uncertainty as to the location of a particle at the instant it enters the classification chamber.

(9) Particle Reynolds numbers quickly exceed unity for typical operating conditions and Stokes drag law is invalid for accurate estimates of drag coefficients.

(10) Analog computer solutions of the more general form of the equations of particle motion wherein linear approximations of the best experimental values for the drag coefficients were used yielded results which were in excellent agreement with experimental values.

(11) An experimental particle classifier was developed and demonstrated to be highly effective in the classification by size of spherical particles having diameters from about one to 50 microns and a wide range of particle densities.

(12) Separating irregular particles according to size was also shown to be possible.

CHAPTER VII

RECOMMENDATIONS

This investigation created new problems worthy of further study even though it achieved most of the results desired initially. One of the first of these involves the fluid mechanics of various types of vortex flow. More detailed studies in this area would probably first require either analog computer or numerical solution of the more complete Navier-Stokes equations. Experimental studies, such as extensions of the flow visualization portion of this investigation, might be used to confirm or reject these later theoretical results. A specific problem of interest would be the interaction of a near-perfect forced vortex with a flat jet emerging into a semi-infinite chamber. This model closely approximates the physical situation within the classifier rotor of this study.

The aerosol flow rates employed herein were based primarily on the maximum diameter of the hole located in the rotor wall directly opposite the aerosol entry slot which gave a near-perfect forced vortex at 1,600 rpm. This was the lowest speed at which stable rotor speeds could be maintained, therefore the flow rate which would permit satisfactory operation at this and higher speeds. To permit larger quantities of materials to be classified per unit time, further studies should be made to determine the optimum aerosol flow rates as a function of rotor speed which permit satisfactory operation.

A narrower aerosol entry slot should be provided to locate more precisely each particle as it enters the classification chamber. This, of course, would lessen the deviation in deposition angles and permit more complete separations at each angular location on the rotor wall.

Additional studies should be made under conditions such that non-steady drag effects and lift components are significant. These forces are undoubtedly important when the densities of the suspending fluid and particles are comparable and might be expected to yield valuable information on performance limitations of centrifugal clarifiers, filters, and the like. Operation of the classifier rotor used in this study at very high speeds, i.e. 25,000 rpm, and reduced pressures might well result in extension of the operating range to sub-micron levels. The slip effect for sub-micron particles at reduced pressures would probably be significant and should be included in theoretical analyses.

A classifier rotor such as built for this work should be operated under very high speed conditions to allow the air flow spirals to intersect the rotor wall at about 40 degrees, for example. Since there is no hole in the rotor wall at 40 degrees, the fluid must reverse its direction and move toward the hole in the rotor wall located at zero degrees. This flow pattern would permit all of those particles larger than about one micron to deposit at angular positions greater than 40 degrees. Hopefully, the sub-micron particles would then be separated in the angular region from 40 to zero degrees. Innovations such as this, possibly combined with low pressure operation, might extend the separation range well down into the sub-micron region.

A slotted web should be used to prevent those particles which

impinge on the web from sliding outward to the rotor wall. This modification would extend the effective deposition range from 160 degrees to about 240 degrees.

Further analog and digital computer solutions should be sought for the equations of particle motion under many different conditions. One area of particular interest would be solutions for the case in which the particle moves radially inward as in the free-vortex types of classifiers. Such solutions would be quite useful in establishing performance limits for this type of classifier.

APPENDIX A

ANALOG COMPUTER PROGRAM

Equations (45) and (46) which are the most general forms of the equations of particle motion for the conditions of this study were transformed from real to machine parameters, time-scaled, and solved by the analog computer. Provision was made in the computer program to vary the type of fluid vortex motion by making the exponent n of equation (23) continuously variable from zero to minus two. A diode function generator was used to approximate the best experimental values of the product of the particle drag coefficient and Reynolds number versus Reynolds number. Figure 3 illustrated the experimental values used and the straight line approximations of the function generator. Representing the data in this manner was particularly satisfactory because the output of the function generator was, in effect, the product of the drag coefficient and the relative particle velocity. This type of output eliminated the need for an additional multiplier which would have been required had the drag coefficient alone been the output.

The major components used in the analog computer circuit and their purpose is given by Figure 31. The complete circuit required for the solution of equations (45) and (46) is given by Figure 32. Recorder outputs were provided to permit plots of absolute particle trajectories, trajectories relative to the fluid or rotor, particle Reynolds number and any other intermediate parameters of interest.

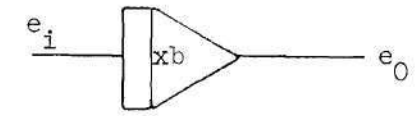

Integrating Amplifier

$$e_0 = -b\int_0^t e_i dt$$

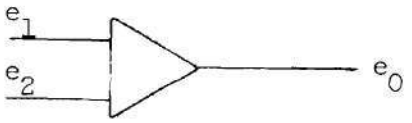

Summing or Inverting Amplifier

$$e_0 = -\sum e_i$$

Special Purpose Amplifier

$$e_0 = -e_i$$

Potentiometer

$$e_0 = ke_i$$

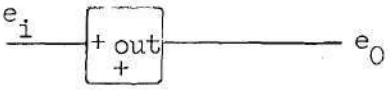

Fixed Diode Function Generator

$$e_0 = -k \log e_i$$

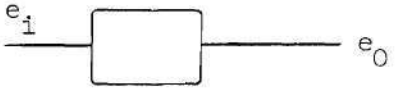

Diode Function Generator

$$e_0 = f(e_i)$$

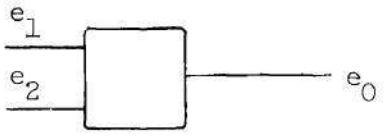

Electronic Multiplier

$$e_0 = -ke_1e_2$$

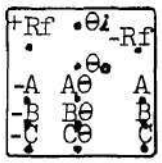

Electro-Mechanical Resolver

Multi-Purpose

$$e_0 = ke_i$$
$$e_0 = ke_1/e_2$$
$$e_0 = ke_1e_2, \text{ etc.}$$

Figure 31. Major Analog Computer Components

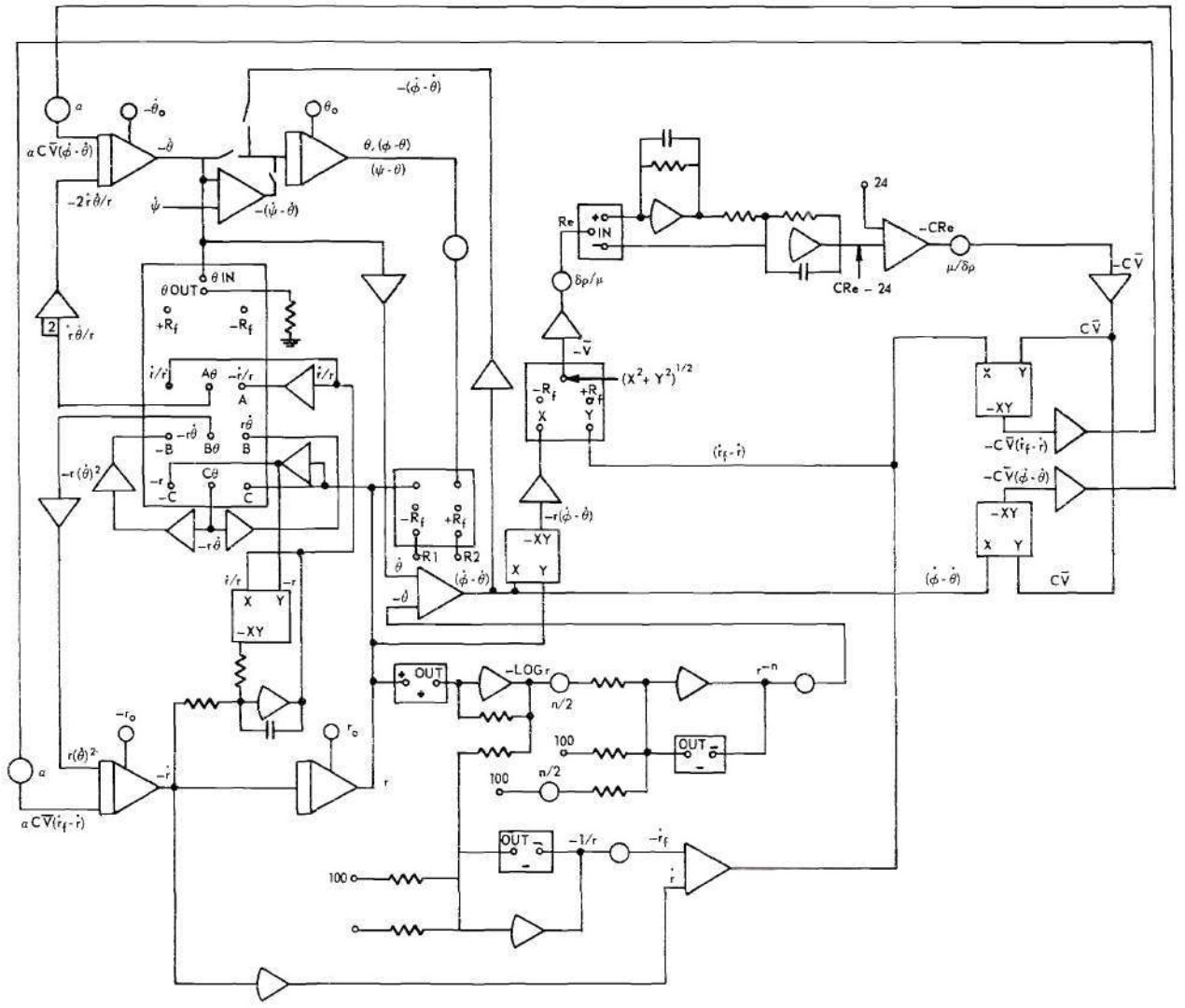

Figure 32. Analog Computer Circuit Diagram.

APPENDIX B

ANALOG COMPUTER SOLUTIONS

This section contains the analog computer solutions for the trajectories of spherical particles relative to a constant speed rotor. All solutions were calculated with the assumption of forced vortex conditions and the applicability of a general drag law.

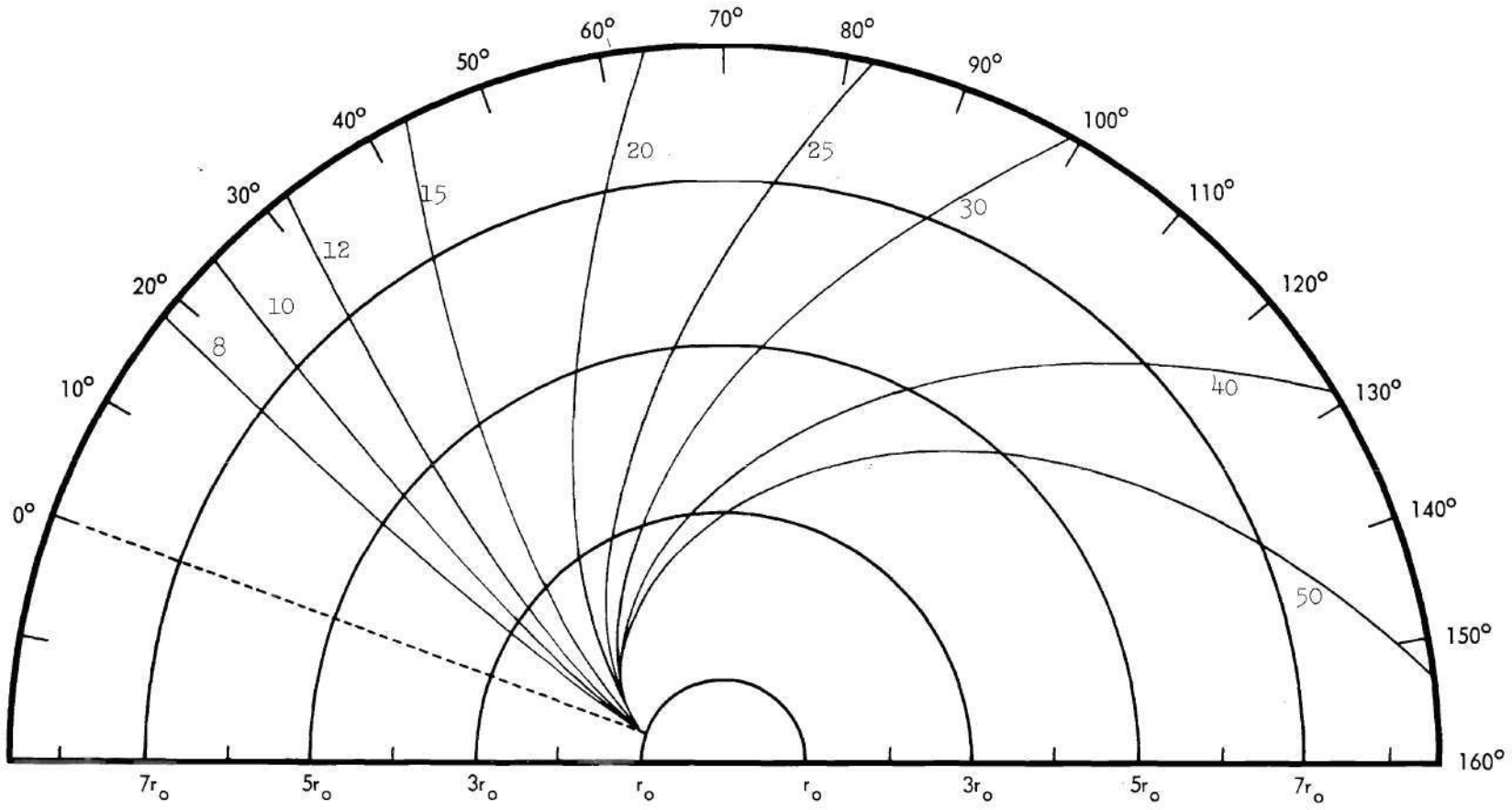

Figure 33. Analog Computer Solutions for the Trajectories of Spherical Particles having a Density of 1.25 gm/cm^3 Relative to a Constant Speed Rotor for Forced Vortex Conditions in which a General Drag Relationship is Assumed Valid. (Rotor Speed: 2400 rpm).

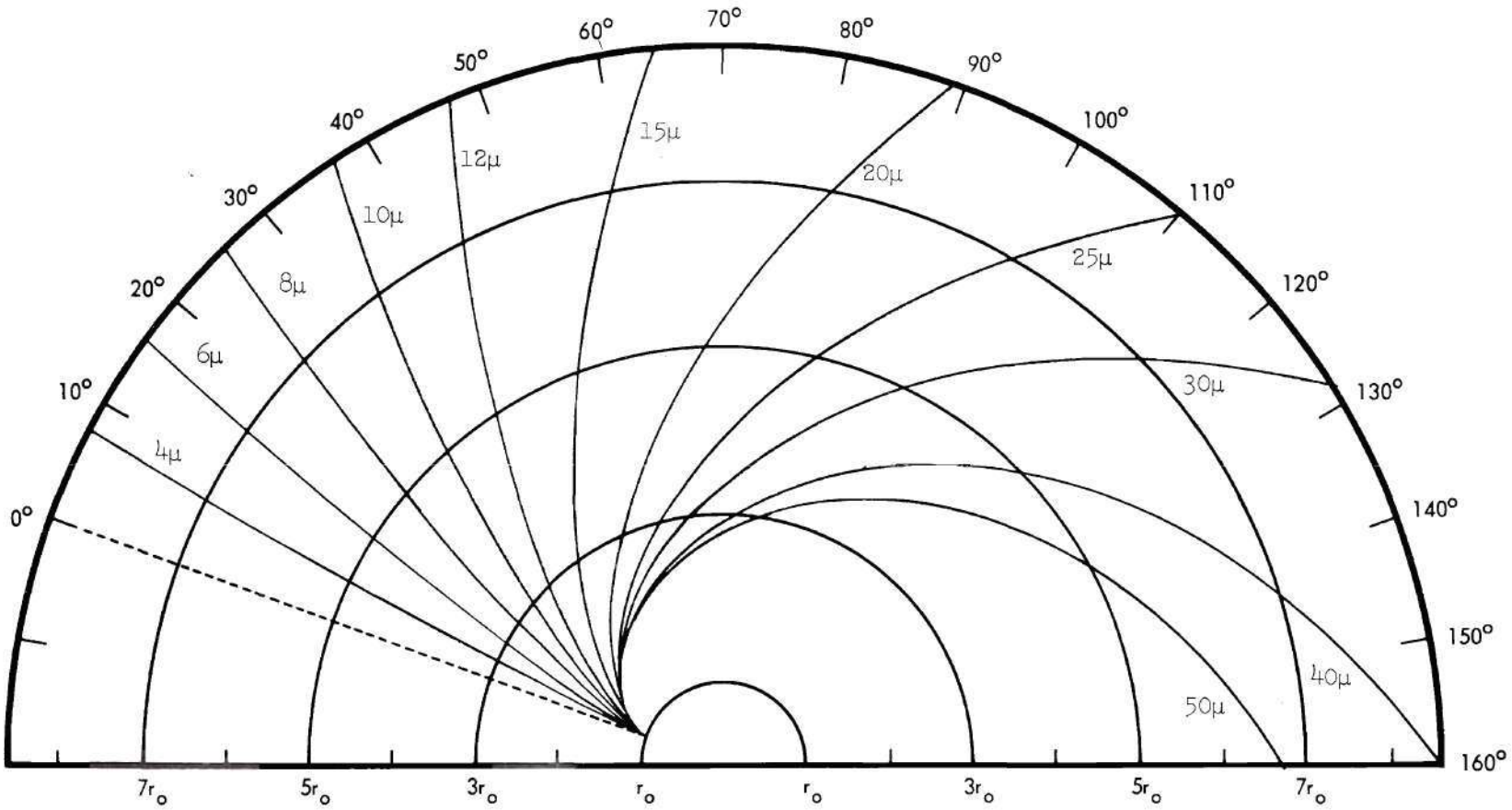

Figure 34. Analog Computer Solutions for the Trajectories of Spherical Particles having a Density of 1.25 gm/cm^3 Relative to a Constant Speed Rotor for Forced Vortex Conditions in which a General Drag Relationship is Assumed Valid. (Rotor Speed: 4800 rpm).

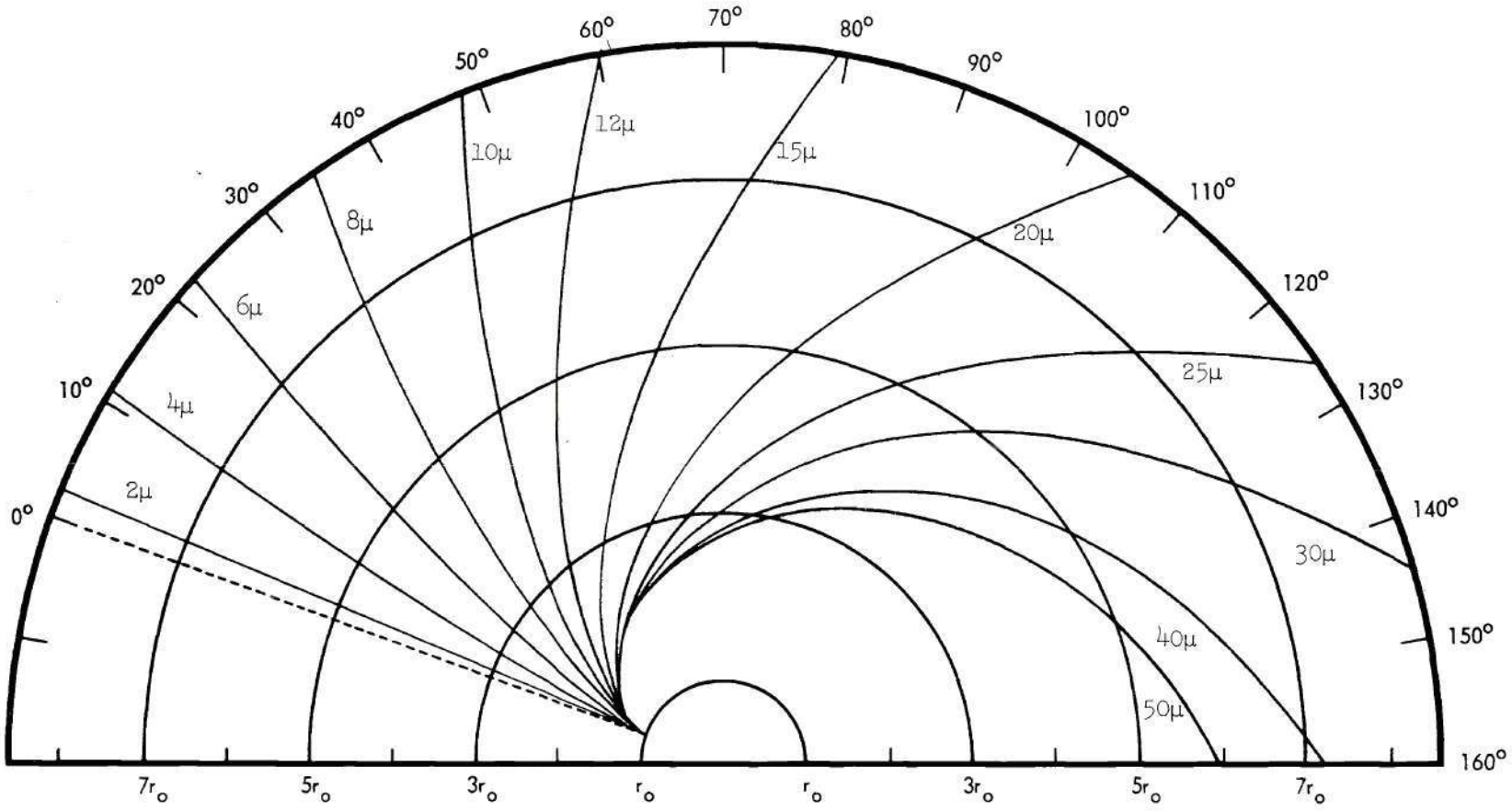

Figure 35. Analog Computer Solutions for the Trajectories of Spherical Particles having a Density of 1.25 gm/cm^3 Relative to a Constant Speed Rotor for Forced Vortex Conditions in which a General Drag Relationship is Assumed Valid. (Rotor Speed: 7200 rpm).

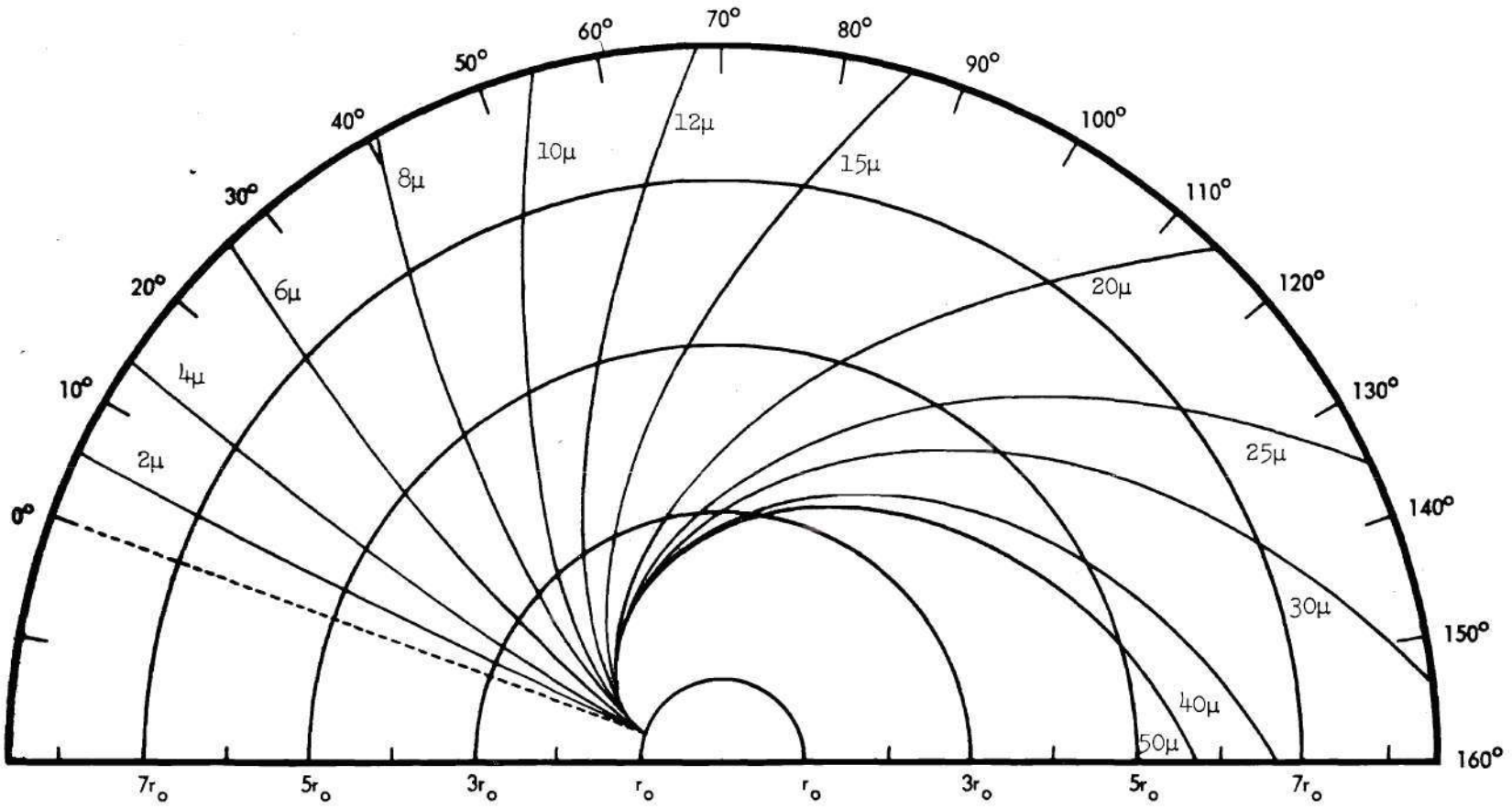

Figure 36. Analog Computer Solutions for the Trajectories of Spherical Particles having a Density of 1.25 gm/cm^3 Relative to a Constant Speed Rotor for Forced Vortex Conditions in which a General Drag Relationship is Assumed Valid. (Rotor Speed: 9600 rpm).

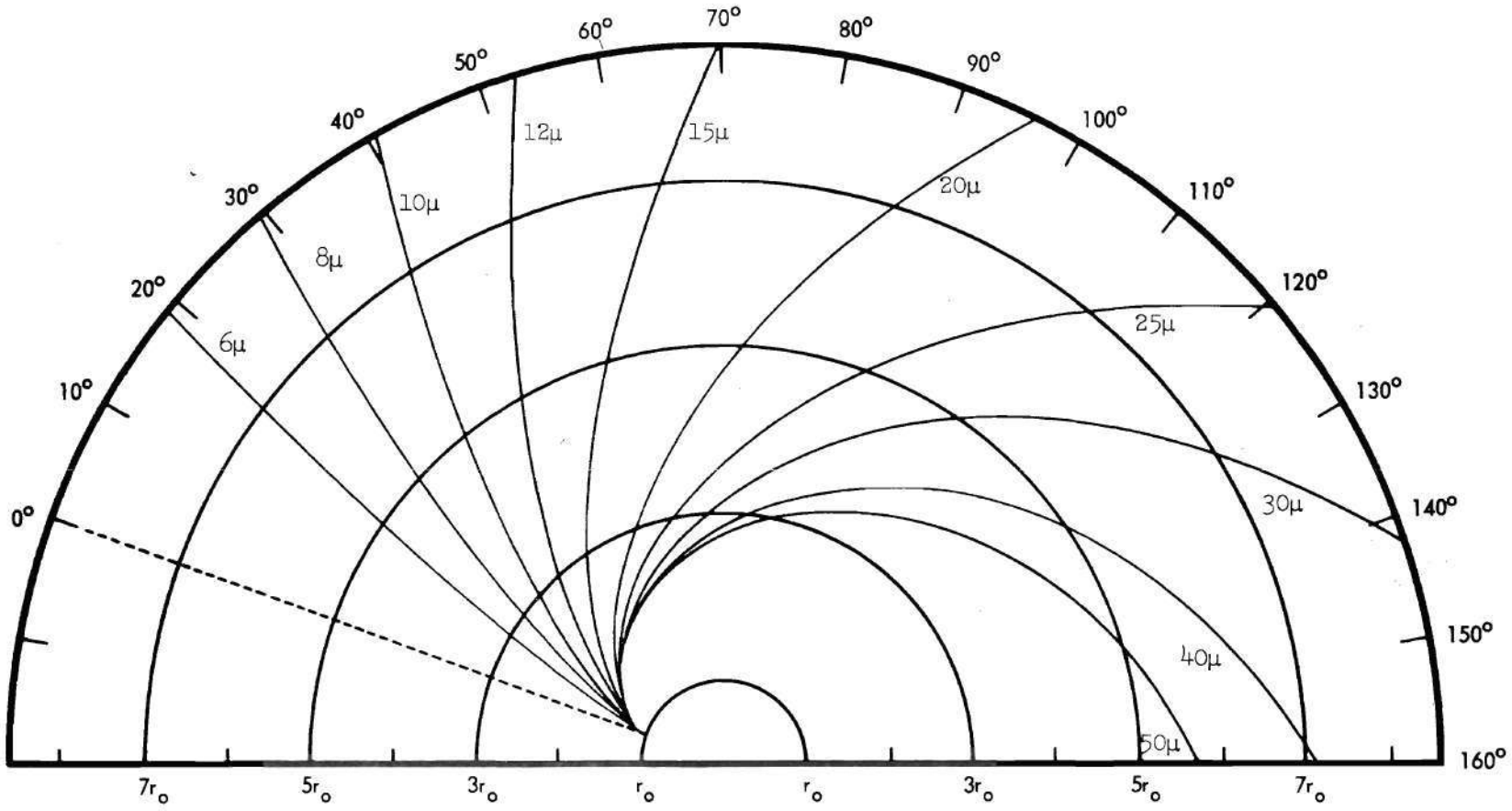

Figure 37. Analog Computer Solutions for the Trajectories of Spherical Particles having a Density of 2.5 gm/cm^3 Relative to a Constant Speed Rotor for Forced Vortex Conditions in which a General Drag Relationship is Assumed Valid. (Rotor Speed: 2400 rpm).

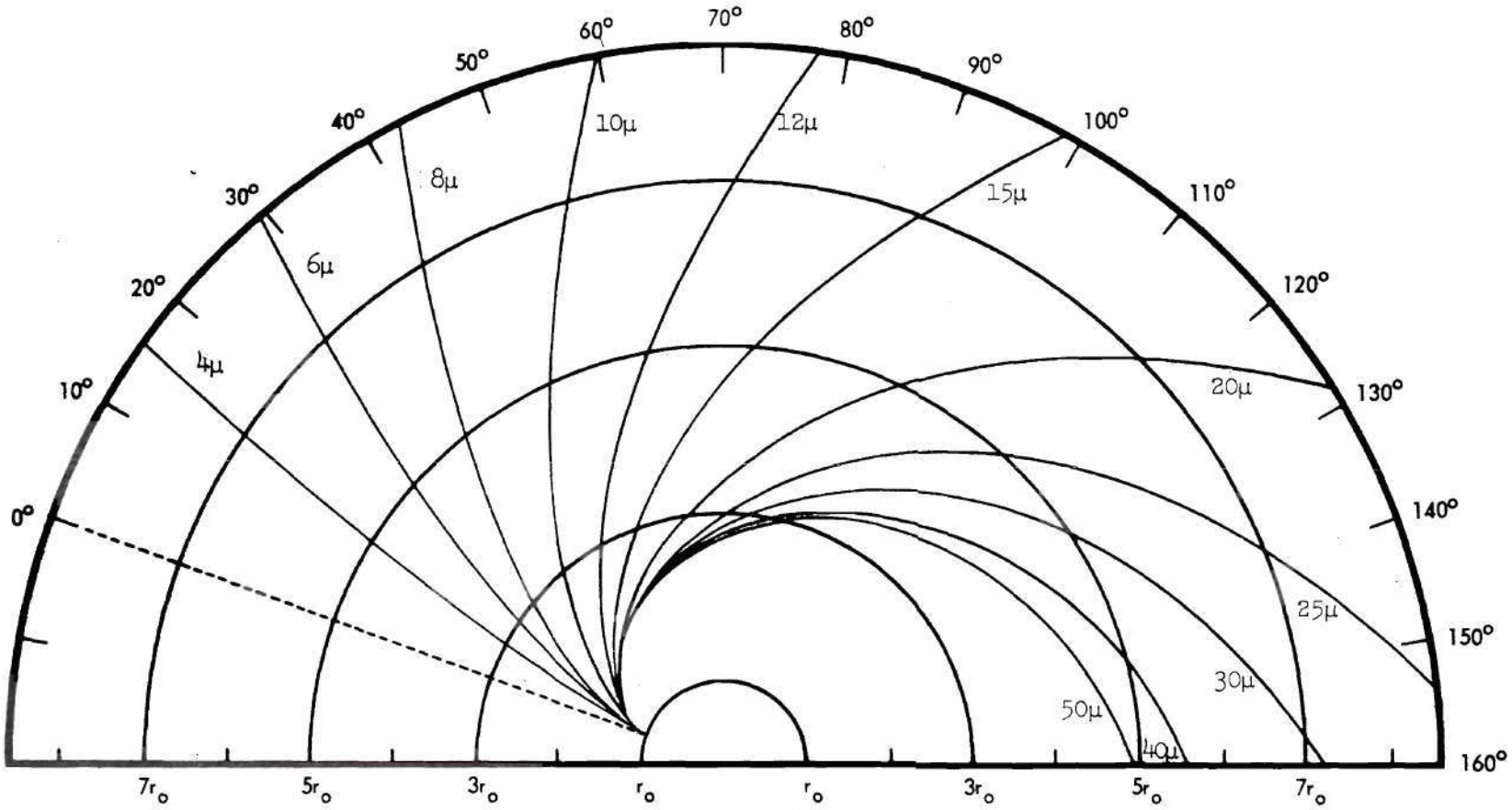

Figure 38. Analog Computer Solutions for the Trajectories of Spherical Particles having a Density of 2.5 gm/cm^3 Relative to a Constant Speed Rotor for Forced Vortex Conditions in which a General Drag Relationship is Assumed Valid. (Rotor Speed: 4800 rpm).

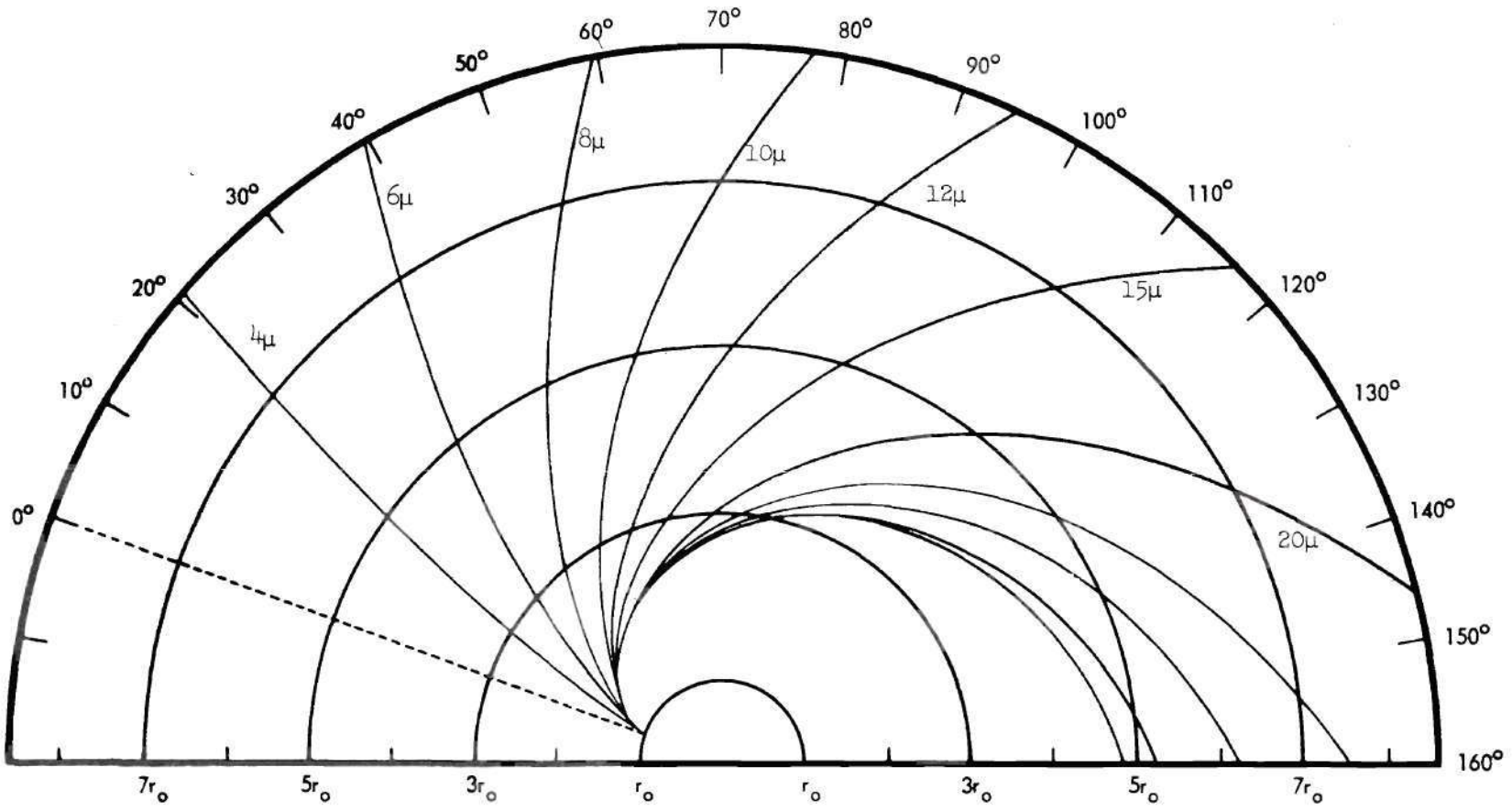

Figure 39. Analog Computer Solutions for the Trajectories of Spherical Particles having a Density of 2.5 gm/cm^3 Relative to a Constant Speed Rotor for Forced Vortex Conditions in which a General Drag Relationship is Assumed Valid. (Rotor Speed: 7200 rpm).

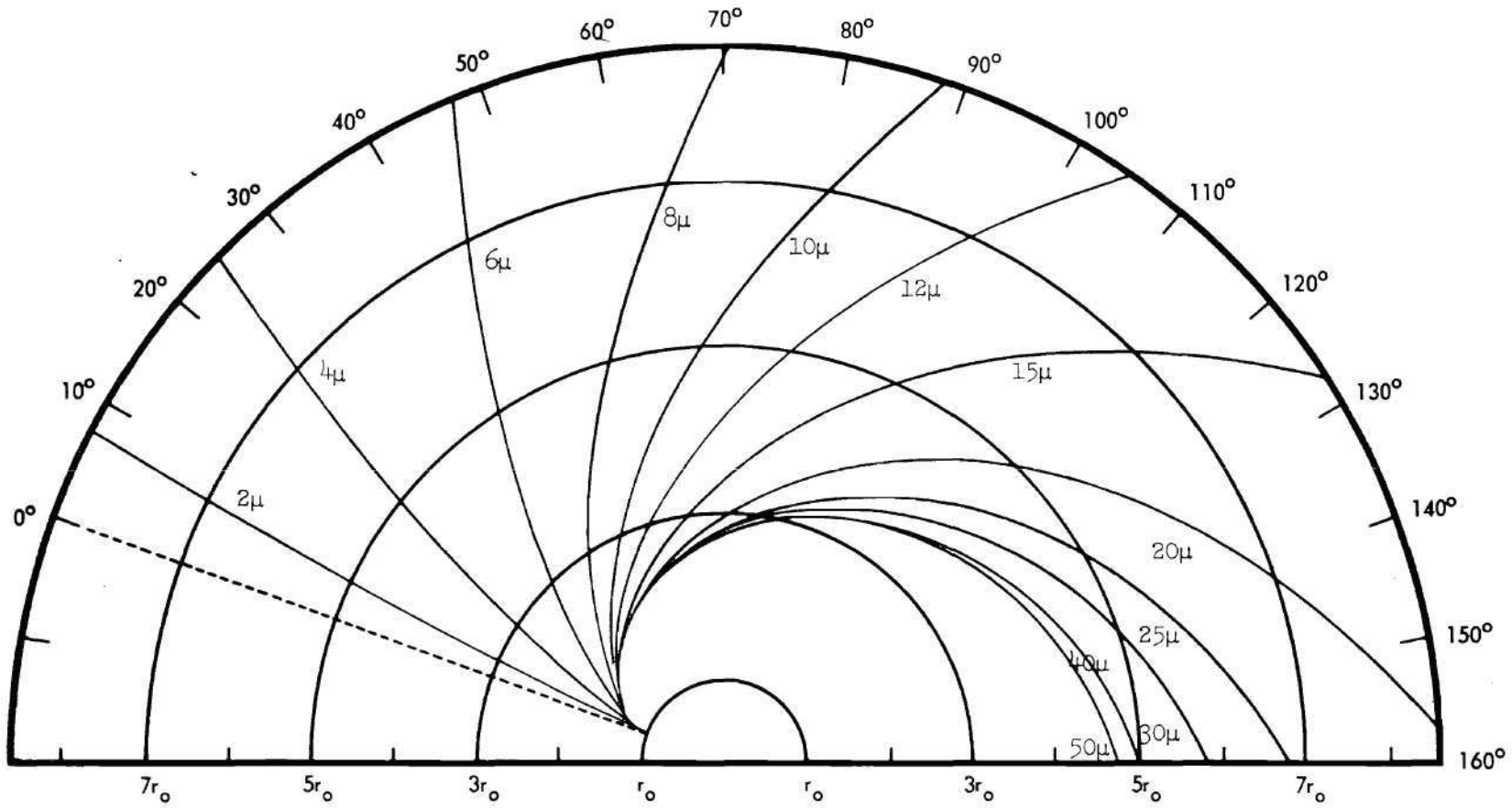

Figure 40. Analog Computer Solutions for the Trajectories of Spherical Particles having a Density of 2.5 gm/cm^3 Relative to a Constant Speed Rotor for Forced Vortex Conditions in which a General Drag Relationship is Assumed Valid. (Rotor Speed: 9600 rpm).

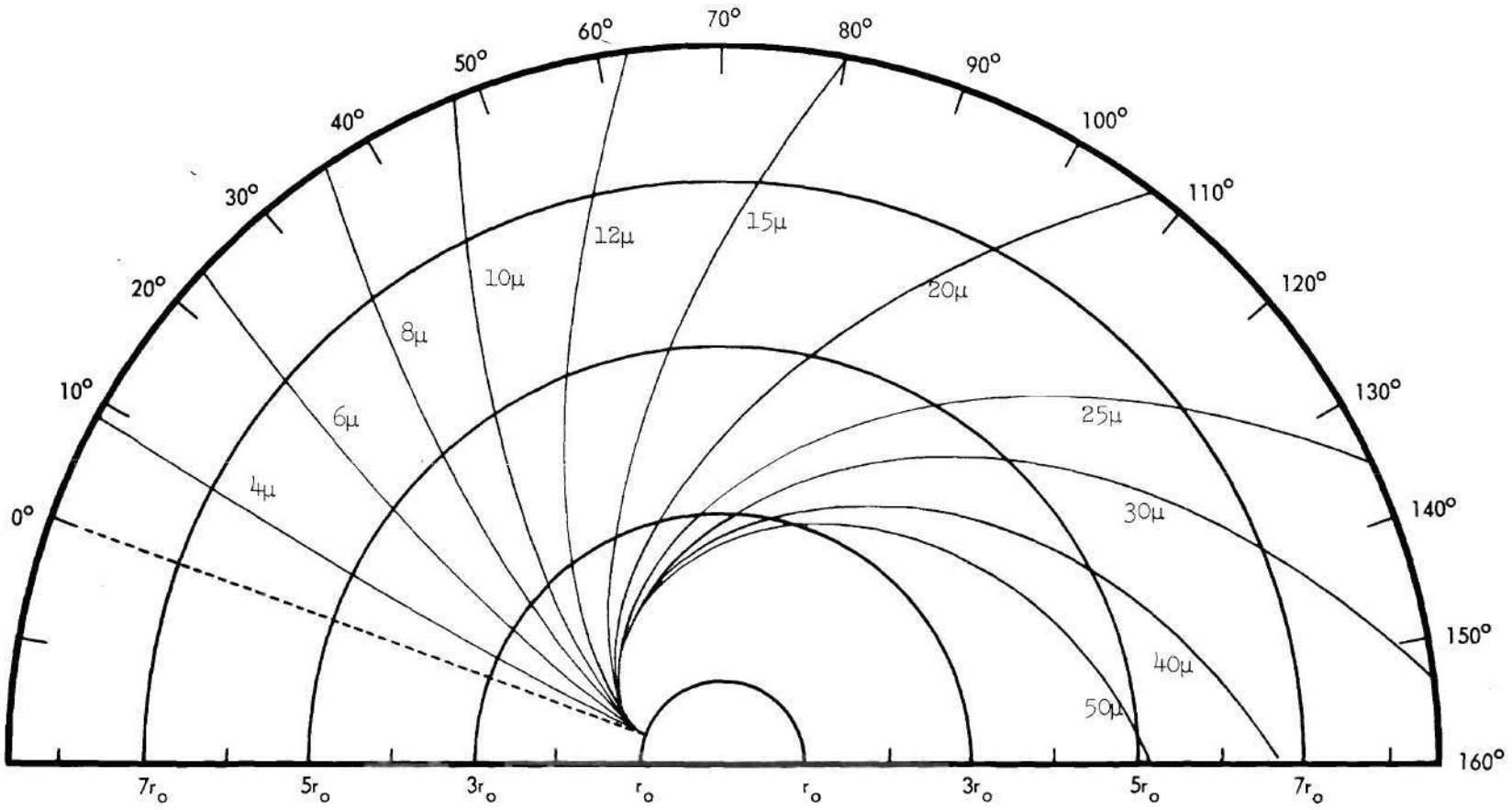

Figure 41. Analog Computer Solutions for the Trajectories of Spherical Particles having a Density of 3.0 gm/cm^3 Relative to a Constant Speed Rotor for Forced Vortex Conditions in which a General Drag Relationship is Assumed Valid. (Rotor Speed: 2400 rpm).

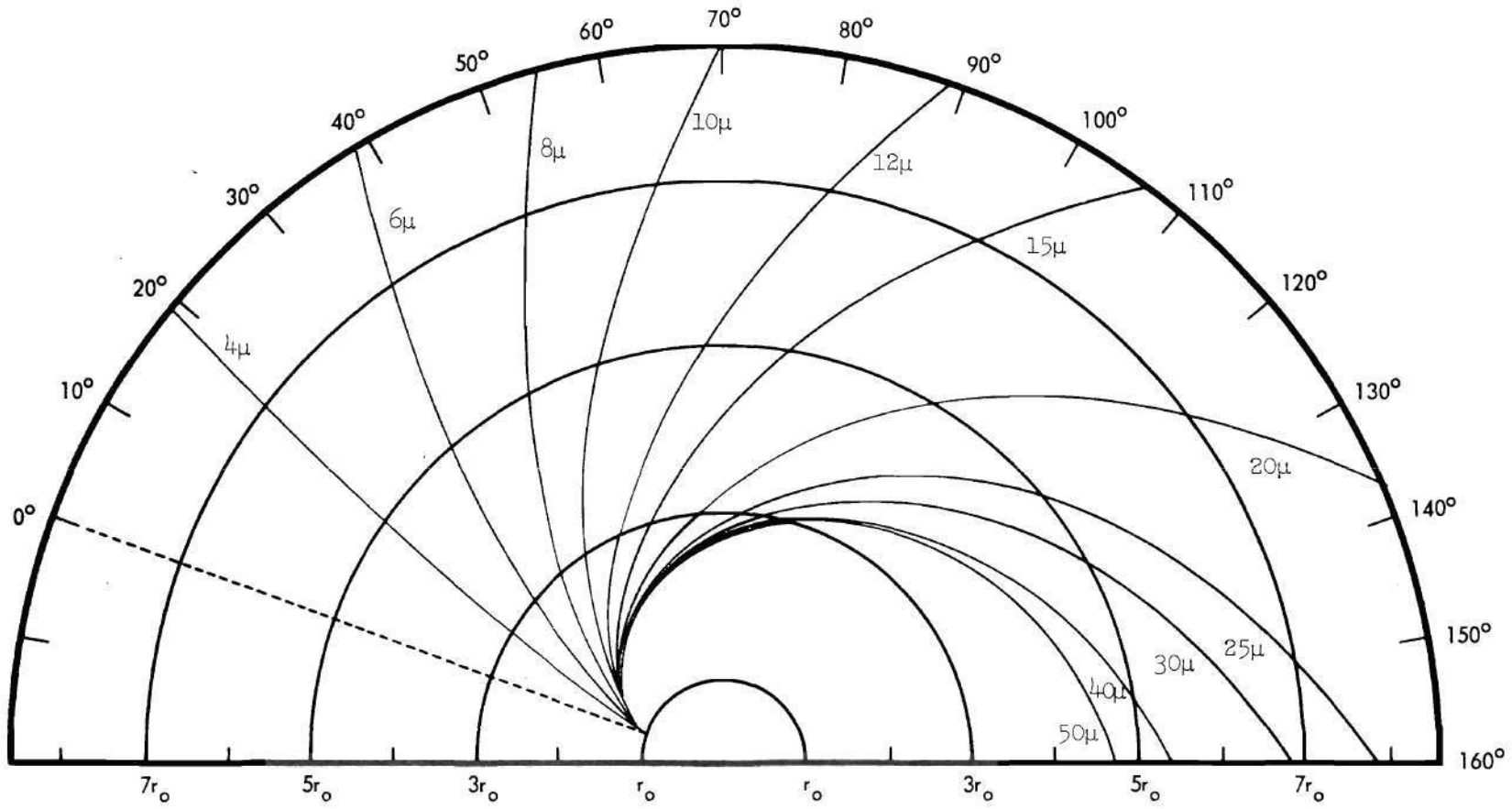

Figure 42. Analog Computer Solutions for the Trajectories of Spherical Particles having a Density of 3.0 gm/cm^3 Relative to a Constant Speed Rotor for Forced Vortex Conditions in which a General Drag Relationship is Assumed Valid. (Rotor Speed: 4800 rpm).

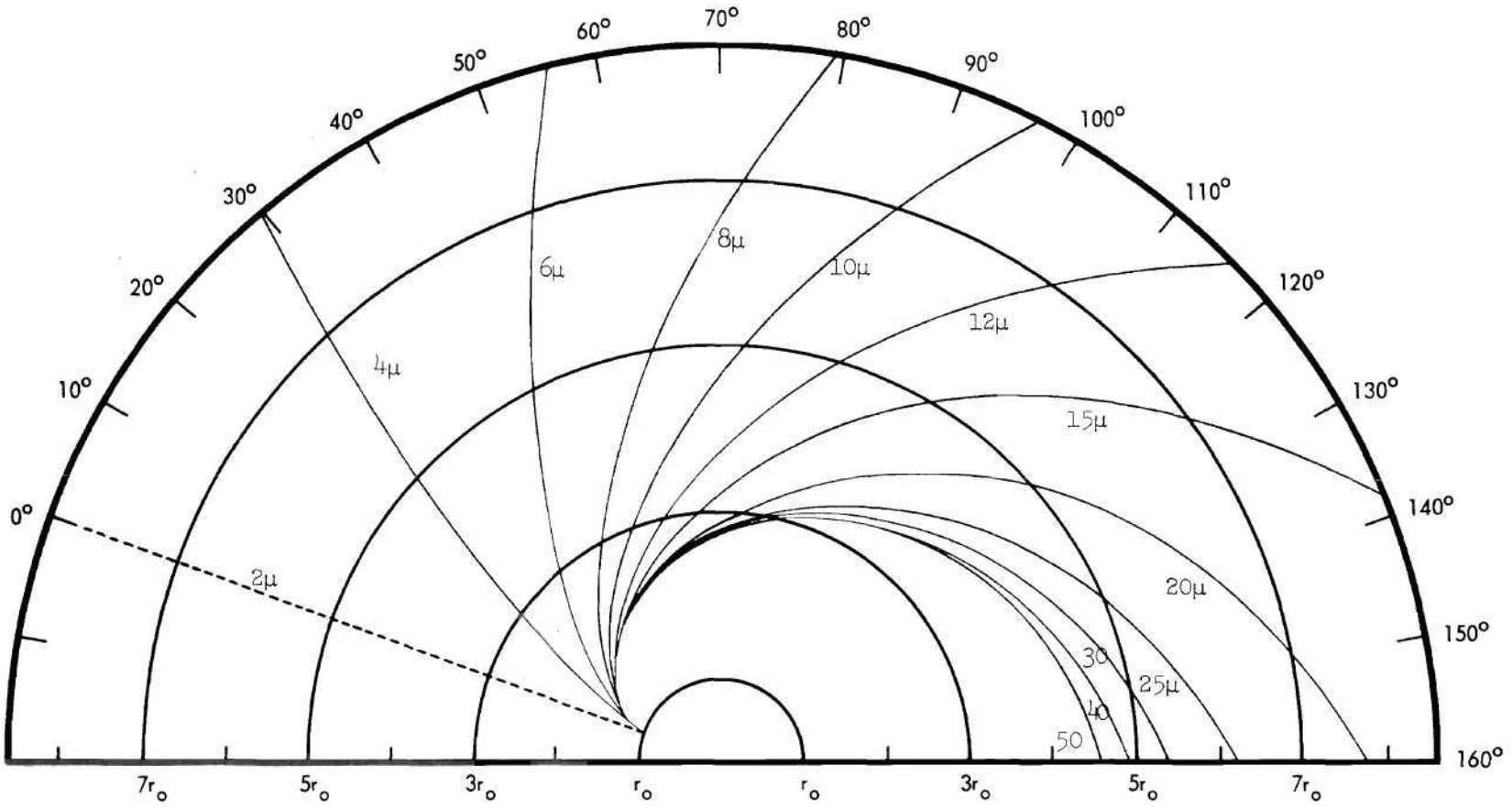

Figure 43. Analog Computer Solutions for the Trajectories of Spherical Particles having a Density of 3.0 gm/cm^3 Relative to a Constant Speed Rotor for Forced Vortex Conditions in which a General Drag Relationship is Assumed Valid. (Rotor Speed: 9600 rpm).

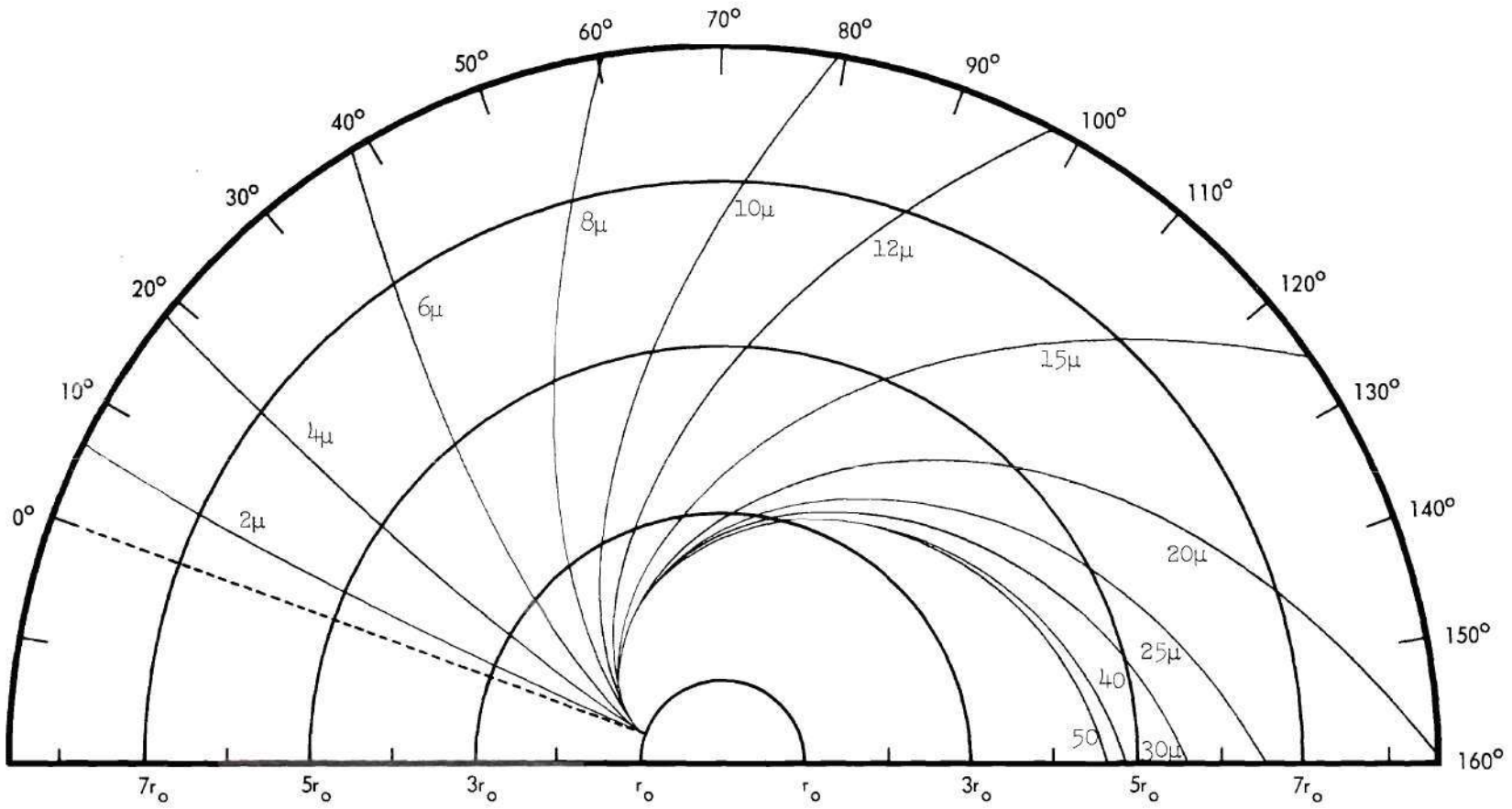

Figure 44. Analog Computer Solutions for the Trajectories of Spherical Particles having a Density of 7.0 gm/cm^3 Relative to a Constant Speed Rotor for Forced Vortex Conditions in which a General Drag Relationship is Assumed Valid. (Rotor Speed: 2400 rpm).

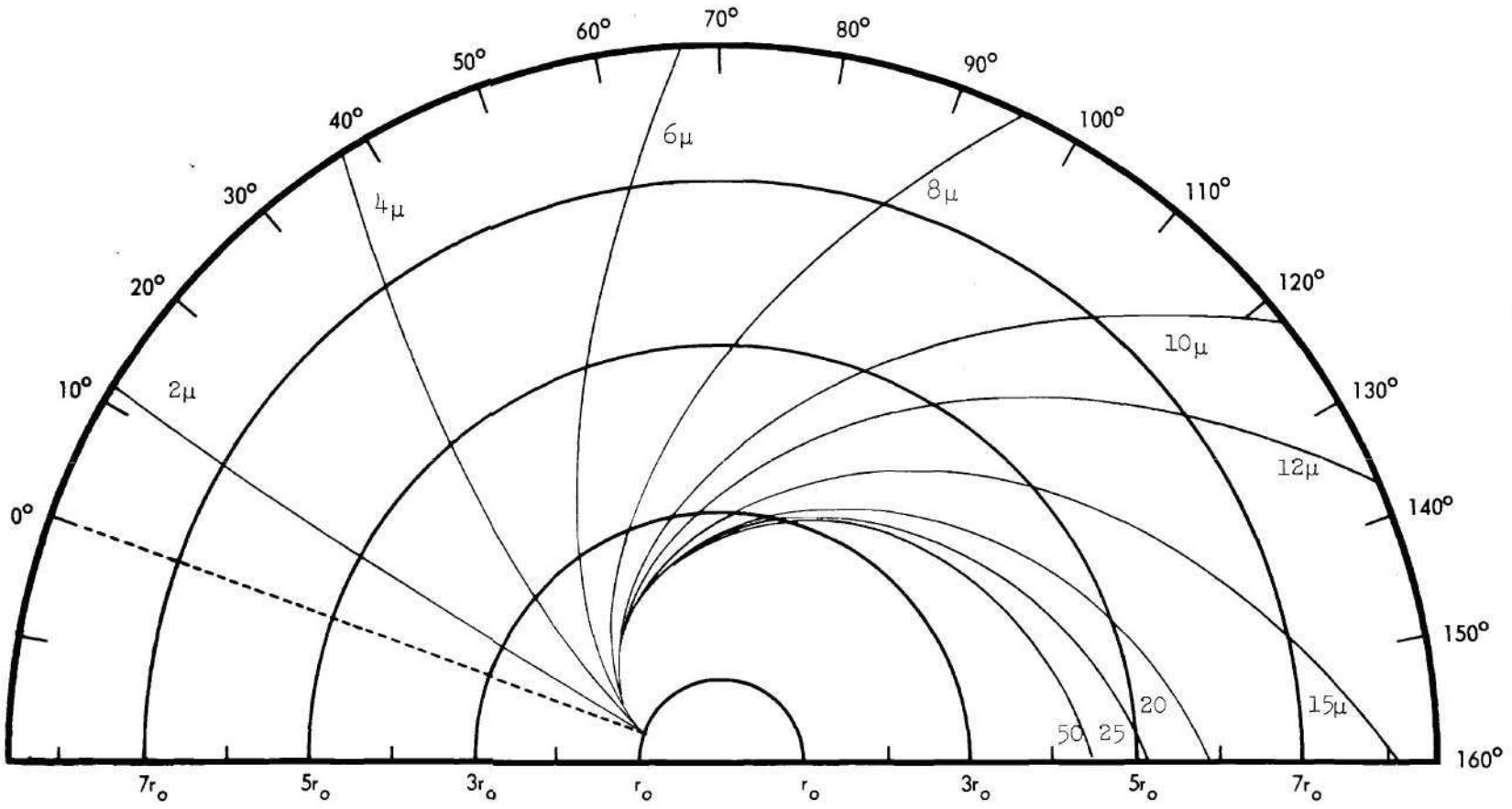

Figure 45. Analog Computer Solutions for the Trajectories of Spherical Particles having a Density of 7.0 gm/cm^3 Relative to a Constant Speed Rotor for Forced Vortex Conditions in which a General Drag Relationship is Assumed Valid. (Rotor Speed: 4800 rpm).

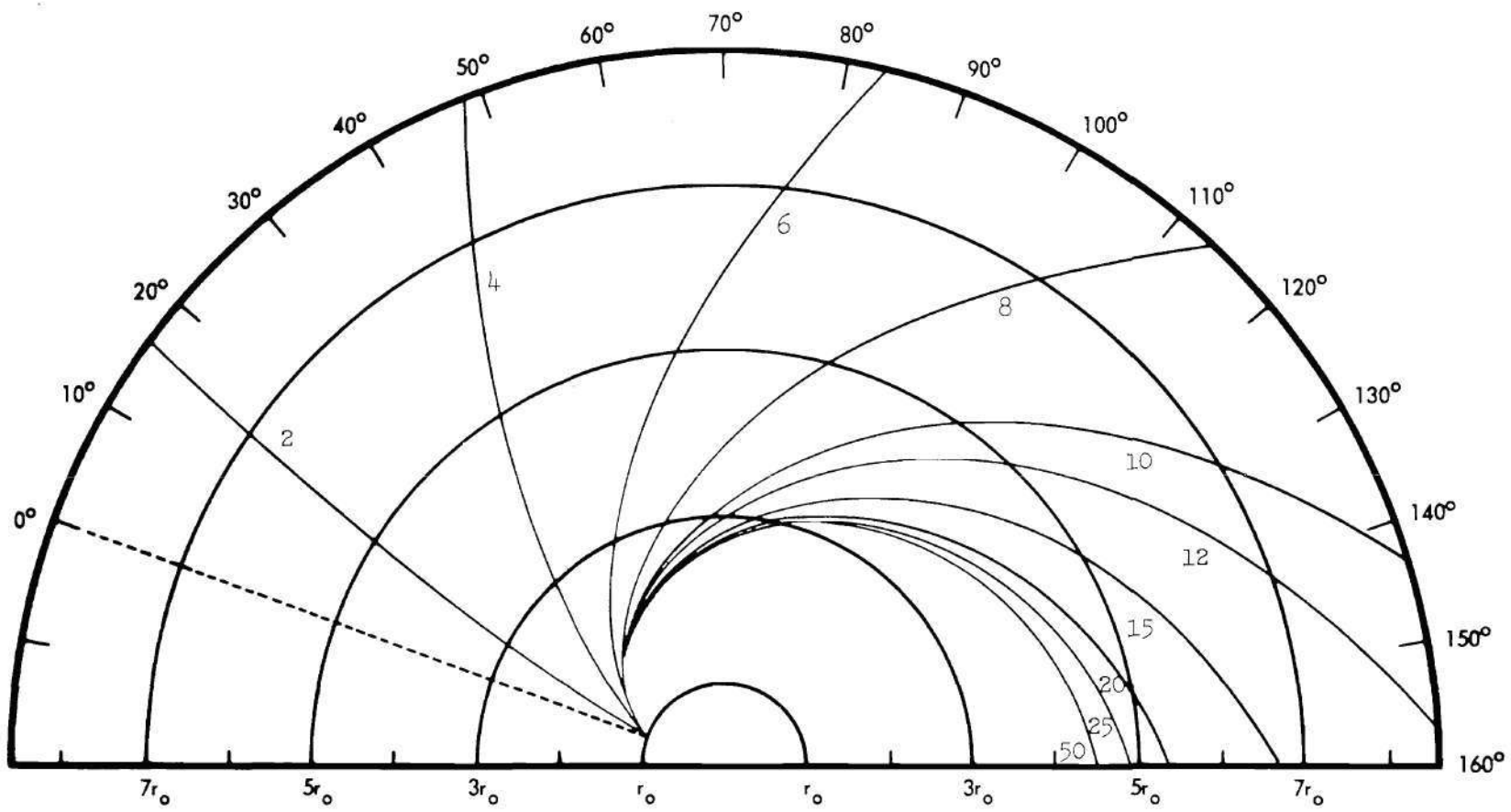

Figure 46. Analog Computer Solutions for the Trajectories of Spherical Particles having a Density of 7.0 gm/cm^3 Relative to a Constant Speed Rotor for Forced Vortex Conditions in which a General Drag Relationship is Assumed Valid. (Rotor Speed: 7200 rpm).

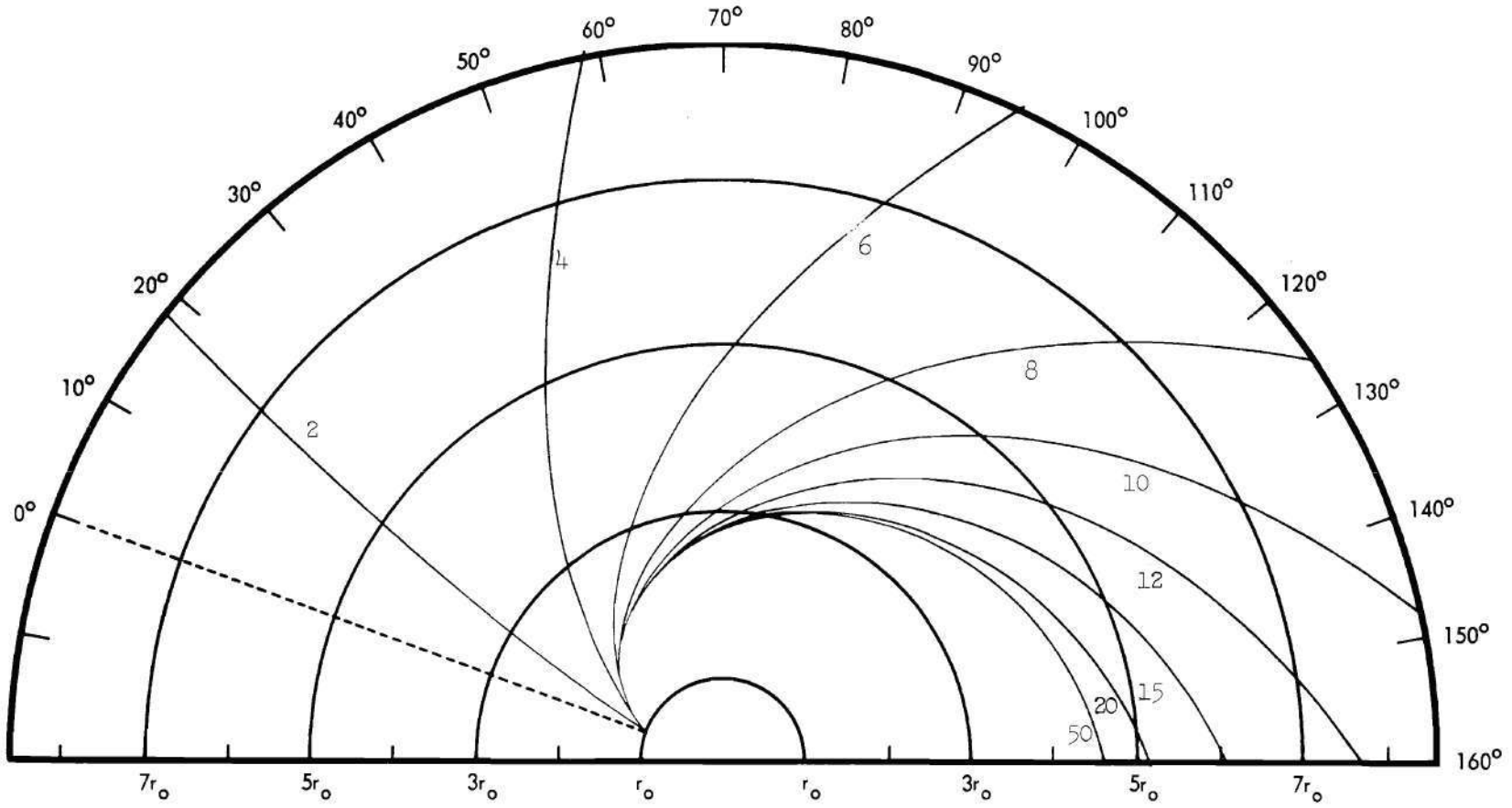

Figure 47. Analog Computer Solutions for the Trajectories of Spherical Particles having a Density of 7.0 gm/cm^3 Relative to a Constant Speed Rotor for Forced Vortex Conditions in which a General Drag Relationship is Assumed Valid. (Rotor Speed: 9600 rpm).

APPENDIX C

EQUIPMENT CONSTRUCTIONAL DETAILS

The main rotor component of the centrifugal classifier assembly was fabricated from a hand-forged billet of aluminum-zinc alloy, 7075-T6. This material has a high strength-to-weight ratio and is particularly suited for high speed applications. Figure 48 is a line drawing of the main rotor component. The rotor shaft, which is shown by Figure 49, was also the means by which the aerosol particles entered the classification chambers. A narrow (1/16 inch) slot was provided at the intersection of the rotor shaft and main rotor component to introduce particles into the classification chamber. A plastic insert was provided in the rotor shaft to confine the path of the aerosol particles as they progressed from the aerosol feed tube to the entry slots and thereby prevent plugging of the entry slots.

Several plastic rotor tops similar to the one shown in Figure 50 were constructed. The various thicknesses of these tops were designed to permit a convenient means of varying the height of the classification chambers. An O-ring was used to seal the rotor top to the main rotor component and a rubber gasket sealed the top and rotor shaft connection. The final rotor assembly which was shown by Figure 9 was thus completely sealed except for the incoming aerosol slots and the desired holes open in the rotor wall.

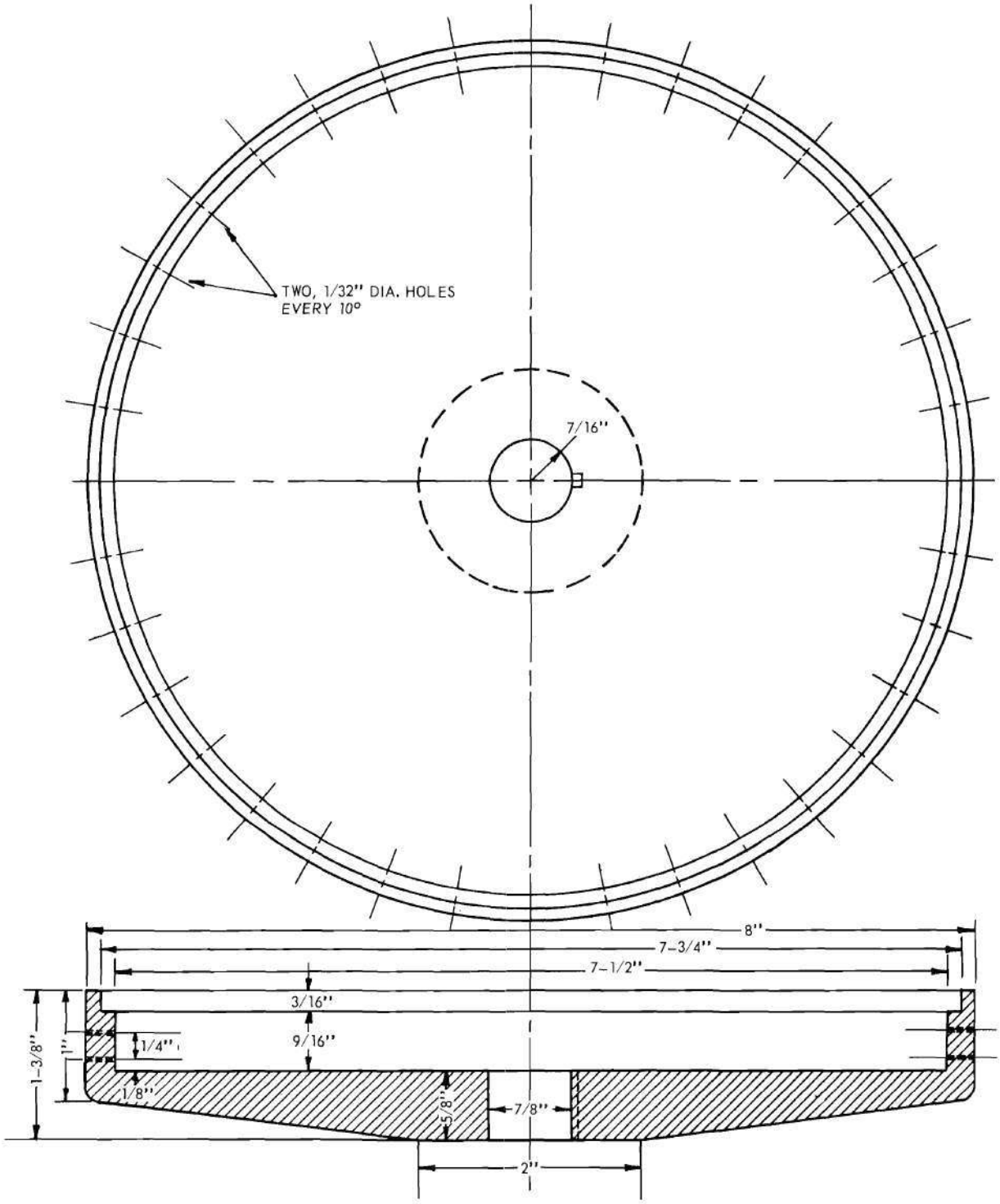

Figure 48. Centrifugal Classifier Main Rotor Component.

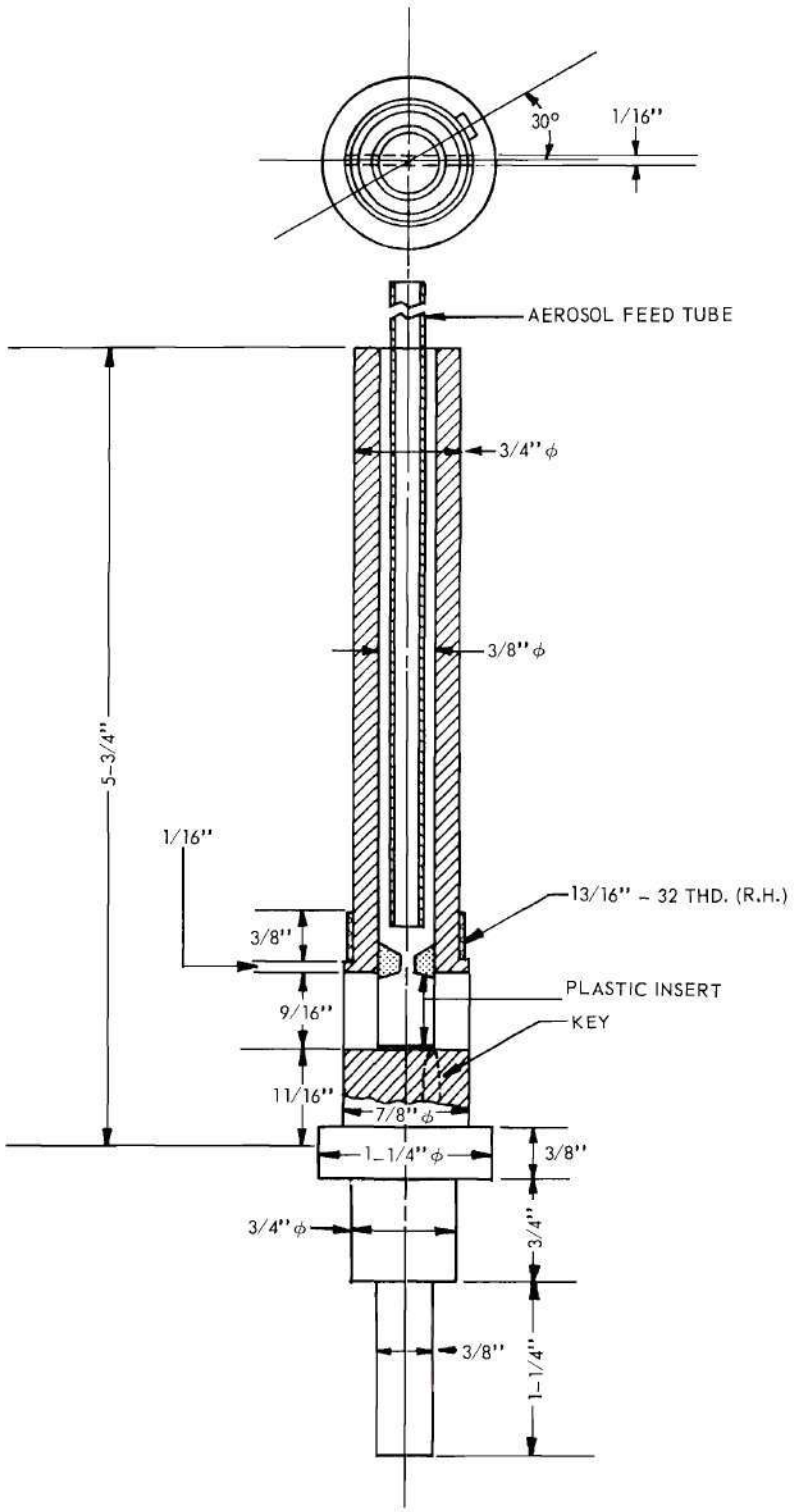

Figure 49. Centrifugal Classifier Rotor Shaft and Aerosol Feed Tube.

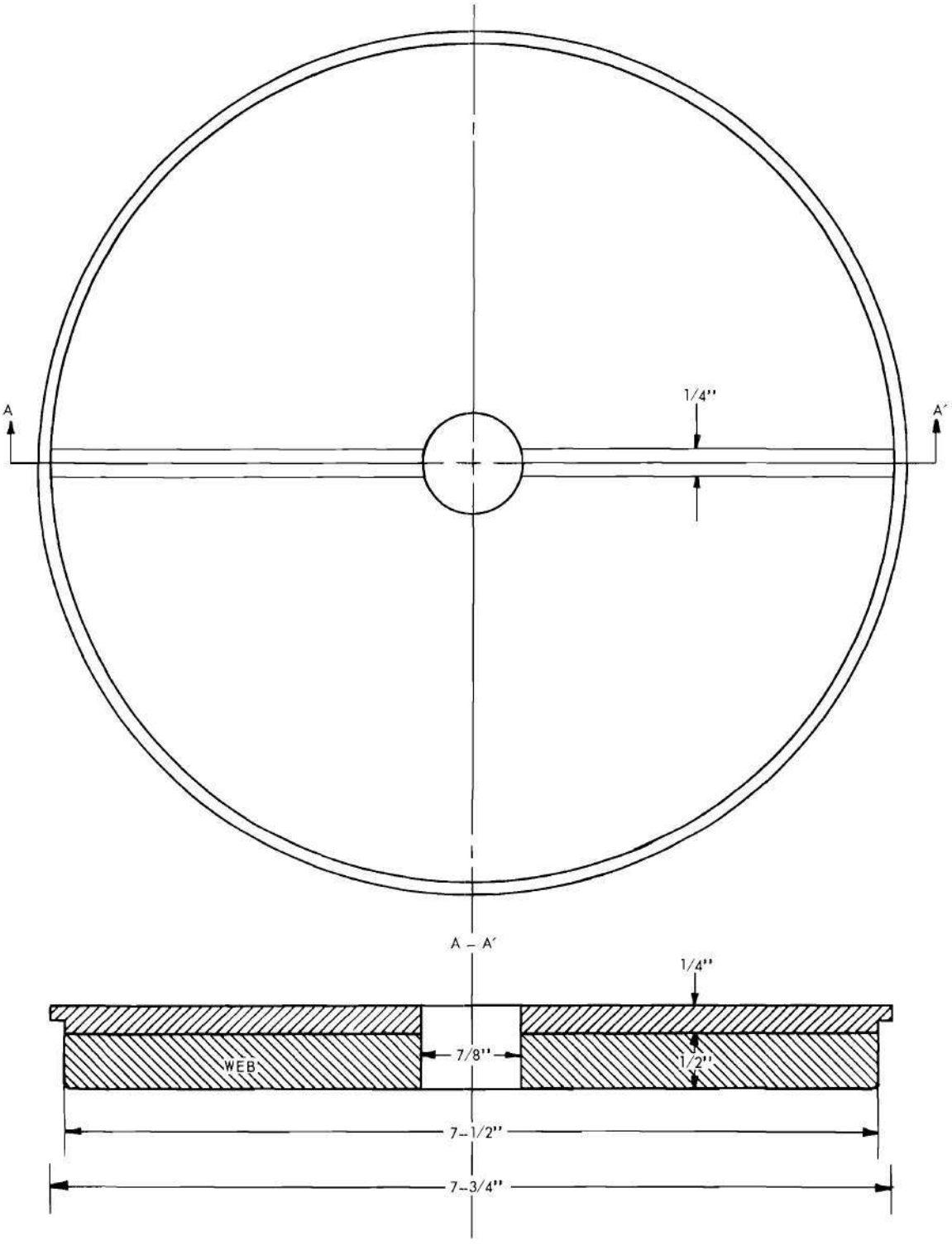

Figure 50. Plastic Rotor Top for the Centrifugal Classifier.

APPENDIX D

SIZE DISTRIBUTION DATA

This section contains the original size distributions and size distributions measured at specified angular locations on the wall of an experimental particle size classifier for various experimental conditions.

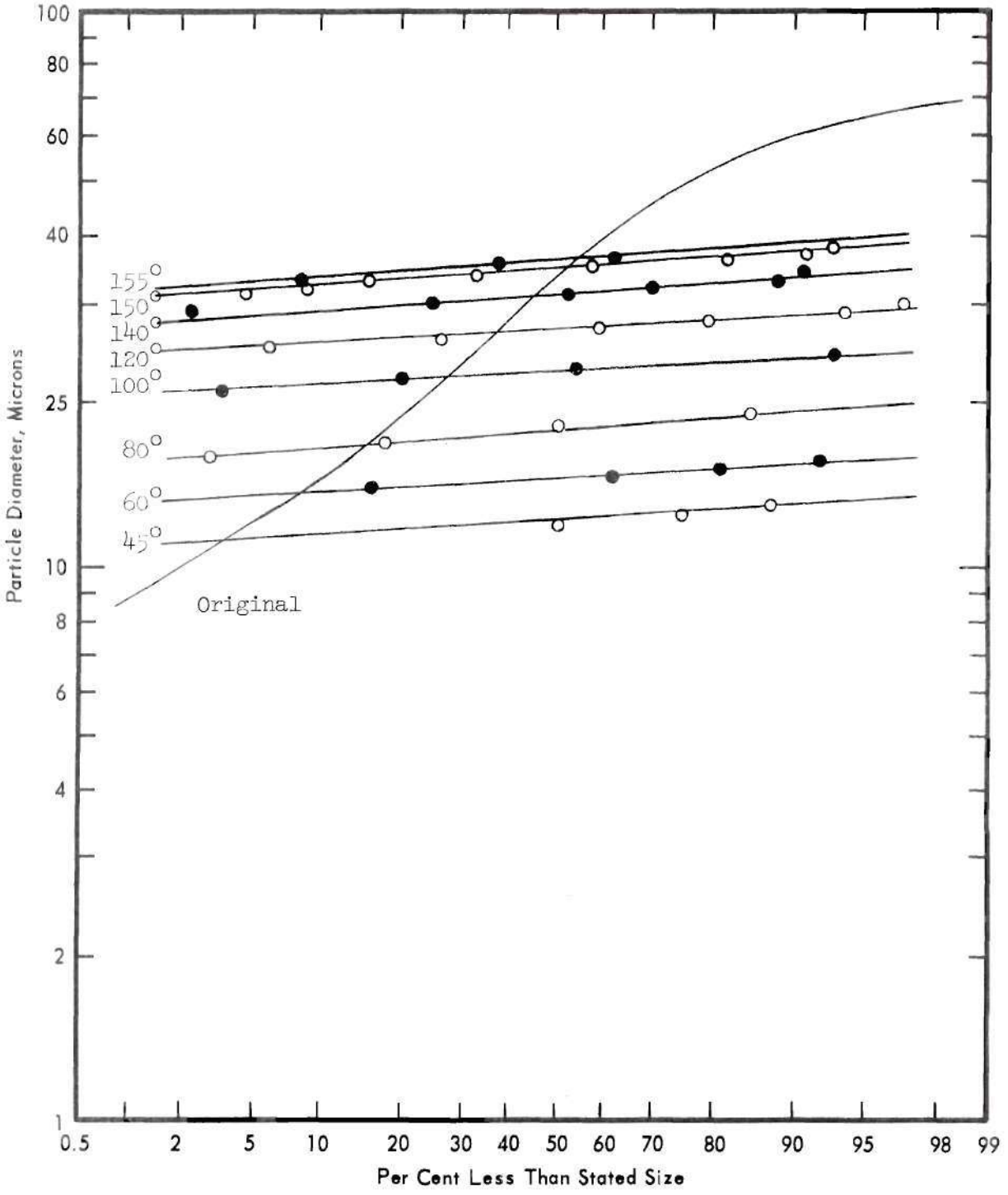

Figure 51. Size Distributions of Plastic Spheres before Classification and as Deposited at Specified Angular Locations on the Rotor Wall. (Rotor Speed: 4800 rpm).

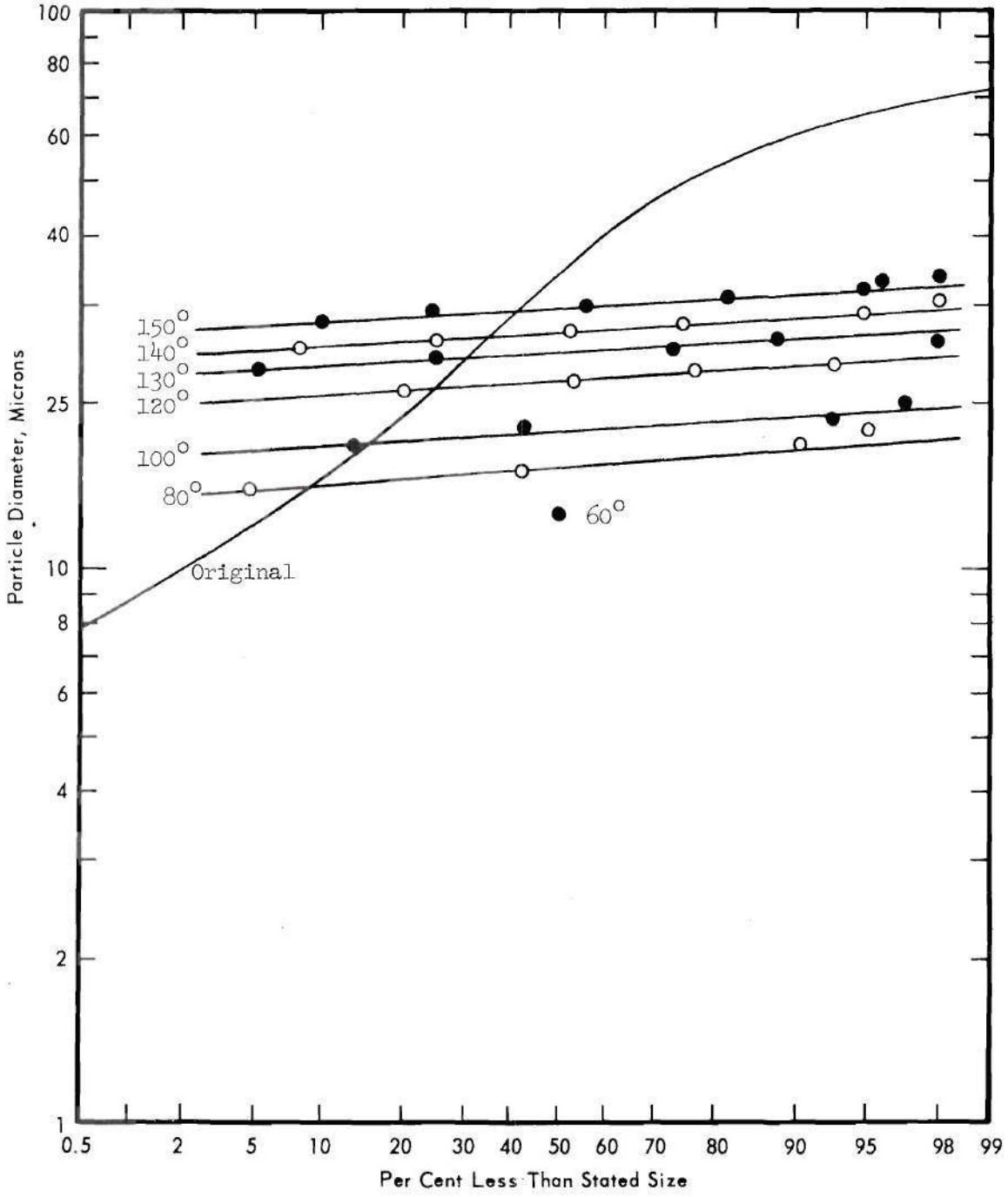

Figure 52. Size Distributions of Plastic Spheres before Classification and as Deposited at Specified Angular Locations on the Rotor Wall. (Rotor Speed: 7200 rpm).

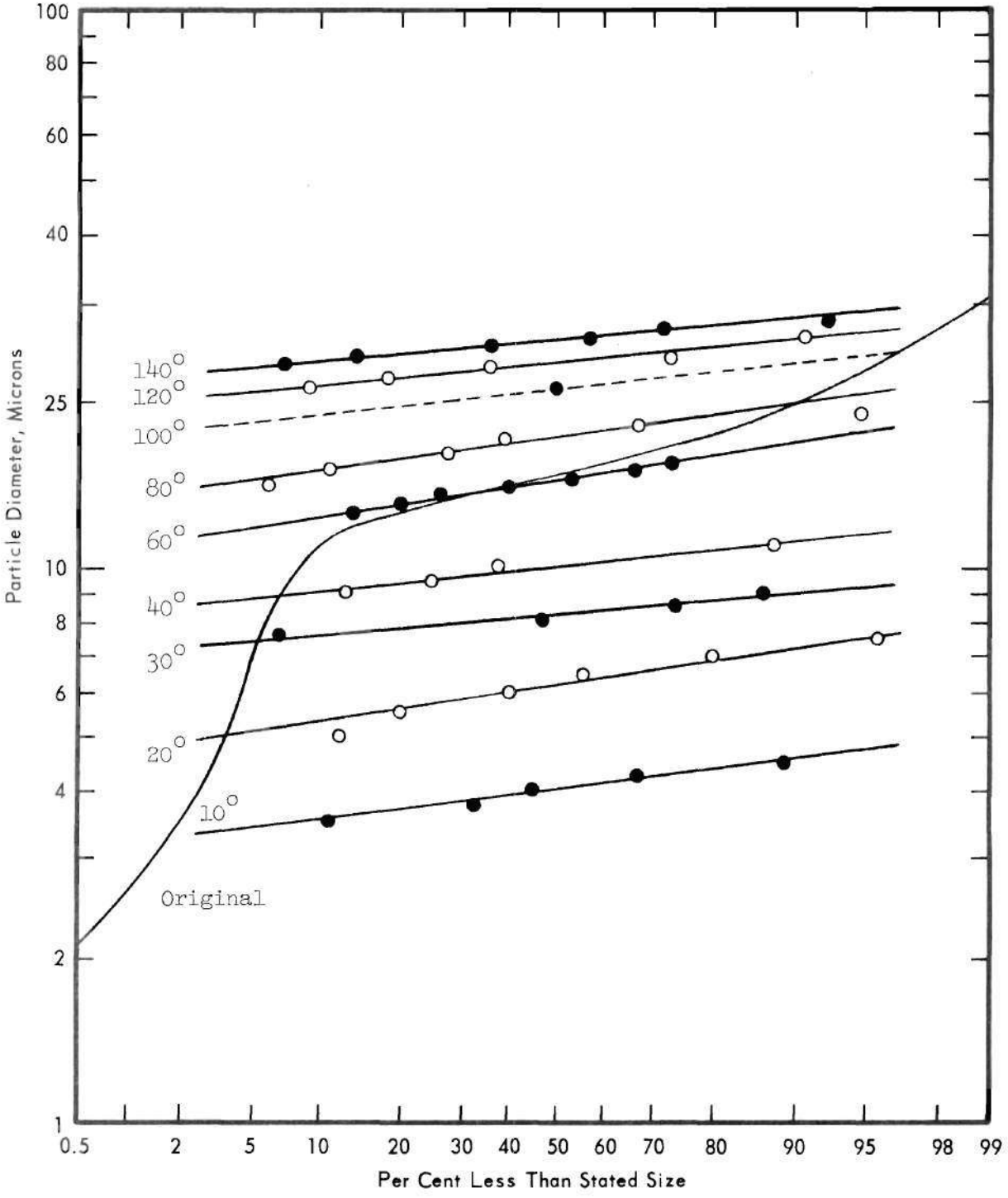

Figure 53. Size Distributions of Glass Spheres before Classification and as Deposited at Specified Angular Locations on the Rotor Wall. (Rotor Speed: 1600 rpm).

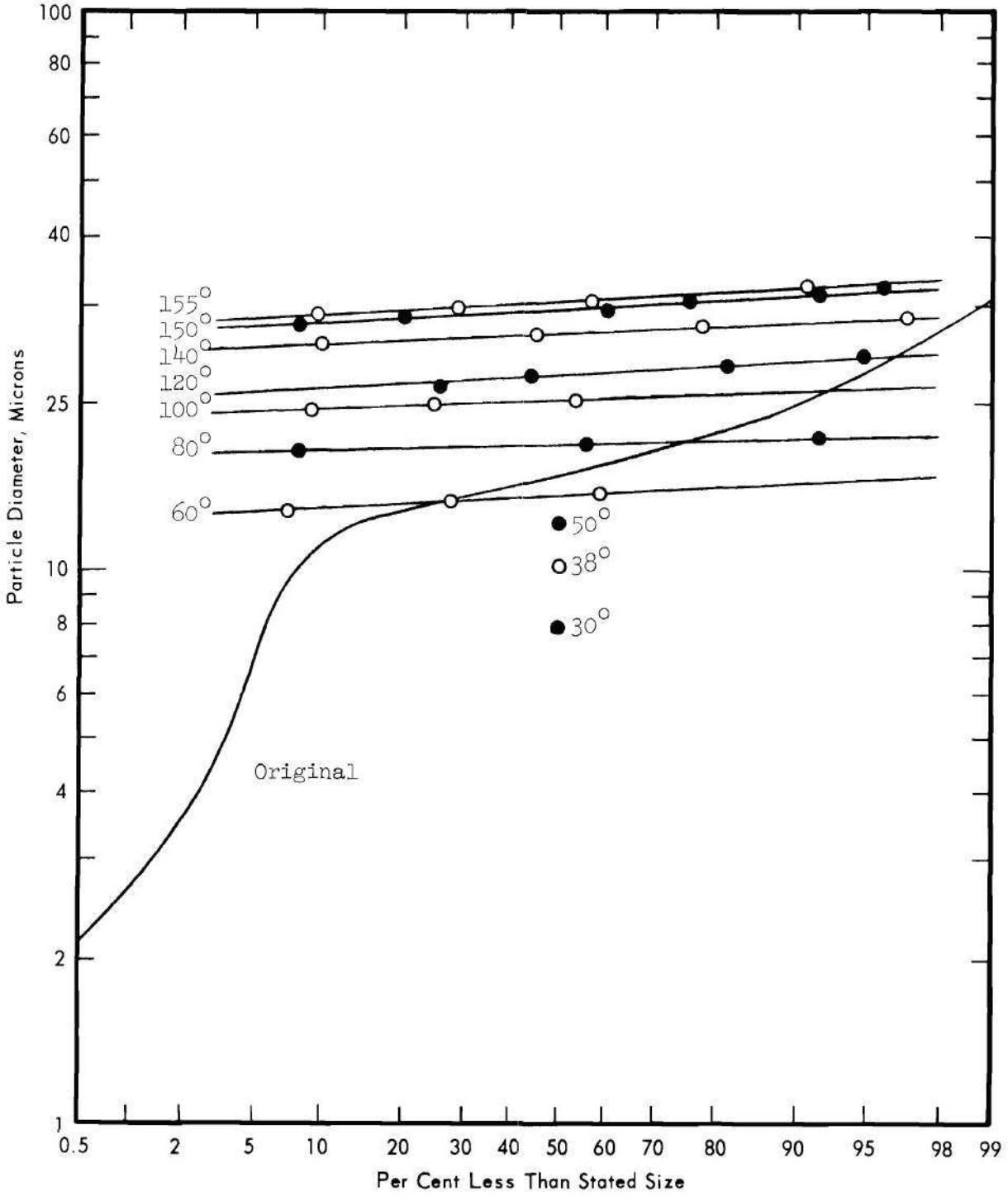

Figure 54. Size Distributions of Glass Spheres before Classification and as Deposited at Specified Angular Locations on the Rotor Wall. (Rotor Speed: 2400 rpm).

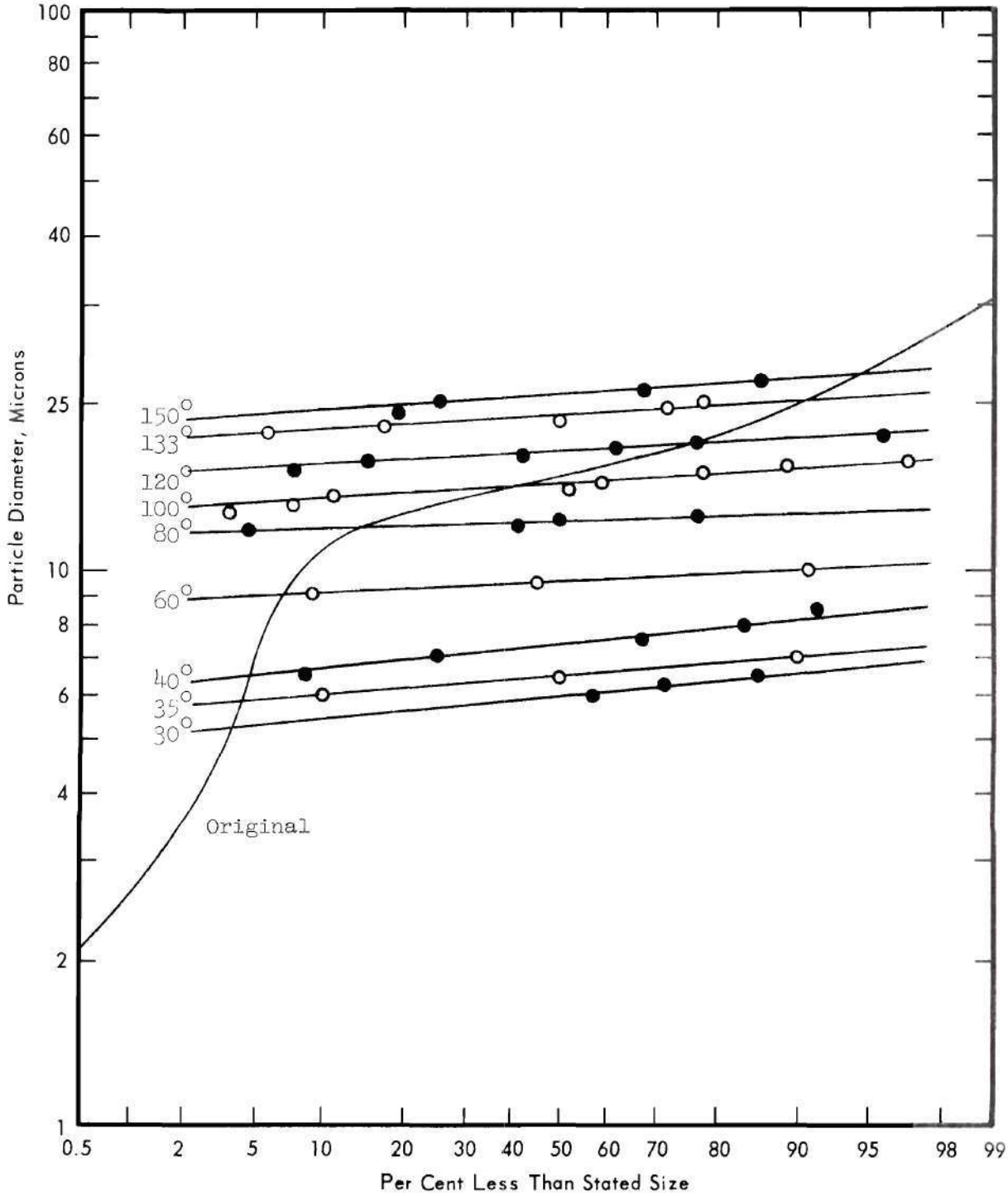

Figure 55. Size Distributions of Glass Spheres before Classification and as Deposited at Specified Angular Locatio s on the Rotor Wall. (Rotor Speed: 4800 rpm).

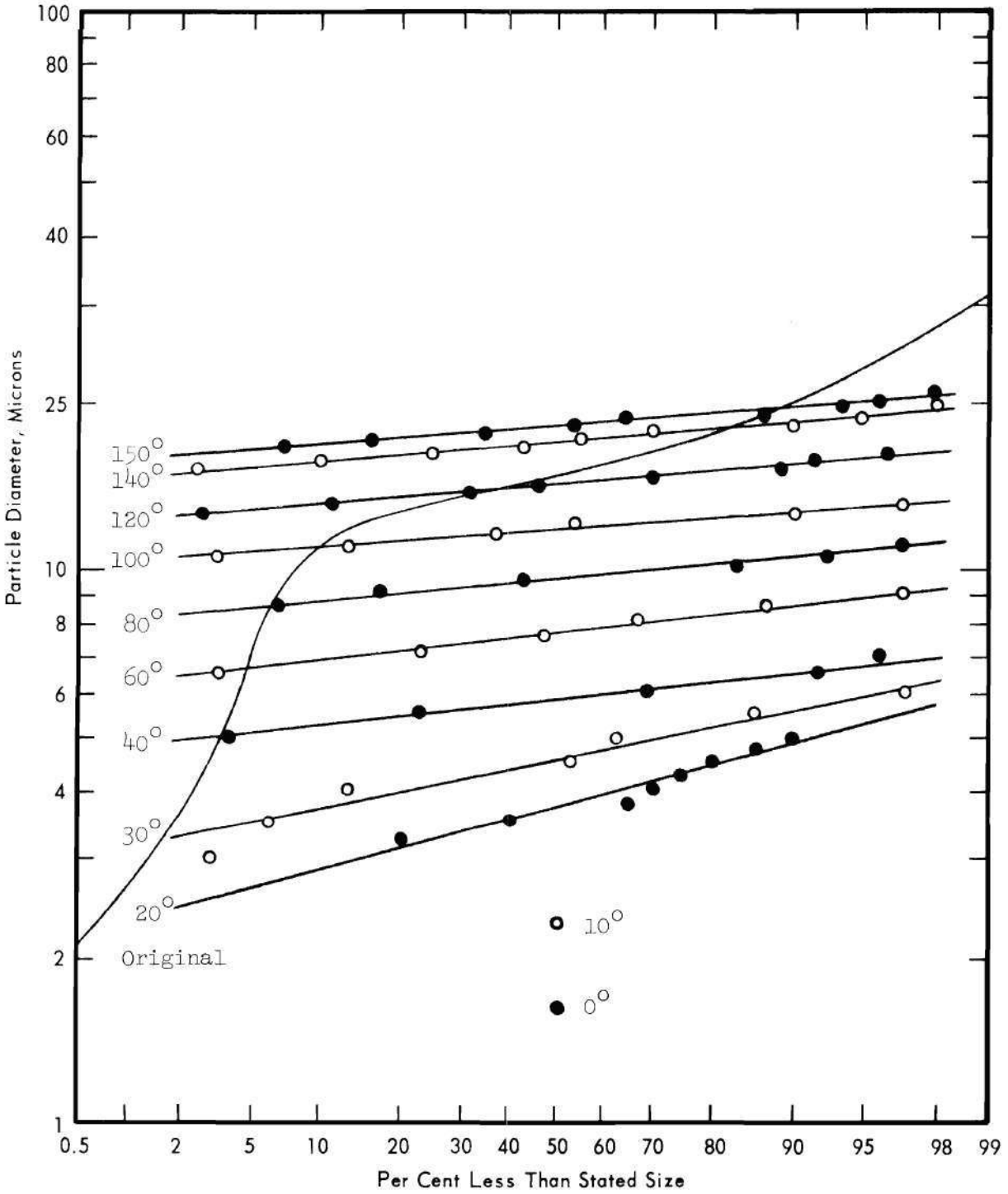

Figure 56. Size Distributions of Glass Spheres before Classification and as Deposited at Specified Angular Locations on the Rotor Wall. (Rotor Speed: 9600 rpm).

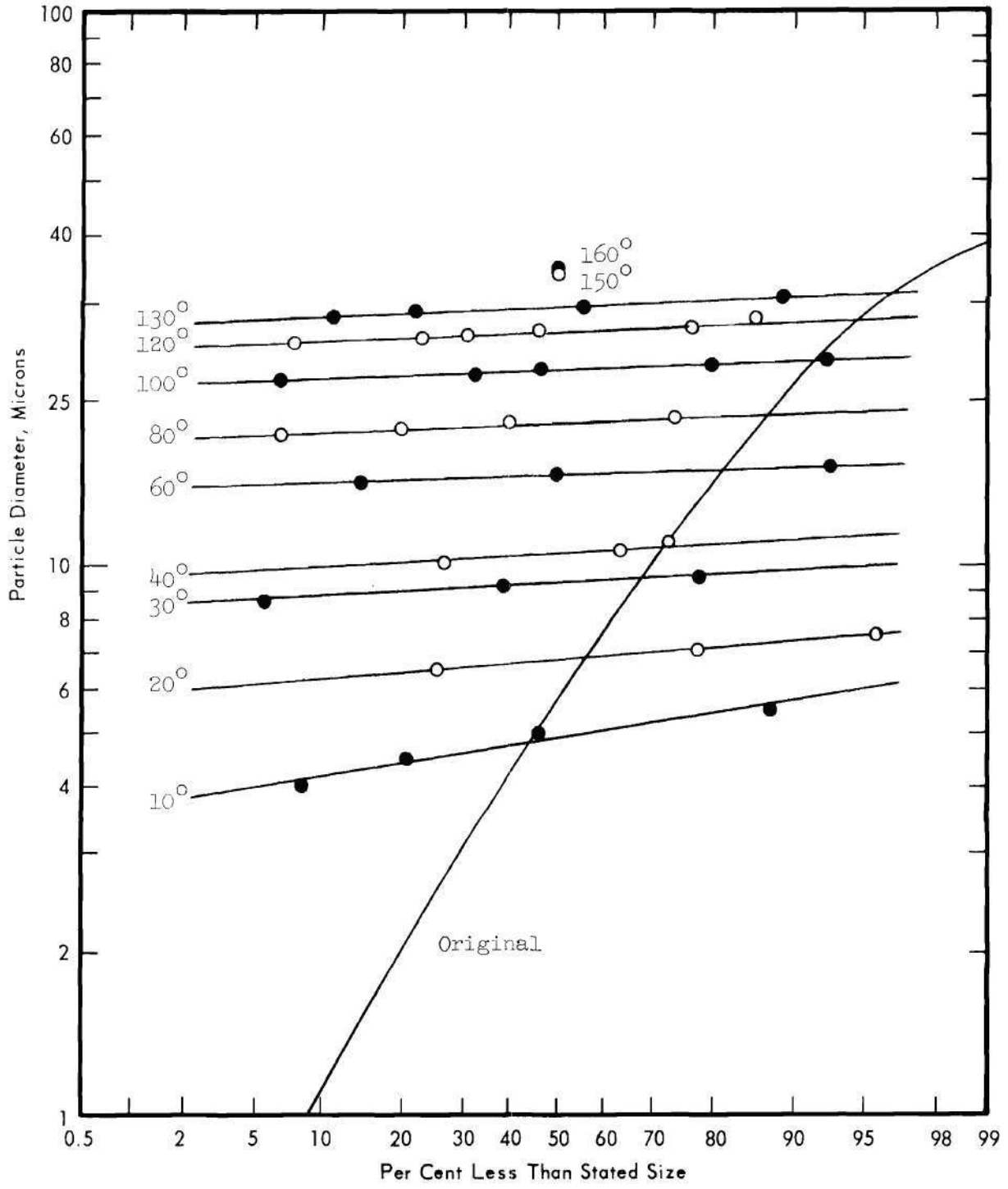

Figure 57. Size Distributions of Aluminum Spheres before Classification and as Deposited at Specified Angular Locations on the Rotor Wall. (Rotor Speed: 1600 rpm).

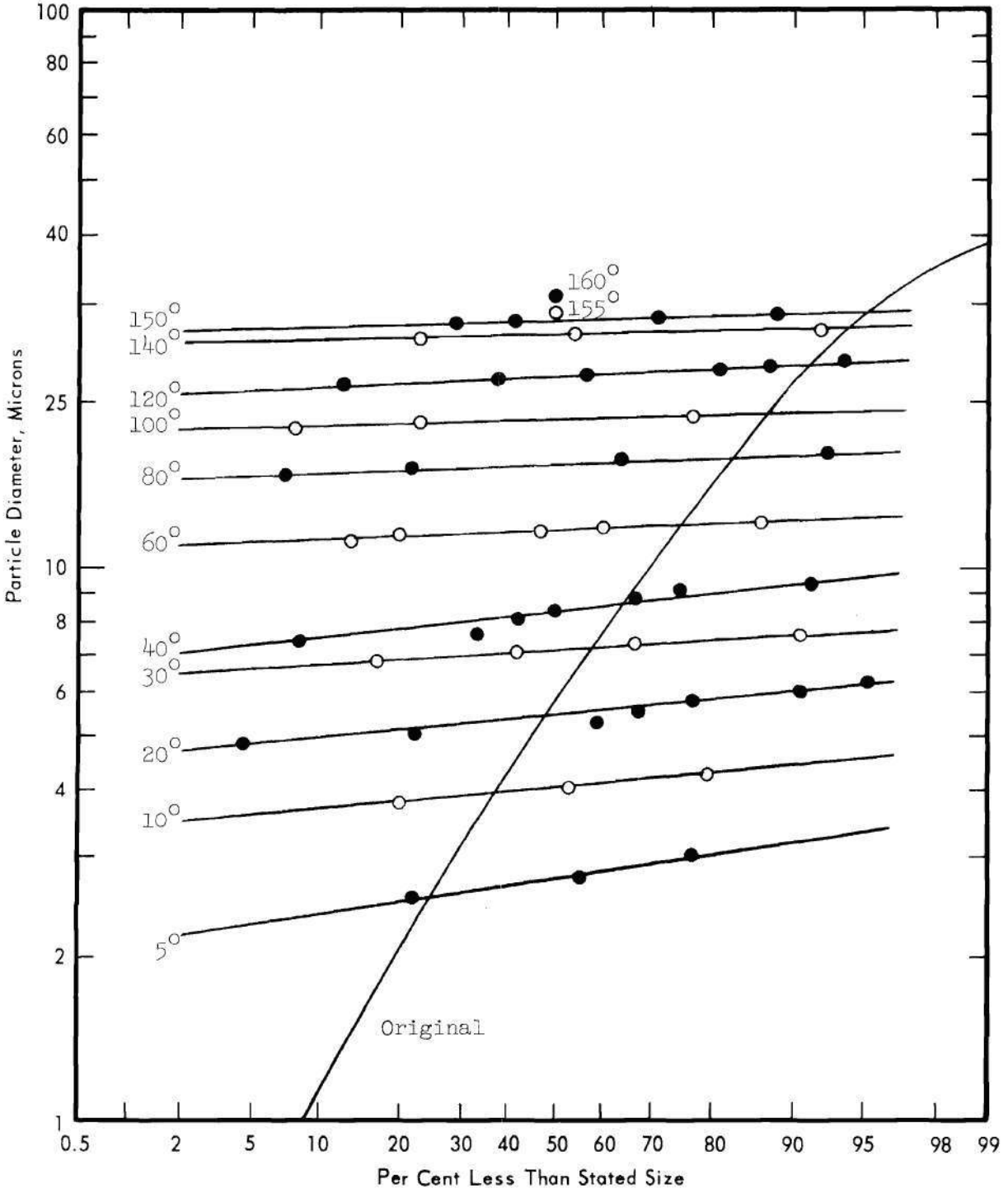

Figure 58. Size Distributions of Aluminum Spheres before Classification and as Deposited at Specified Angular Locations on the Rotor Wall. (Rotor Speed: 2400 rpm).

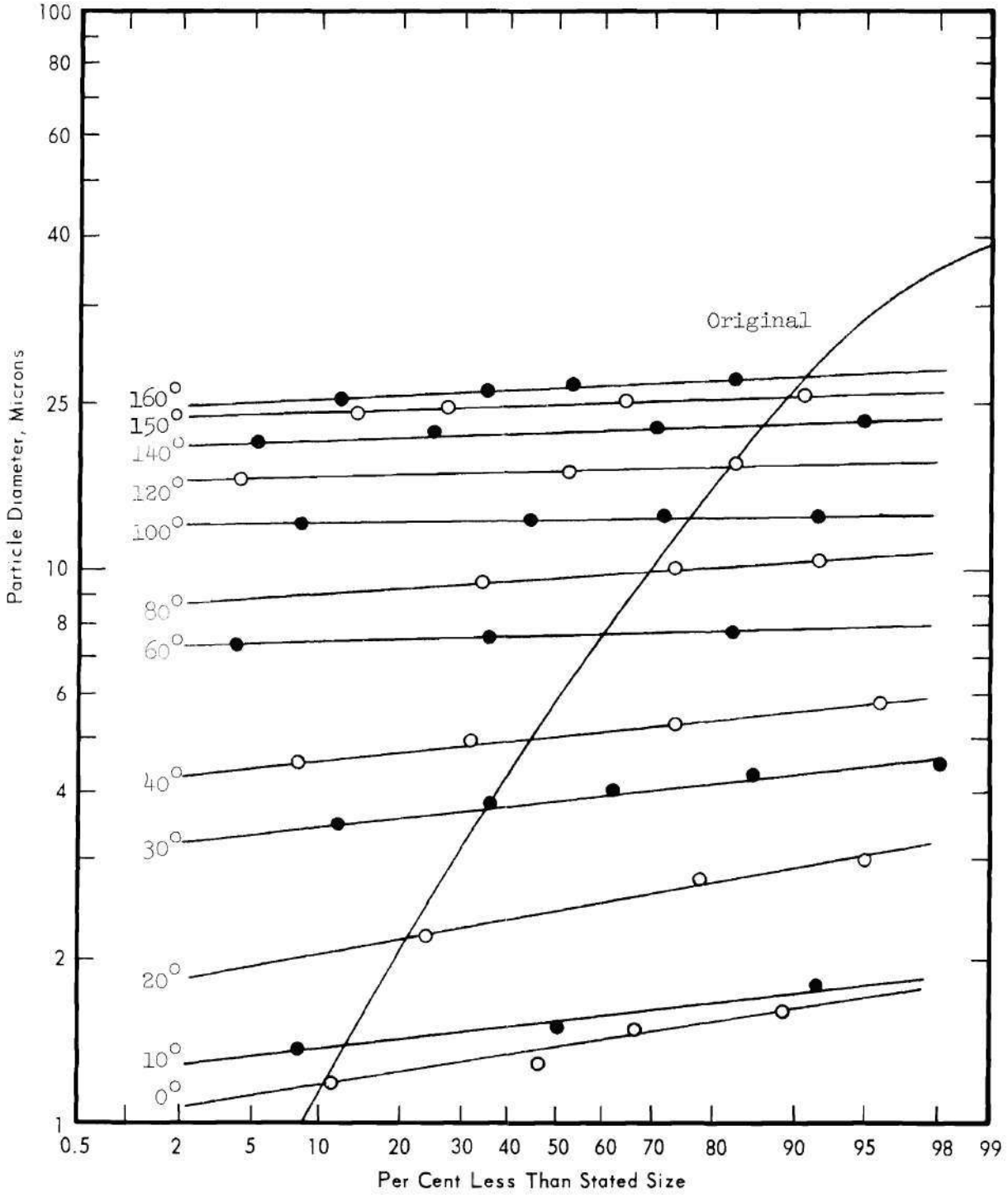

Figure 59. Size Distributions of Aluminum Spheres before Classification and as Deposited at Specified Angular Locations on the Rotor Wall. (Rotor Speed: 4800 rpm).

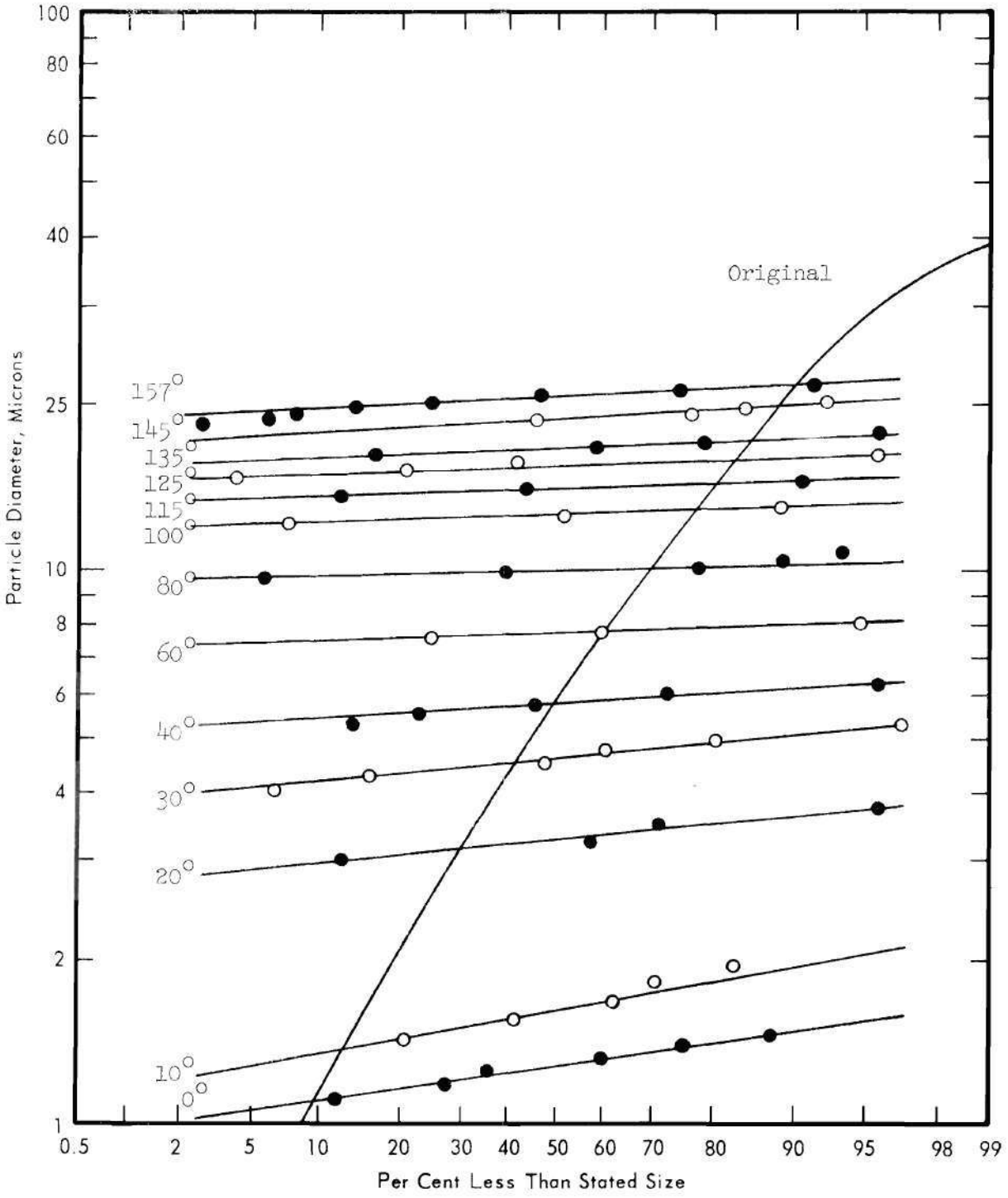

Figure 60. Size Distributions of Aluminum Spheres before Classification and as Deposited at Specified Angular Locations on the Rotor Wall. (Rotor Speed: 7200 rpm).

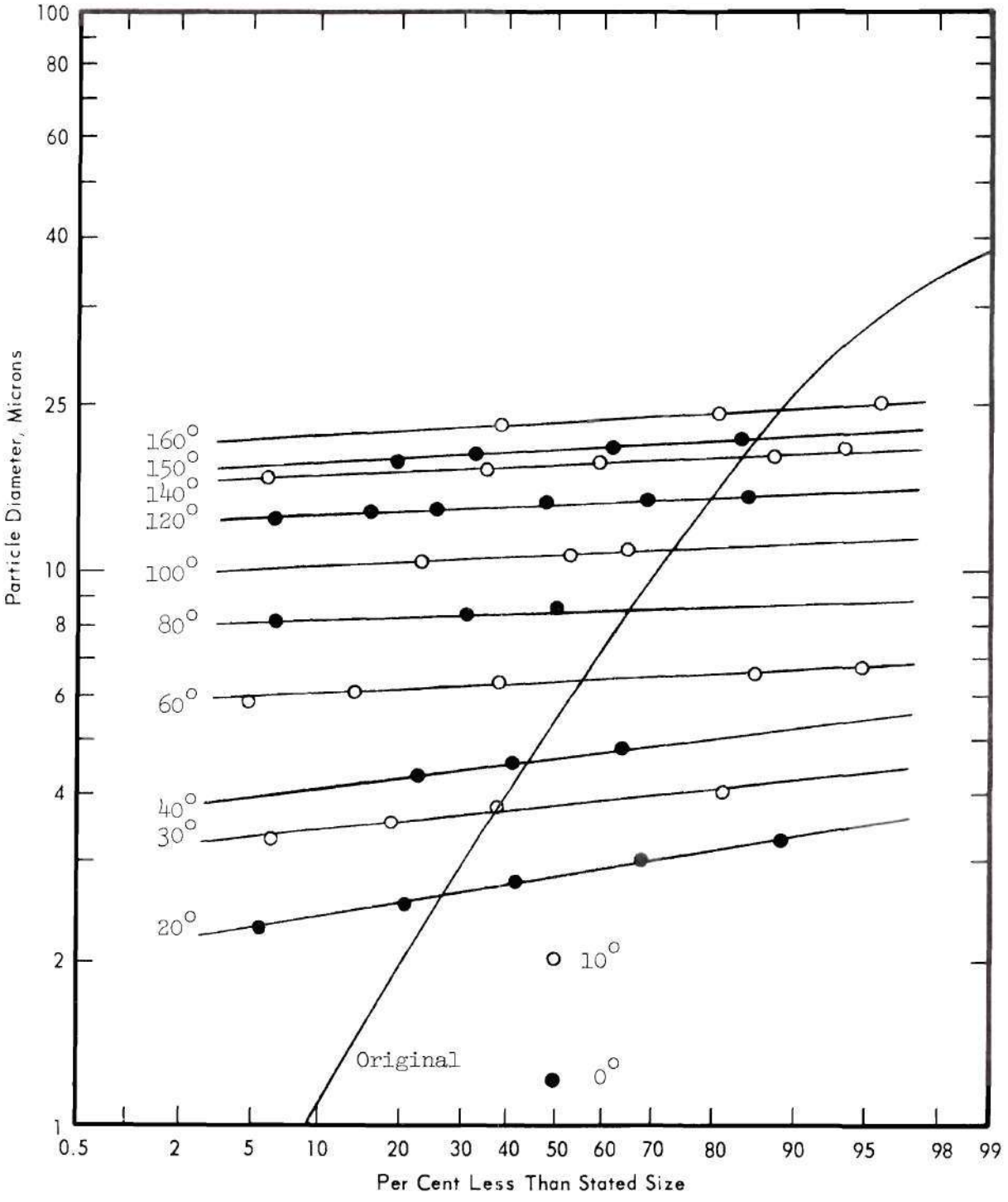

Figure 61. Size Distributions of Aluminum Spheres before Classification and as Deposited at Specified Angular Locations on the Rotor Wall. (Rotor Speed: 9600 rpm).

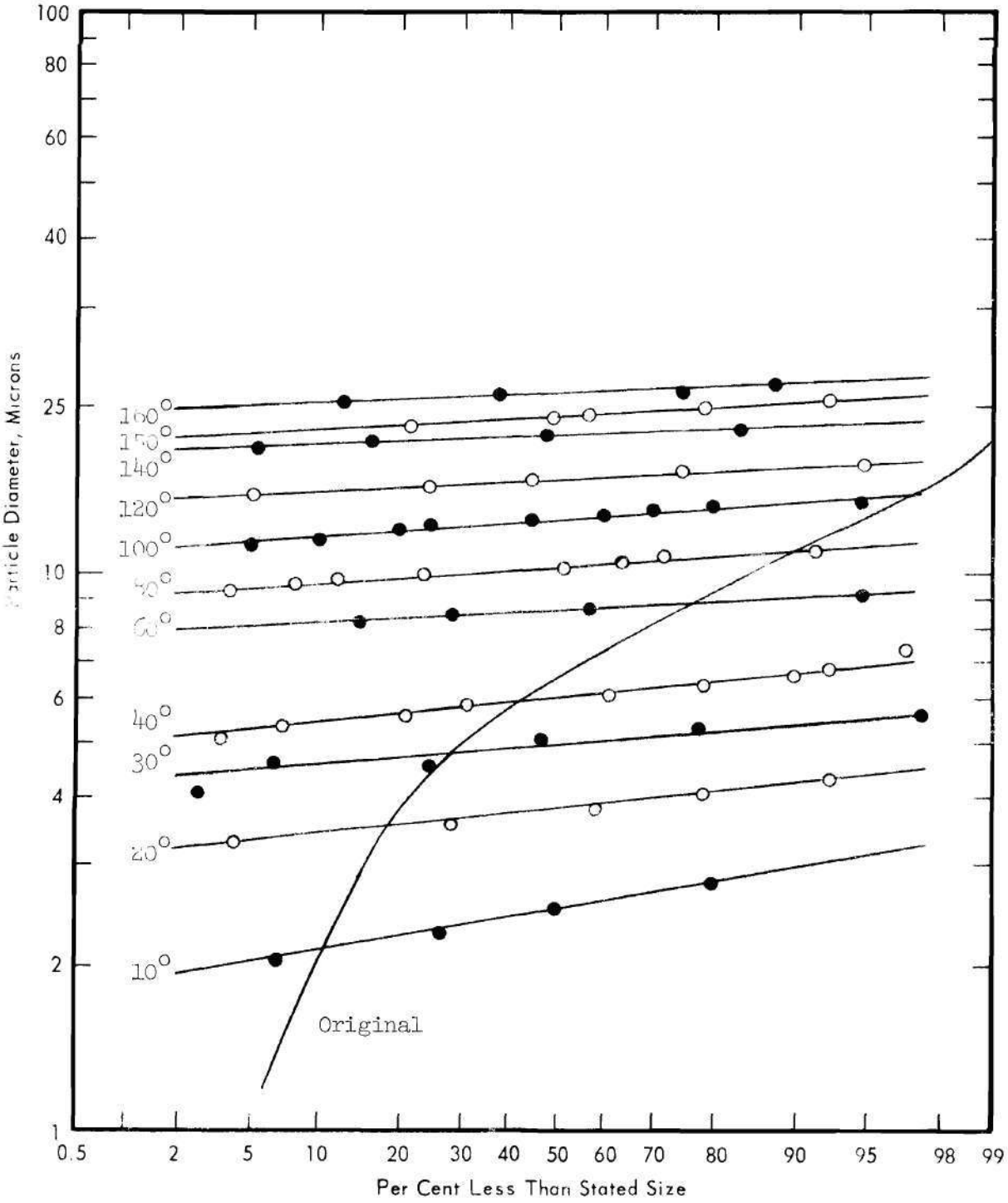

Figure 62. Size Distributions of Zinc Spheres before Classification and as Deposited at Specified Angular Locations on the Rotor Wall. (Rotor Speed: 1600 rpm).

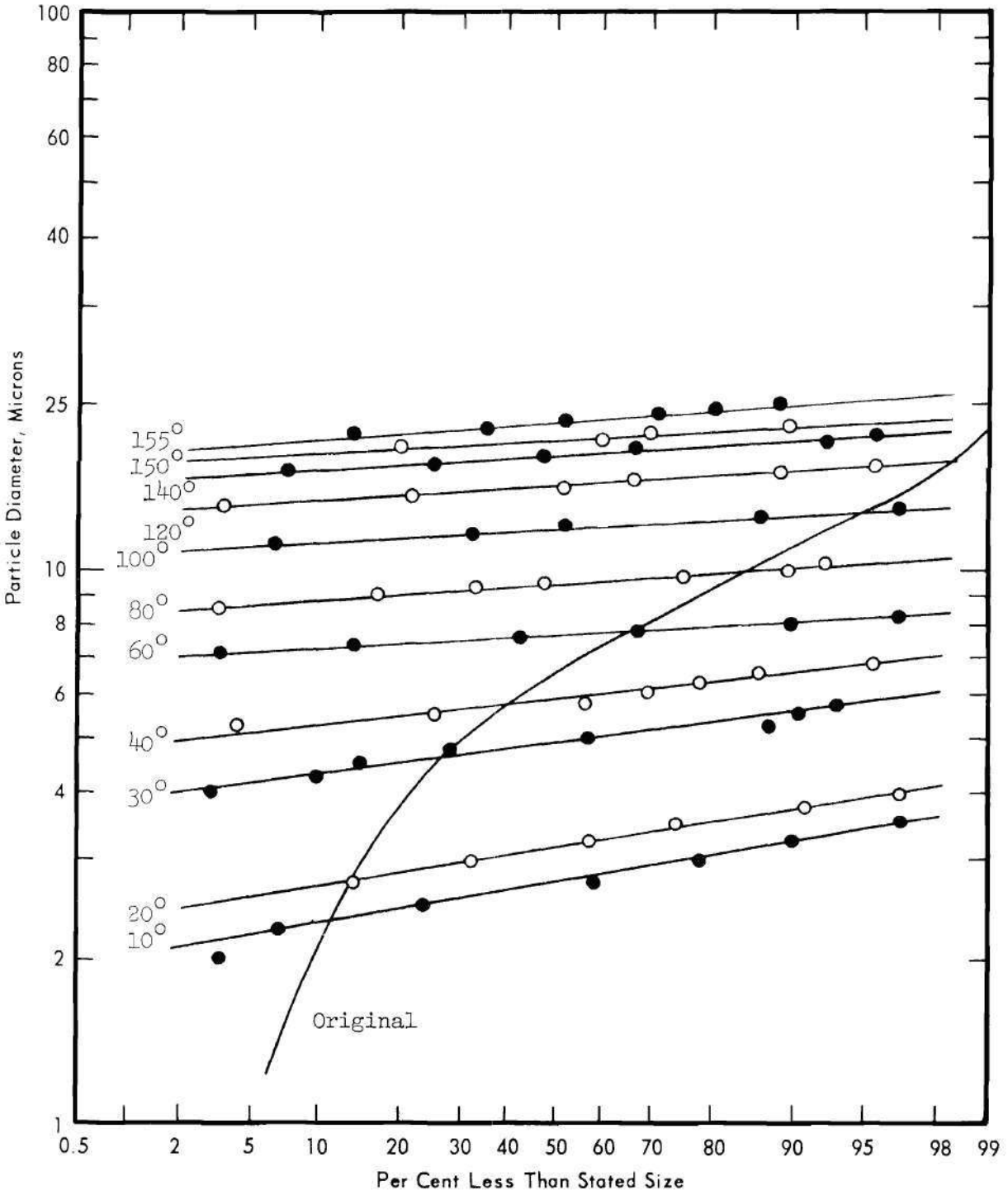

Figure 63. Size Distributions of Zinc Spheres before Classification and as Deposited at Specified Angular Locations on the Rotor Wall. (Rotor Speed: 2400 rpm).

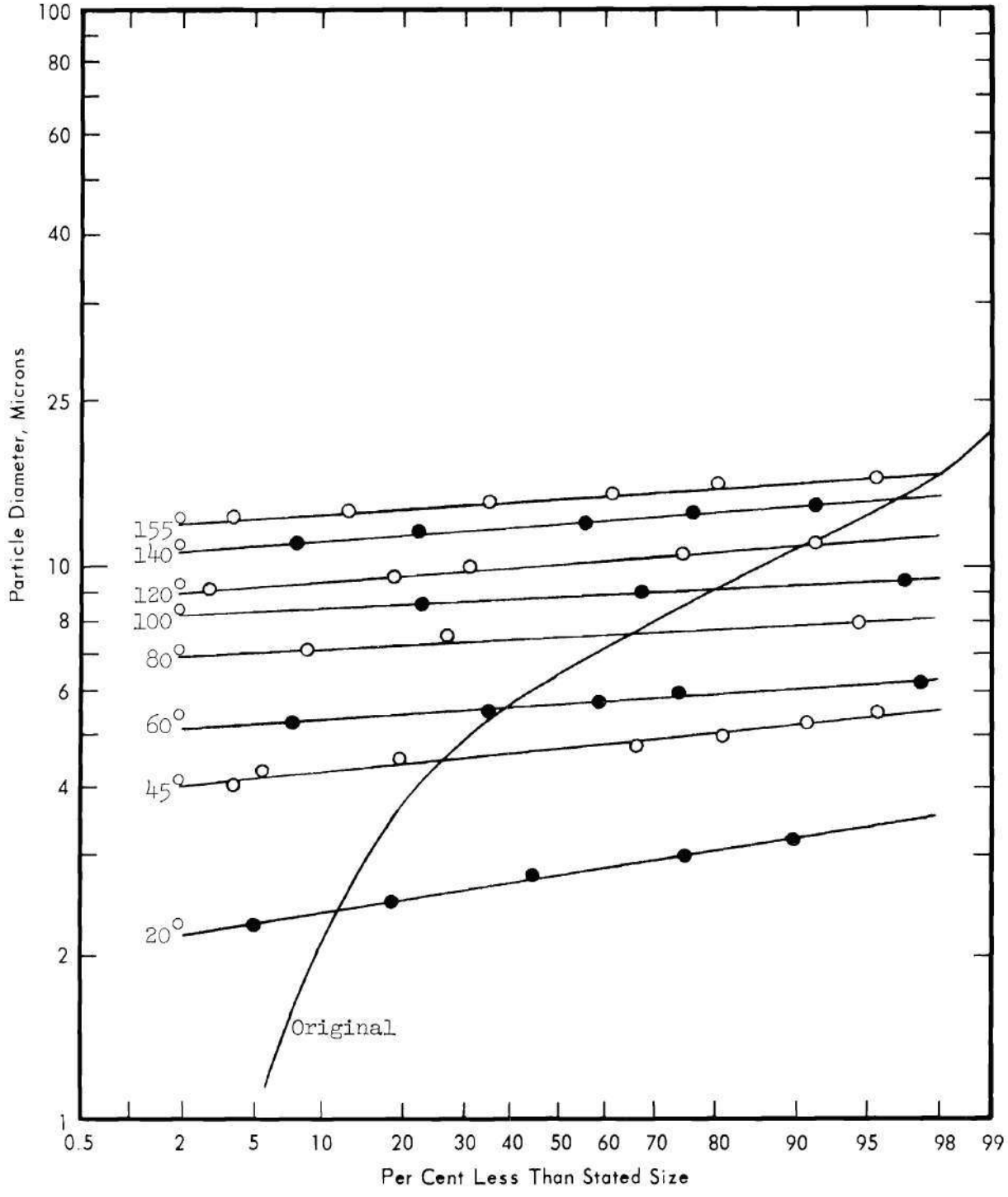

Figure 64. Size Distributions of Zinc Spheres before Classification and as Deposited at Specified Angular Locations on the Rotor Wall. (Rotor Speed: 4800 rpm).

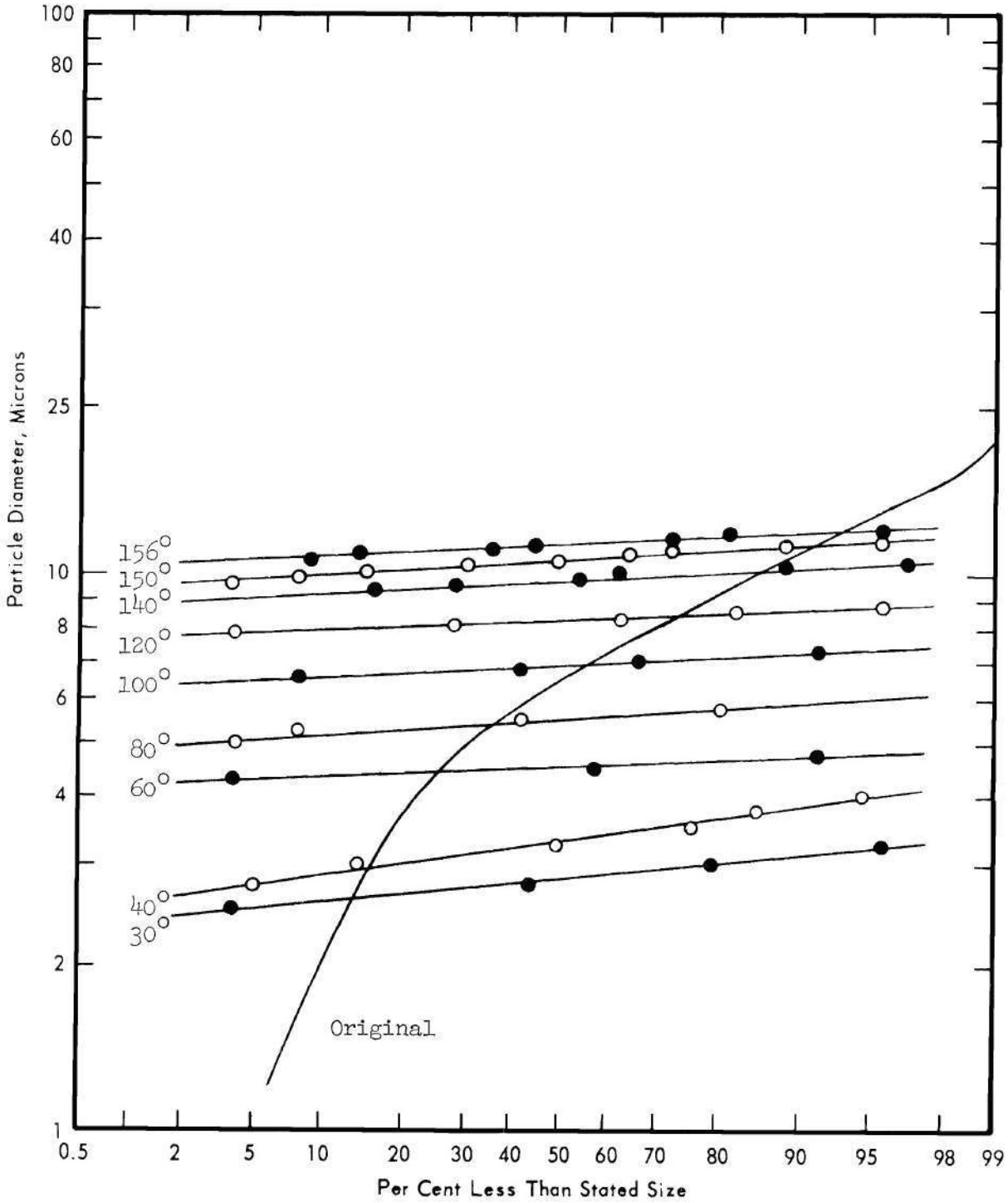

Figure 65. Size Distributions of Zinc Spheres before Classification and as Deposited at Specified Angular Locations on the Rotor Wall. (Rotor Speed: 7200 rpm).

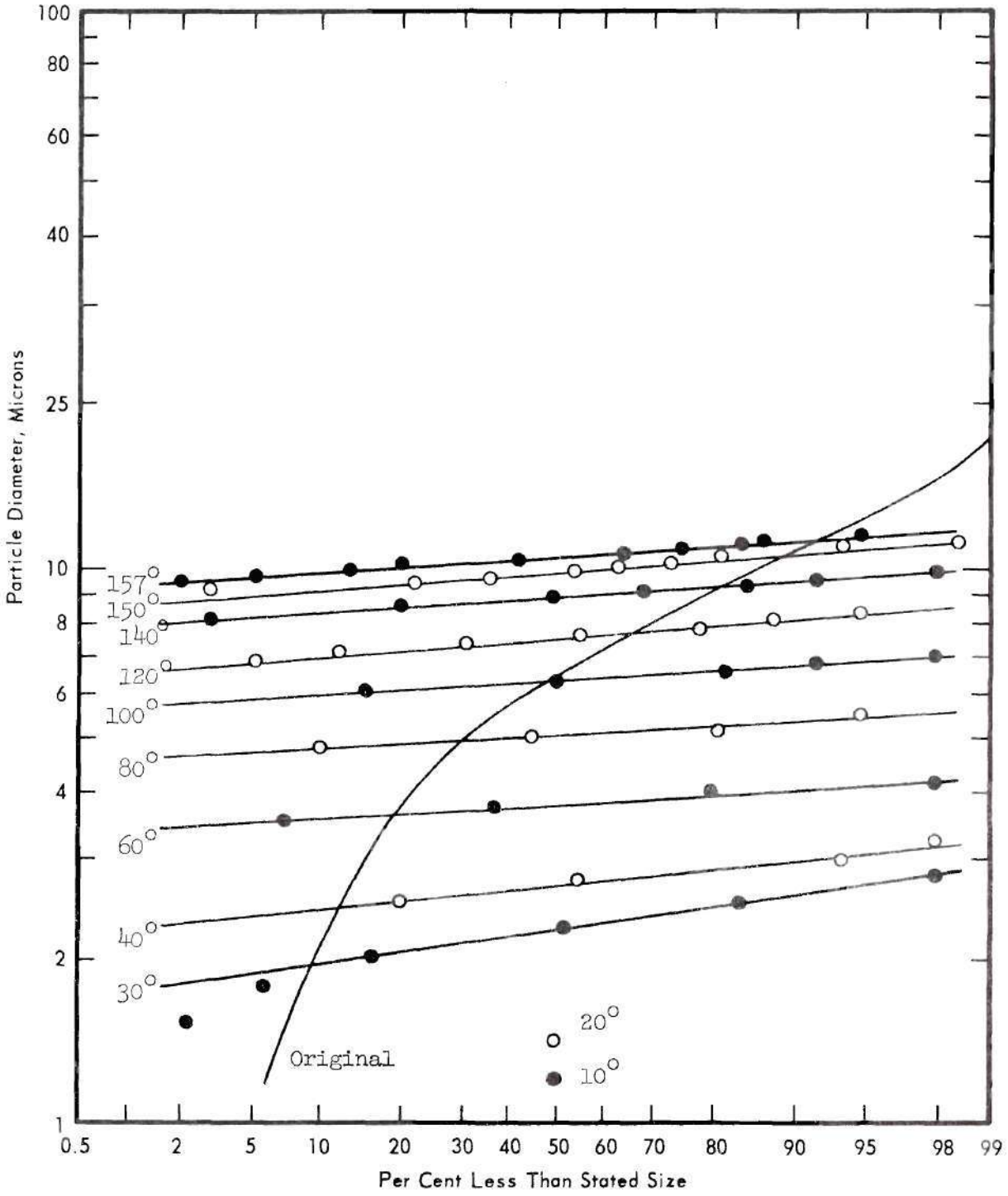

Figure 66. Size Distributions of Zinc Spheres before Classification and as Deposited at Specified Angular Locations on the Rotor Wall. (Rotor Speed: 9600 rpm).

APPENDIX E

COMPARISON OF RESULTS

This section contains comparisons of analog computer solutions obtained using the Stokes drag relation and a more general drag relation with experimental data for several types of spherical particles and various operating conditions.

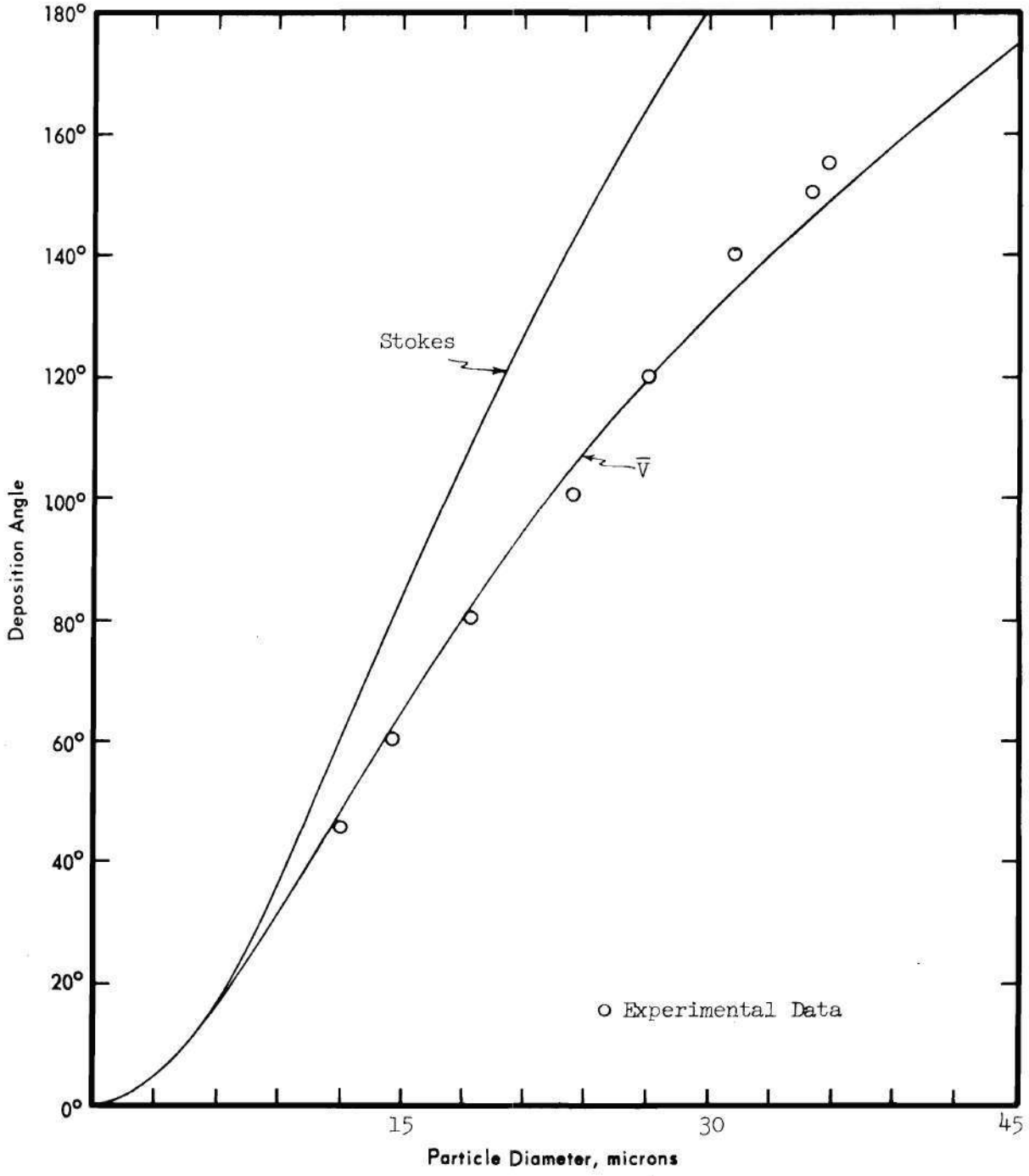

Figure 67. Comparison of Analog Computer Solutions Obtained Using Stokes Law and a More General Drag Relation with Experimental Data for Plastic Spheres. (Rotor Speed: 4800 rpm).

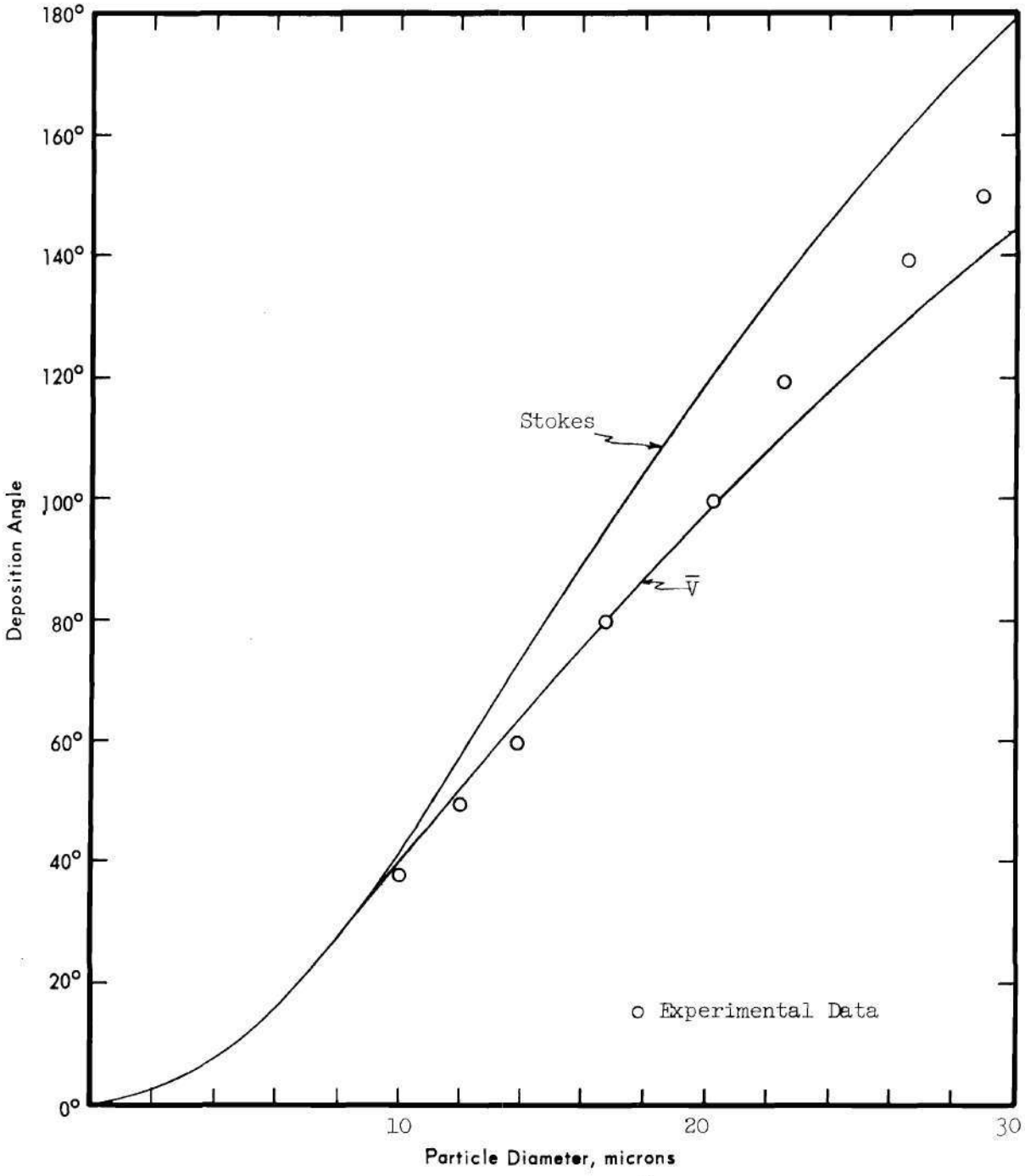

Figure 68. Comparison of Analog Computer Solutions Obtained Using Stokes Law and a More General Drag Relation with Experimental Data for Glass Spheres. (Rotor Speed: 2400 rpm).

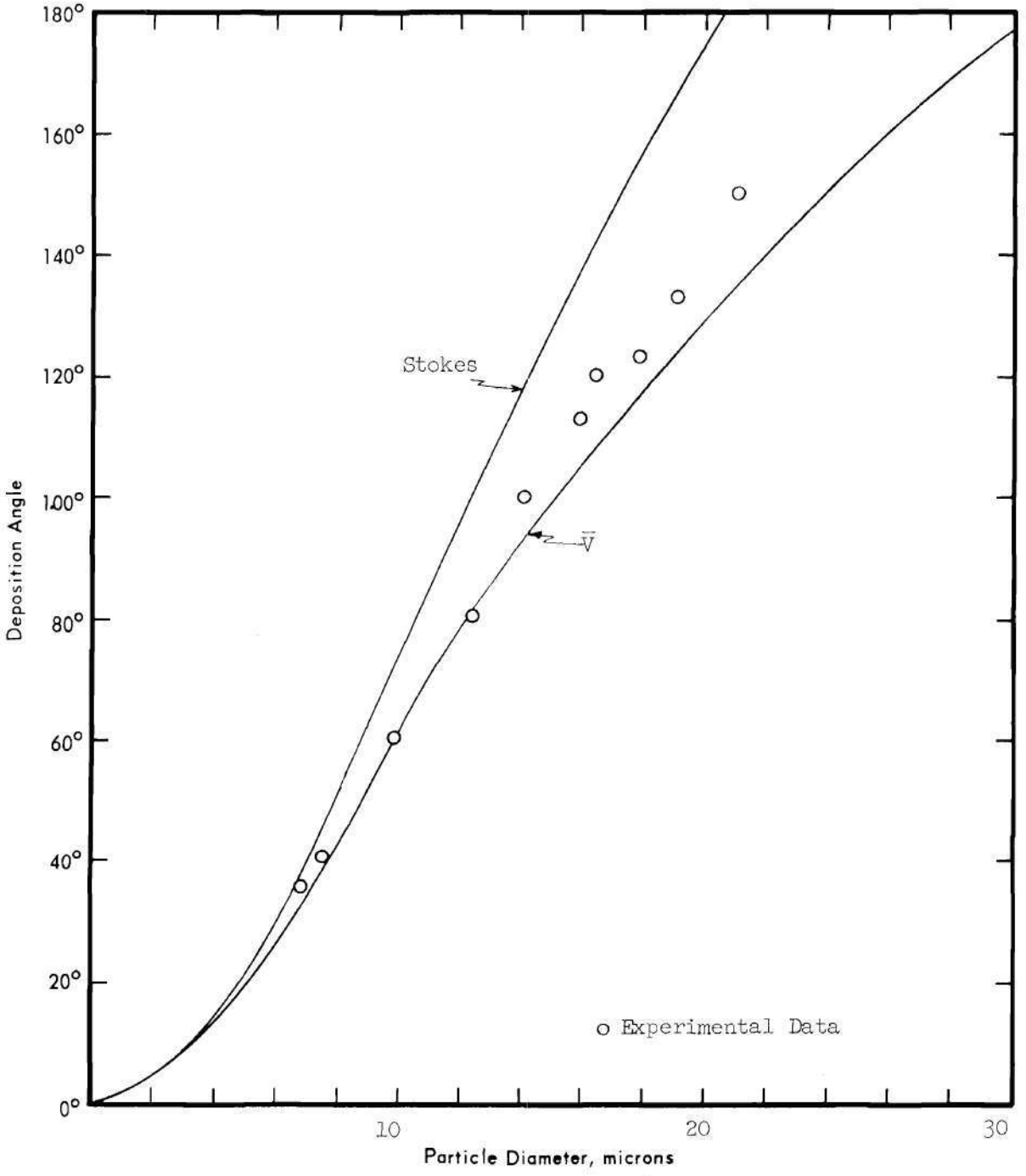

Figure 69. Comparison of Analog Computer Solutions Obtained Using Stokes Law and a More General Drag Relation with Experimental Data for Glass Spheres. (Rotor Speed: 4800 rpm).

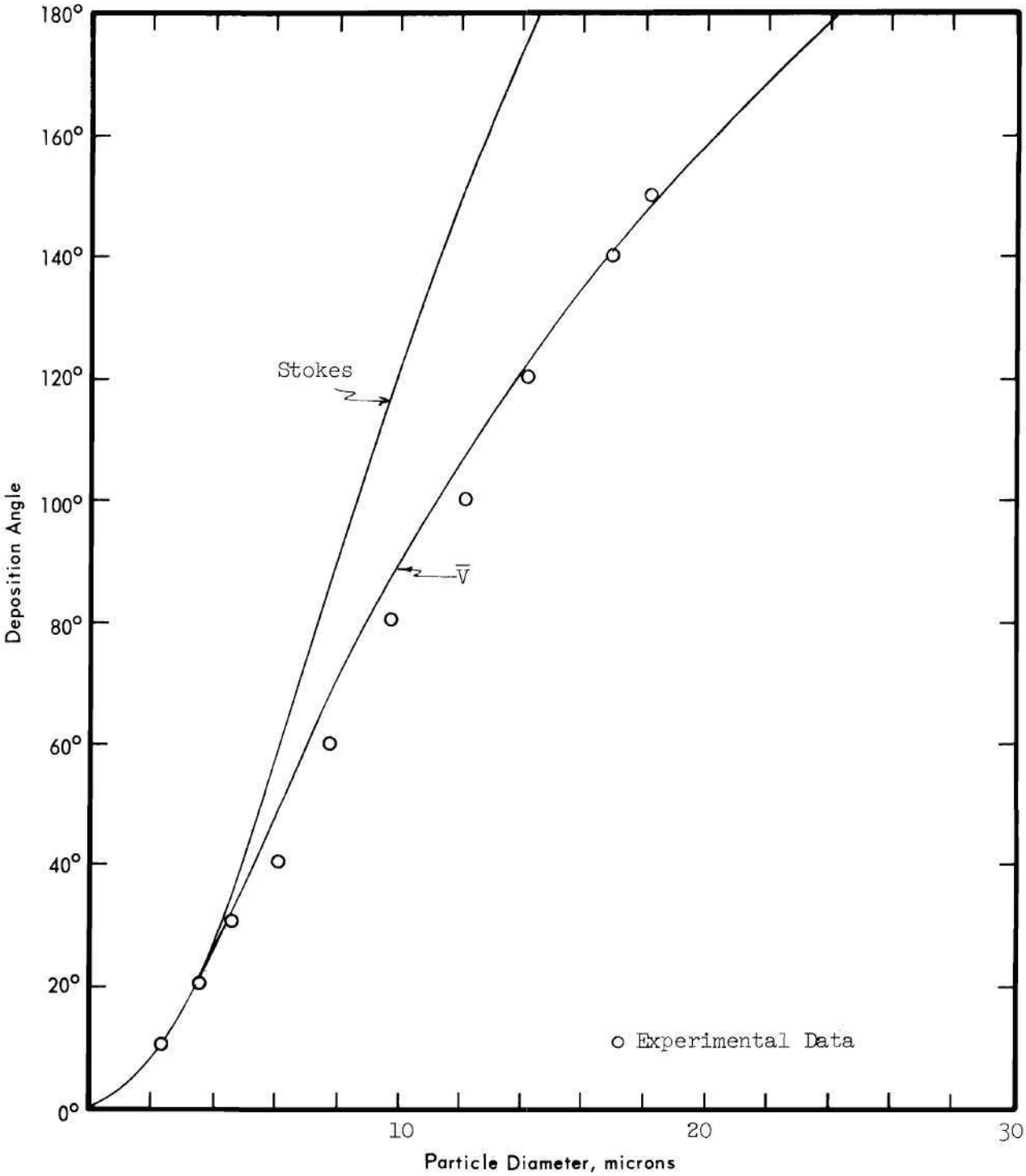

Figure 70. Comparison of Analog Computer Solutions Obtained Using Stokes Law and a More General Drag Relation with Experimental Data for Glass Spheres. (Rotor Speed: 9600 rpm).

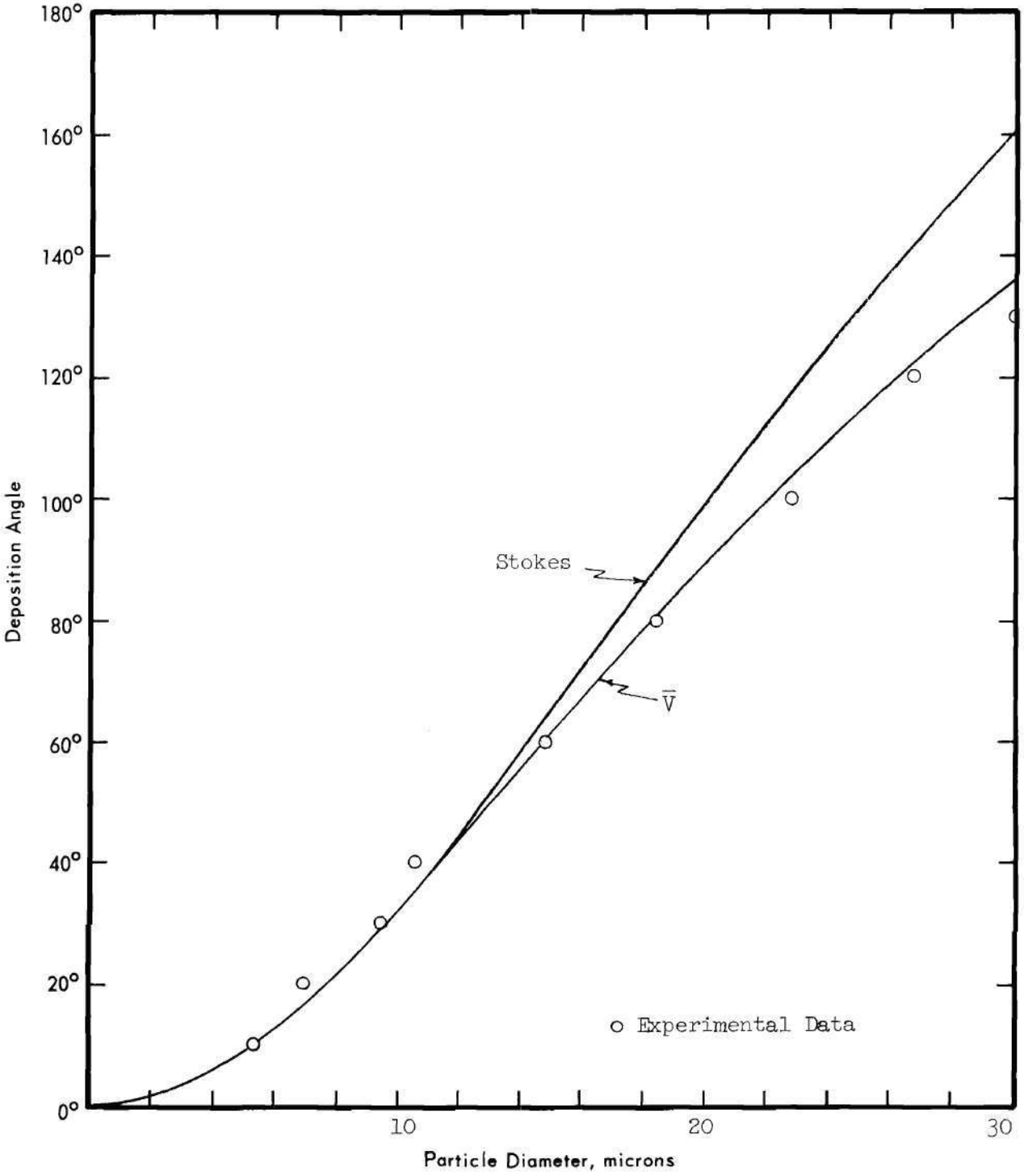

Figure 71. Comparison of Analog Computer Solutions Obtained Using Stokes Law and a More General Drag Relation with Experimental Data for Aluminum Spheres. (Rotor Speed: 1600 rpm).

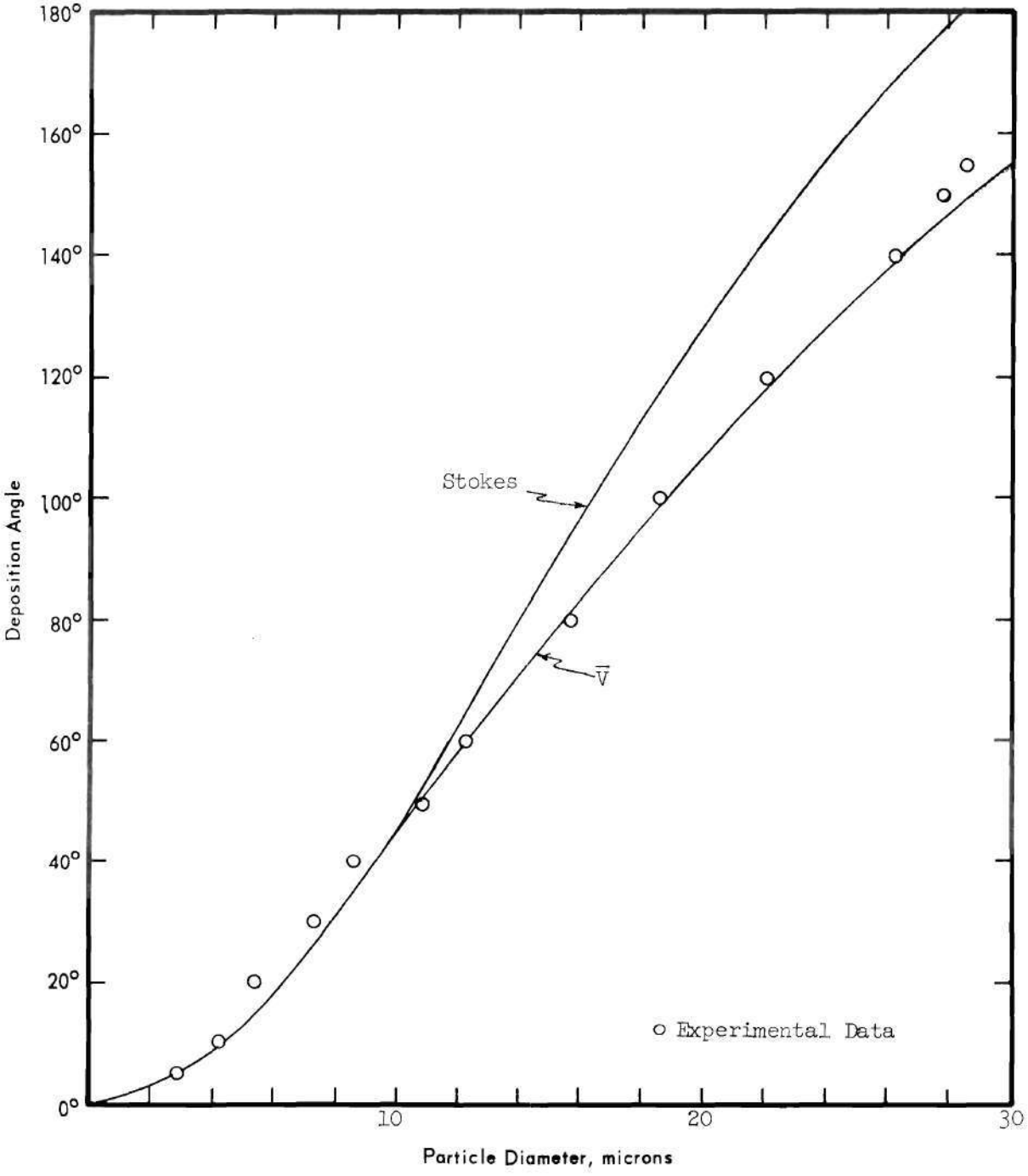

Figure 72. Comparison of Analog Computer Solutions Obtained Using Stokes Law and a More General Drag Relation with Experimental Data for Aluminum Spheres. (Rotor Speed: 2400 rpm).

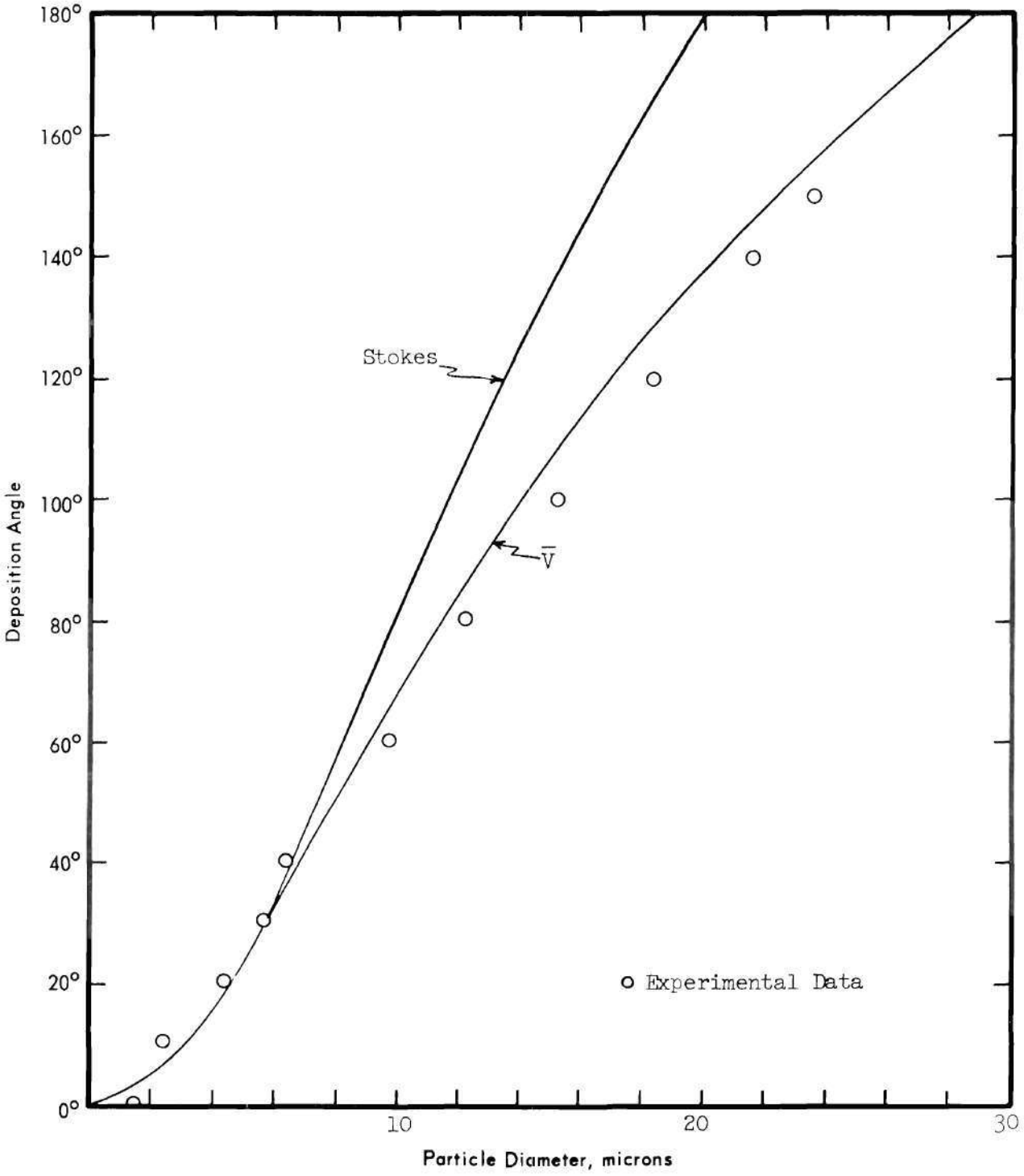

Figure 73. Comparison of Analog Computer Solutions Obtained Using Stokes Law and a More General Drag Relation with Experimental Data for Aluminum Spheres.(Rotor Speed: 4800 rpm).

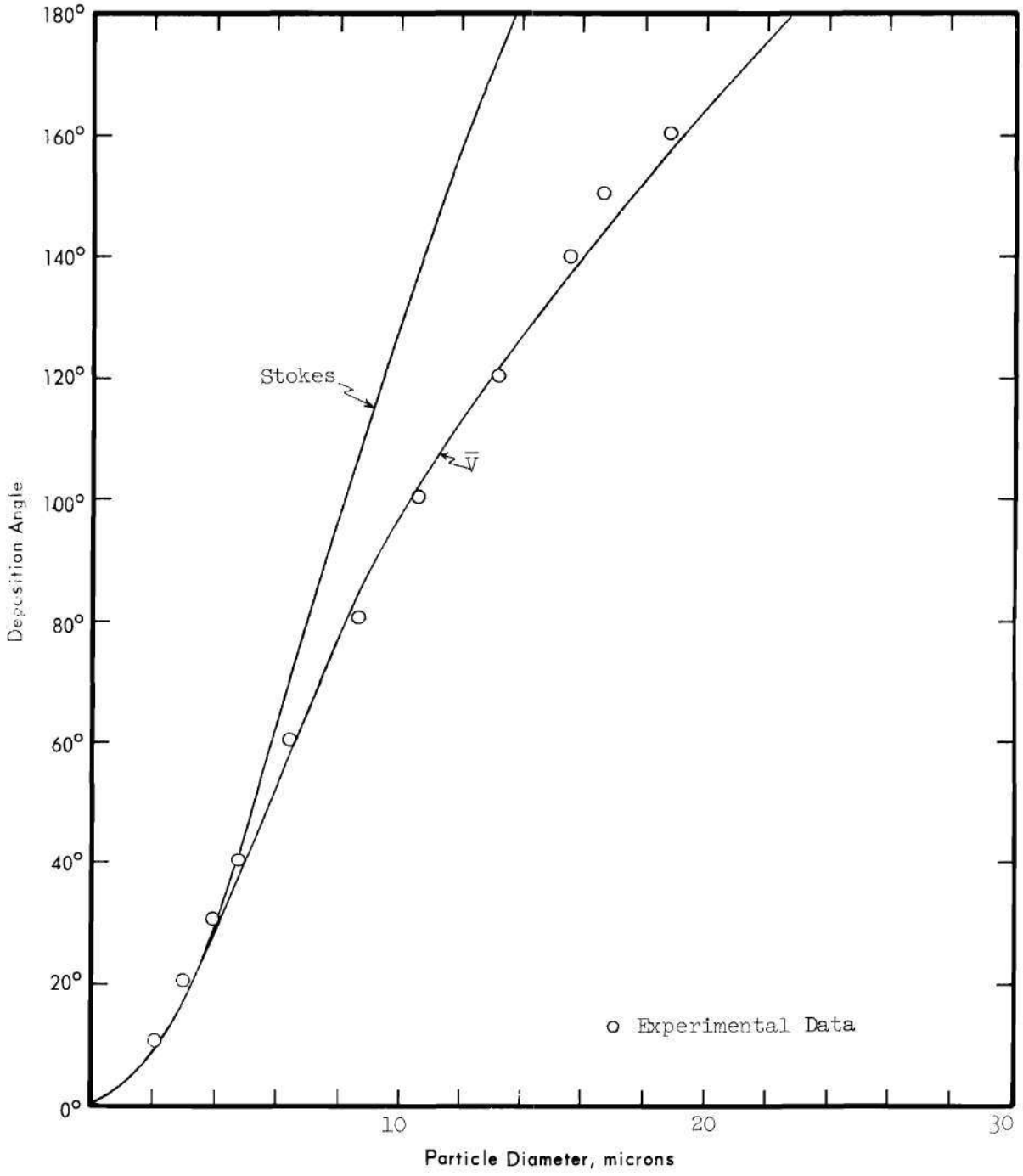

Figure 74. Comparison of Analog Computer Solutions Obtained Using Stokes Law and a More General Drag Relation with Experimental Data for Aluminum Spheres. (Rotor Speed: 9600 rpm).

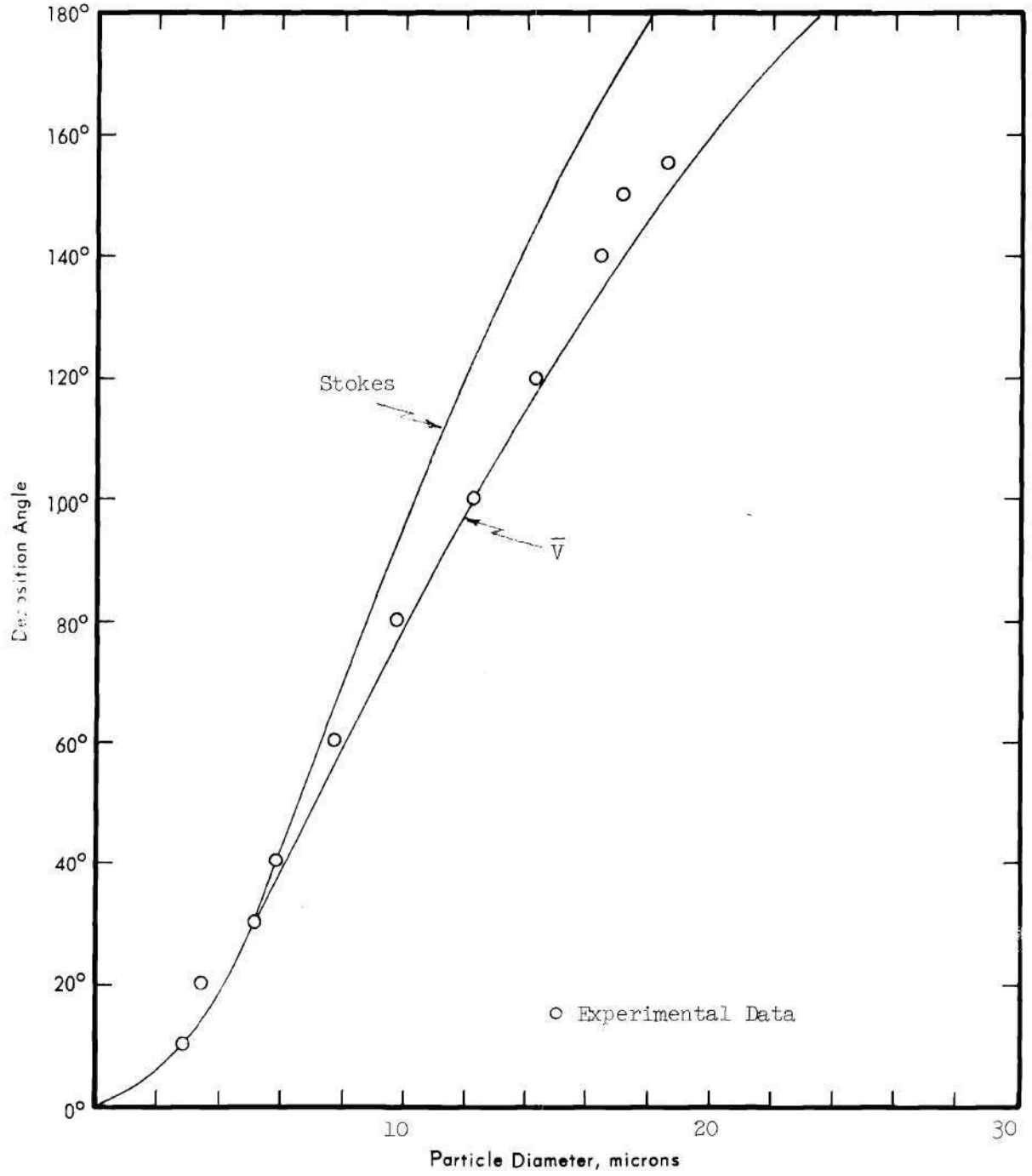

Figure 75. Comparison of Analog Computer Solutions Obtained Using Stokes Law and a More General Drag Relation with Experimental Data for Zinc Spheres. (Rotor Speed: 2400 rpm).

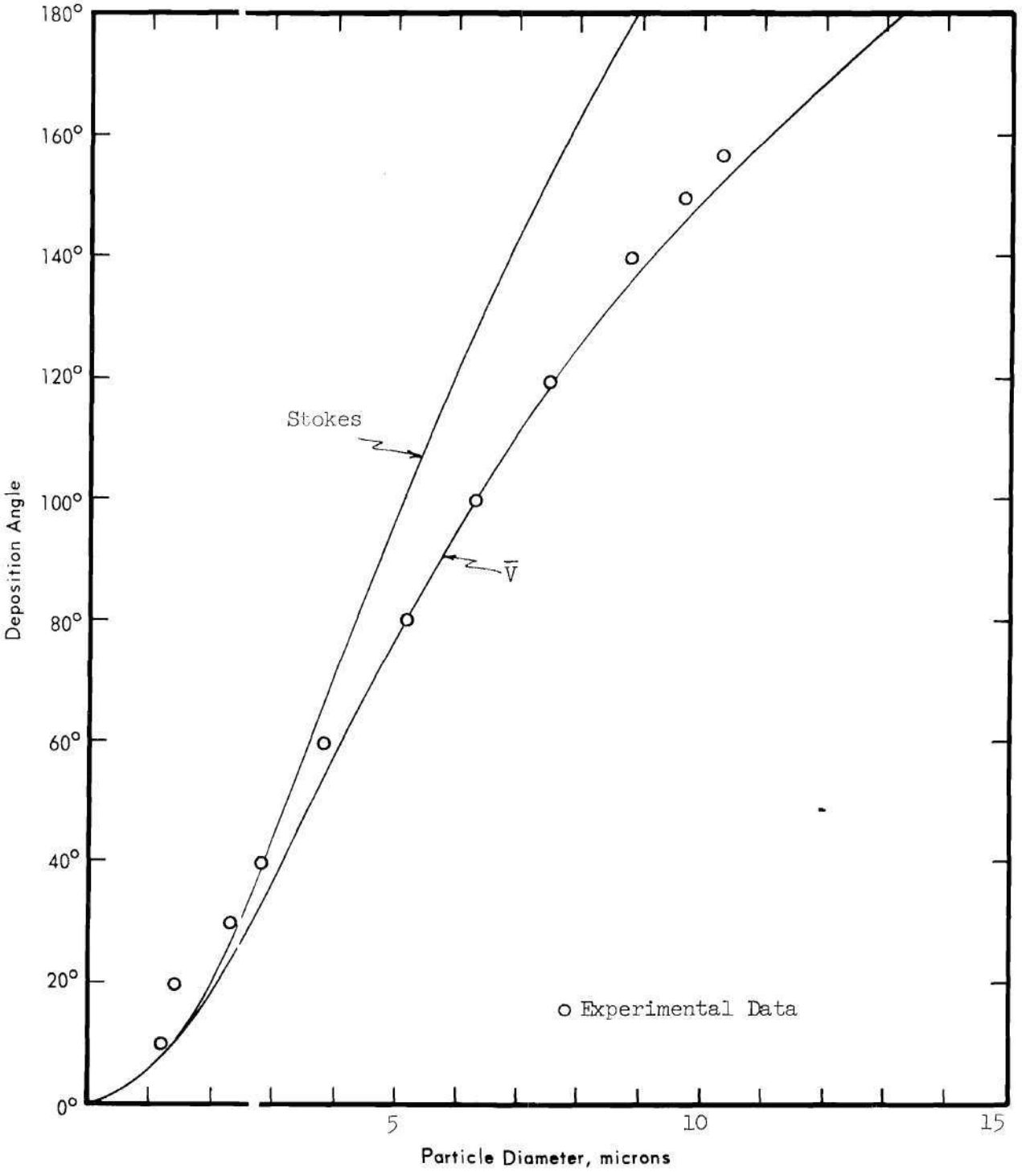

Figure 76. Comparison of Analog Computer Solutions Obtained Using Stokes Law and a More General Drag Relation with Experimental Data for Zinc Spheres. (Rotor Speed: 9600 rpm).

LITERATURE CITED*

1. G. G. Stokes, "On the Effect of the Internal Friction of Fluids on the Motion Pendulum," Trans. Camb. Phil. Soc. 9, 8-15 (1851).

2. Lord Rayleigh, "On the Motion of Solid Bodies Through Viscous Liquid," Phil. Mag., Sixth Series, 21, 697-711 (1911).

3. J. Proudman, "On the Motion of Solids in a Liquid Possessing Vorticity," Proc. Roy. Soc., 92A, 408-424 (1916).

4. G. I. Taylor, "Motion of Solids in Fluids when the Flow is not Irrotational," Proc. Roy. Soc., 93A, 99-113 (1917).

5. G. I. Taylor, "The Motion of a Sphere in a Rotating Liquid," Proc. Roy. Soc., 102A, 180-189 (1922).

6. G. I. Taylor, "Experiments on the Motion of Solid Bodies in Rotating Fluids," Proc. Roy. Soc., 104A, 213-218 (1923).

7. Lord Rayleigh, "On the Dynamics of Revolving Fluids," Proc. Roy. Soc., 93A, 148-154 (1917).

8. G. I. Taylor, "Experiments with Rotating Fluids," Proc. Roy. Soc. 100A, 114-121 (1921).

9. T. Okaya and M. Hasegawa, "On the Friction to the Disc Rotating in a Cylinder," Jap. J. Phys., 13, No. 1, 29-37 (1938).

10. G. K. Batchelor, "Note on a Class of Solutions of the Navier-Stokes Equations Representing Steady Rotationally-Symmetric Flow," Quart. Jnl. Mech. and Appl. Math., 4, 29-41 (1951).

11. J. Gillis, "Stability of a Column of Rotating Viscous Liquid," Proc. Camb. Phil. Soc., p. 152, (January 1961).

12. A. Reynolds, "On the Dynamics of Turbulent Vortical Flow," Zeit. angew. Math. und Physik, p. 149, (March 25, 1961).

13. W. F. Tanner, "Spiral Flow in Rivers, Shallow Seas, Dust Devils, and Models," Science, p. 41, (January 4, 1963).

14. J. S. Turner, "The Flow into an Expanding Spherical Vortex," J. Fluid Mech., 18, 195-199 (1964).

* Abbreviations for journals follow the form used by the American Chemical Society as found in Chemical Abstracts (1964).

15. F. Schultz-Grunow, "Der Reibungswiderstand rotierender Scheiben in Gehausen," Zeit. angew. Math. und Mech., 15, 191-204 (1935).

16. Th. von Karman, "Laminare and Turbulente Reibung," Zeit. angew. Math. und Mech., 1, 233-252 (1921).

17. F. Albrecht, "Theoretische Untersuchungen uber die Ablagerung von Staub aus stromender Luft und ihre Anwendung auf die Theorie der Staubfilter," Physik Zeit, 32, 48-56 (1931).

18. C. E. Lapple and C. B. Shepherd, "Calculation of Particle Trajectories," Ind. and Eng. Chem., 32, 605-617, (1940).

19. G. Narsimhan, "On the Equation of Motion of a Spherical Particle in a Centrifugal Force Field," J. Phys. Chem., 60, pp. 1476-1480, (1956).

20. K. L. Calder, "Some Theoretical Aspects of the Rotating Drum Aerosol Chamber," BWL Technical Study No. 13, October 1958, Army Biological Warfare Laboratory, Frederick, Md. ASTIA AD-207-865.

21. A. R. Kriebel, "Particle Trajectories in a Gas Centrifuge," Trans. Am. Soc. Mech. Engr., J. Basic Engr., 333-340, (1960).

22. C. W. Bouchillon, "Particle Trajectories in a Hydrocyclone," Georgia Institute of Technology Ph. D. Thesis, 1963.

23. K. Muller and J. Wessel, "Berechnung von Teilchenbahnen im Windsichter mit dem electronishen Analogrechner," Aufbereitungs Technik, 6, 235-242, (1963).

24. K. Wolf and H. Rumpf, "Uber die Sichtwirkung einer ebenen spiralformigen Luftstromung," Zeit. Verein Chem. Ing. 85, 601-604 (1941).

25. M. Nord, "Classifier Uses New Theory," Chem. Engr., 384-385, (1953).

26. R. E. Payne, "The Optimal Vortex Classifier," Mining Engr., 9, 1113-17 (1957).

27. W. Wieland, "Der Korngrossenanalysator System Holderbank," Aufbereitungs Technik, 4, 157-160 (1963).

28. G. Brown et al., Unit Operations, John Wiley and Sons, Inc., New York, p. 264, 1950.

29. "Bahco Micro-Particle Classifier," Technical Bulletin, Harry W. Dietert Co., Detroit, Michigan, 1960.

30. K. F. Sawyer and W. H. Walton, "The 'Conifuge' - A Size-separating Sampling Device for Airborne Particles," J. Sci. Inst., 27, 272-276, (1950).

31. A. Goetz, H. J. R. Stevenson, and O. Preining, "The Design and Performance of the Aerosol Spectrometer," J. Air Poll. Assn., 10, 378-383, (1960).

32. A. R. Kriebel, "Particle Trajectories in a Gas Centrifuge," Trans. Am. Soc. Mech. Engr., J. Basic Engr., 83, Series D, 333-340, (1961).

33. C. W. Oseen, "Uber den Gultigkeitsbereich der Stokesschen Widerstandsformel," Arkiv Math. Astr. Fys., 9, 1-15, (1913).

34. S. Goldstein, "The Steady Flow of Viscous Fluid Past a Fixed Spherical Object at Low Reynolds Numbers," Proc. Roy. Soc., A123, p. 225, (1929).

35. A. B. Basset, "On the Motion of Two Spheres in a Liquid," Quart. Jnl. Math., 22, 369, (1887).

36. H. Lamb, Hydrodynamics, Cambridge University Press, Cambridge, England, p. 423, (1932).

37. Lord Rayleigh, "On the Motion of Solid Bodies Through Viscous Liquid," Phil. Mag., Sixth Series, 21, 697-711, (1911).

38. N. A. Fuks, The Mechanics of Aerosols, U. S. Department of Commerce, Office of Technical Services, Washington 25, D. C. (1959).

39. R. A. Millikan, "Coefficients of Slip in Gasses and the Law of Reflection of Molecules from the Surfaces of Solids and Liquids," Phys. Revs., 21, 217-238, (1923).

40. C. N. Davies, "Definitive Equations for the Fluid Resistance of Spheres," Phys. Soc., 57, 259-270, (1954).

41. C. E. Lapple and C. B. Shepherd, "Calculation of Particle Trajectories," Ind. Eng. Chem., 32, 605-617, (1940).

42. W. M. Swanson, "The Magnus Effect: A Summary of Investigations to Date," Trans. Am. Soc. Mech. Engr., J. Basic Engr., 83, 461-470, (1961).

43. S. I. Rubinow and J. B. Keller, "The Transverse Force on a Spinning Sphere Moving in a Viscous Fluid," J. Fluid Mech., 11, 447-457, (1961).

44. C. W. Bouchillon, "Particle Trajectories in a Hydrocyclone," Georgia Institute of Technology Ph.D. Thesis, 1963.

VITA

John Henry Burson, III was born in Carrollton, Georgia, on July 30, 1934. He attended elementary school in Carrollton and graduated from Carrollton High School in 1951. He entered the Cooperative Division of the Georgia Institute of Technology in June, 1951, and graduated in 1956, receiving the degree of Bachelor of Chemical Engineering.

In January of 1956, Mr. Burson joined Testworth Laboratories in Carrollton, Georgia as Chief Chemist. He remained at this position until September, 1959, except for a six month tour of duty in the Chemical Corps of the United States Army from February, 1957, to August, 1957. In September of 1959, he entered the Graduate Division of the Georgia Institute of Technology on a part-time basis and joined the staff of the Engineering Experiment Station as a Research Assistant. He was promoted to the position of Assistant Research Engineer in 1962. In March, 1963, he received the degree Master of Science in Metallurgy. He has also served as a part-time instructor in the School of Chemical Engineering and the Engineering Evening School. He is the author or co-author of eleven major reports and publications and a member of Sigma Xi. He is presently a Captain in the United States Army Reserve.

Mr. Burson was married in 1955 to the former Barbara Anne Vaughn. They have two daughters and two sons.